The Pennsylvania State University

The Graduate School

College of Earth and Mineral Sciences

BIOGEOCHEMICAL CYCLING OF COPPER IN ACID MINE DRAINAGE

A Dissertation in

Geosciences and Biogeochemistry

by

Bryn E. Kimball

Submitted in Partial Fulfillment
of the Requirements
for the Degree of

Doctor of Philosophy

December 2009

The dissertation of Bryn E. Kimball was reviewed and approved* by the following:

Susan L. Brantley
Professor of Geosciences
Dissertation Adviser
Co-Chair of Committee

Jennifer L. Macalady
Assistant Professor of Geosciences
Co-Chair of Committee

Matthew S. Fantle
Assistant Professor of Geosciences

Brian A. Dempsey
Professor of Environmental Engineering

Katherine H. Freeman
Professor of Geosciences
Associate Department Head of Graduate Programs

*Signatures are on file in the Graduate School

ABSTRACT

Metal contamination in surface water and soil environments is largely due to acid rock drainage (ARD) or acid mine drainage (AMD), which results from dissolution of metal sulfide minerals. This dissertation focuses on characterizing the biogeochemical processes that solubilize and sequester copper (Cu) in environments impacted by AMD.

Copper isotope measurements are a novel approach to characterizing Cu mobility. A review of published Cu isotope data (Chapter 2) show that, on average, Cu(I)-sulfides and secondary Cu(I)/(II) minerals are depleted in ^{65}Cu (based on $^{65}Cu/^{63}Cu$) relative to AMD-impacted streamwater, seawater, and large rivers. Based on published experiments, including those described in this dissertation, aqueous Cu(II) is enriched in ^{65}Cu relative to aqueous and solid Cu(I) phases (Chapter 2). Enrichment of aqueous Cu in ^{65}Cu relative to Cu-bearing minerals is best explained by a redox isotope effect, whereby isotopically heavy Cu(I) in sulfide minerals preferentially oxidizes to Cu(II), which is then released to solution. Experiments also show that Cu isotope fractionation (up to 4‰) due to a redox isotope effect can be overprinted by additional isotope effects that are related to mineralogy, kinetics, ligand complexation, and biological processes, which, in combination, may account for the large variation of Cu isotope composition ($\Delta^{65}Cu$ = 12‰) in environmental samples.

Chalcopyrite is the most abundant Cu-bearing mineral on earth, and most commonly occurs in hydrothermal sulfide deposits. Under oxic conditions, dissolution of chalcopyrite releases dissolved Cu and Fe and acidifies surrounding solutions. Understanding how this and other sulfide minerals dissolve is important for abating anthropogenic release of metals in association with mining activies. In Chapter 3, chalcopyrite dissolution kinetics are synthesized and analyzed in order to derive empirical chalcopyrite dissolution rate laws. Using multiple linear regression analysis, we determine a rate law for nonoxidative chalcopyrite dissolution and for oxidation of chalcopyrite by Fe(III).

Chapter 4 is a survey of Cu isotope compositions in primary chalcopyrite and enargite and leached Cu in an AMD-impacted area in southwestern Colorado, USA. To aid our interpretation of Cu isotope fractionation measured among field samples, we also

conducted chalcopyrite and enargite leach experiments in the absence and presence of the Proteobacterium *Acidithiobacillus ferrooxidans*. When bacteria are present, leached Cu is isotopically lighter than chalcopyrite ($\Delta_{aq\text{-}min}^{o}$ = -0.57 ± 0.14‰, where min^{o} refers to the starting mineral), and isotopically identical to enargite ($\Delta_{aq\text{-}min}^{o}$ = 0.14 ± 0.14‰). The biotic fractionation differences between chalcopyrite and enargite are likely due to differing mineralogy. Even though microorganisms are present at the field site, Cu isotope fractionation in the field resembles that in abiotic chalcopyrite leach experiments. In abiotic experiments, leached Cu was isotopically enriched in ^{65}Cu relative to chalcopyrite ($\Delta_{aq\text{-}min}^{o}$ = 1.37 ± 0.14‰) and enargite ($\Delta_{aq\text{-}min}^{o}$ = 0.98 ± 0.14‰). Mass balance calculations support the likelihood that partitioning of isotopically heavy dissolved Cu into microbial-associated phases is less significant in the open field system compared to the closed laboratory experiments. Copper isotope measurements in abiotic experiments allow us to infer that heavy Cu is preferentially oxidized at the interface between the isotopically homogeneous mineral and a surface oxidized layer. The isotopically heavy oxidized Cu is then solubilized. The result is leached Cu that is isotopically heavier than the starting material during abiotic leaching. During biotic leaching, additional processes likely affect the Cu isotope composition of leached Cu.

Based on the hypothesis that interaction of isotopically heavy dissolved Cu with *A. ferrooxidans* cells caused part of the biotic fractionation measured in sulfide leach experiments (Chapter 4), we characterized Cu association with cells and related precipitates using transmission electron microscopy (TEM), energy dispersive x-ray spectroscopy (EDS), X-ray fluorescence microscopy (μ-XRF), and micro-x-ray diffraction (μ-XRD). The results, described in Chapter 5, show that within cells, polyphosphate granules have the highest Cu concentration. The μ-XRF observations show that whole cells of *A. ferrooxidans* grown in 1 mM Cu may contain 0.11 ± 0.01 to 6.19 ± 0.28 fg Cu/cell. Outside of cells, Cu may co-precipitate with jarosite minerals (identified with μ-XRD) that form as a result of cell growth. Incorporation of isotopically heavy Cu into jarosite is consistent with equilibrium isotope fractionation theory and the observed bioleach fractionation measured (Chapter 4). Further work is warranted to determine whether isotopic, chemical, and structural characteristics of jarosite function as a biosignature of microbial Fe-oxidation.

TABLE OF CONTENTS

LIST OF TABLES

LIST OF FIGURES

PREFACE

This dissertation is comprised of five chapters.

Chapter 1 is an introduction to the dissertation as a whole. The chapter introduces themes that are found throughout the dissertation and provides reasons for focusing on copper, among the many toxic metals.

Chapter 2 is a synthesis of the advances made in the field of copper isotope biogeochemistry to date. This chapter provides context for the novel tool used in this dissertation: copper isotope measurements.

Chapter 3 is a compilation and analysis of chalcopyrite dissolution kinetics. The chapter will be edited and submitted for publication as a multiple-author work: B. E. Kimball, J. D. Rimstidt, and S. L. Brantley, Chalcopyrite Dissolution Rate Laws. The manuscript will be submitted to *Applied Geochemistry*.

Chapter 4 is a comparison of the copper isotope fractionation measured between sulfide minerals and acid mine drainage samples from the field to the fractionation measured between copper in sulfide minerals and leached copper in abiotic and biotic leach experiments. This chapter is published as it is presented here as: B. E. Kimball, R. Mathur, A. C. Dohnalkova, A. J. Wall, R. L. Runkel, and S. L. Brantley, 2009, Copper Isotope Fractionation in Acid Mine Drainage, *Geochimica et Cosmochimca Acta*, v. 73, p. 1247-1263.

Chapter 5 is a follow-up to Chapter 4. This chapter explores how dissolved copper interacts with *Acidithiobacillus ferrooxidans* cells, and how such interaction may affect the partitioning of copper isotopes in the system. The chapter will be edited and submitted for publication as a multiple-author work: B. E. Kimball, A. C. Dohnalkova, B. Lai, J. L. Macalady, K. M. Kemner, and S. L. Brantley, Bacterially-Mediated Precipitation of Jarosite: Implications for Copper Isotope Mobility. The manuscript will be submitted to *Geobiology*.

ACKNOWLEDGEMENTS

I owe many people thanks for helping me to complete this dissertation. My advisor Sue Brantley has greatly influenced the way I think about the world and pose scientific questions. She has also taught me how to communicate my science efficiently and successfully. I am grateful to have had the honor to work with her. My co-advisor, Jenn Macalady, has also positively shaped the way I view science. Her curiosity about the microbial world reminds me why I love science. I want to thank my original committee member, Peter Heaney, for helping me to understand XRD, TEM, and minerals in general. I appreciate Matt Fantle's willingness to step in as my new committee member, and I thank him for helpful discussions about non-traditional isotope systems. I also want to thank Ryan Mathur for teaching me everything I know about copper isotopes. I thank Brian Dempsey, my outside committee member, for helpful discussions and encouragement.

I learned analytical techniques from many helpful people. Laura Liermann taught me how to do just about everything in the Brantley lab. John Kittleson and Henry Gong taught me to use plasma-source mass spectrometers, and Garret Hart and Jeff Vervoort (Washington State University) taught me how to use their multi-collector ICP-MS. Alice Dohnalkova (EMSL) taught me everything I know about TEM analysis of microbial cells and provided many of the TEM images presented in this dissertation. I owe many thanks to Kenneth Kemner for allowing me to use some of his synchrotron beam time in order to make μ-XRF measurements, and for teaching me about x-ray absorption spectroscopy. I am also grateful to have had the pleasure to work with Don Rimstidt before he retires. He taught me how to synthesize and analyze and large kinetic data set, a task that would have been too daunting without him.

I am greatly indebted to my friends and colleagues at Penn State. The Brantley group, Macalady group, and Heaney group have helped me immensely in carrying out this research. I want to thank Andy Wall in particular for many helpful discussions and for moral support. I also thank Kristin Morrell and Jennifer Williams for encouragement

and friendship. This work would not have been possible without the support of my many wonderful friends and my loving family.

This work was made possible by multiple generous funding sources. Support was provided by the Penn State Biogeochemical Research Initiative for Education (BRIE) (NSF grant DGE-9972759), the EPA Science to Achieve Results (STAR) fellowship program, and the Penn State Center for Environmental Kinetics Analysis (CEKA) (NSF grant CHE-0431328), the National Aeronautics and Space Administration (NASA) grant NNG05GN72G, and the International Association of Geochemistry Student Research Grant. TEM imaging and analyses were performed at the W. R. Wiley Environmental Molecular Sciences Laboratory (EMSL), a national scientific user facility operated by Battelle for the U.S. DOE under Contract DE-AC05-76RLO1830. μ-XRF analysis was performed at the Advanced Photon Source, Argonne National Laboratory, which is supported by the DOE Office of Science, Office of Basic Energy Sciences. General user support for μ-XRF work was also provided by the DOE's Environmental Remediation Sciences division.

Chapter 1
An Introduction to the Biogeochemical Cycling of Copper in Acid Mine Drainage

Metals play an important role in our society. We rely on them for building material and infrastructure, as well as for our good health. Like many things, however, too much metal can be detrimental to the environment, and ultimately our lives. When metals accumulate in water and soils above some threshold concentration, they can circulate in the biosphere at toxic levels, causing health defects or death (Smith and Huyck, 1999). Metal-rich, acidic drainage occurs anywhere that sulfide minerals are exposed to atmospheric oxygen, including road construction and foundation excavation sites, but the most common sites are locations where sulfide-bearing metalliferous ore deposits and sulfide-rich coal are exploited (Blowes et al., 2003). The released metals negatively affect the quality of aquatic life, decrease the productivity of agriculture and ranching, and contaminate the drinking water of many communities (Nordstrom and Alpers, 1999). Nearly 20,000 km of rivers and streams and more than 180,000 acres of lakes and reservoirs in the U.S. have been spoiled with toxic acid mine drainage (AMD) (Kleinmann, 1989). This chronic environmental problem, also referred to as acid rock drainage (ARD), involves the production of acid from oxidative sulfide dissolution, the transport of acidic, metal-rich waters through ecosystems, and the ultimate neutralization of acidity and attenuation of metals.

The most common sulfide mineral found on earth, and in mining environments, is pyrite (FeS_2) (Nesse, 2000; Blowes et al., 2003). Pyrite oxidatively dissolves in the presence of oxygen (O_2) or ferric iron (Fe(III)), releasing dissolved Fe and sulfuric acid, as shown in the following reactions:

$$FeS_2 + 3.5O_2 + H_2O \rightarrow Fe^{2+} + 2SO_4^{2-} + 2H^+ \quad (1.1)$$

$$FeS_2 + 14Fe^{3+} + 8H_2O \rightarrow 15Fe^{2+} + 2SO_4^{2-} + 16H^+ \quad (1.2)$$

The Fe(II) produced is then oxidized by dissolved O_2 in the following reaction:

$$14Fe^{2+} + 3.5O_2 + 14H^+ \rightarrow 14Fe^{3+} + 7H_2O \quad (1.3)$$

Reaction 1.3 is abiotically very slow at low pH (Schwertmann and Fitzpatrick, 1992; Nordstrom and Southam, 1997), but is catalyzed by acidophilic Fe-oxidizing microorganisms. The Fe(III) produced then oxidizes more pyrite or is consumed during hydrolysis and formation of Fe (oxyhydr)oxides ($Fe(OH)_3$) in the following reaction:

$$Fe^{3+} + 3H_2O \rightarrow Fe(OH)_3 + 3H^+ \quad (1.4)$$

Solutions carrying the reactants produced in reactions 1.1, 1.2, and 1.4 tend to have low pH (< 4) and high metal and sulfate contents. Despite these relatively extreme conditions, acidophilic prokaryotes are known to thrive in ARD (Nordstrom and Southam, 1997). Certain lithotrophic bacteria and archaea make a living by oxidizing reduced Fe and S for their energy needs, and acquiring C through autotrophy, making them primary producers in this acidic niche (Johnson, 1998). Other microorganisms pair lithotrophy with the acquisition of C through heterotrophy or mixotrophy (Johnson, 1998). The metabolized, oxidized Fe and S then provide substrates for Fe- and S-reducers that live in nearby suboxic or anoxic zones. Microbial communities in ARD are comprised of members that carry out synergistic Fe- and S-oxidation and reduction, as well as organic carbon oxidation, carbon fixation, nitrogen fixation, and extracellular polymeric film production (Baker and Banfield, 2003). These microbial communities tend to contain few distinct taxa (Baker and Banfield, 2003), with microenvironments containing fewer than five different genera (Bond and Banfield, 2001).

The presence of Fe- and S-oxidizing microorganisms causes sulfide dissolution rates to increase. For example, the rate of pyrite oxidation by O_2 at pH = 2 and 25ºC is $0.3 - 3 \times 10^{-9}$ mol m^{-2} s^{-1} during abiotic dissolution (McKibben and Barnes, 1986; Rimstidt et al., 1994; Nordstrom and Alpers, 1999) and 8.8×10^{-8} mol m^{-2} s^{-1} in the presence of *Acidithiobacillus ferrooxidans* (Olson, 1991; Nordstrom and Alpers, 1999), an Fe- and S-oxidizing Proteobacterium. Microorganisms dissolve sulfides through: 1) indirect bioleaching, whereby dissolved Fe(II) leached from minerals is microbially oxidized to Fe(III) (reaction 1.3), which then attacks sulfides to release more Fe(II) and reduced S, and 2) contact bioleaching, where cells attach to minerals and create a microenvironment optimized for electron extraction from reduced elements (Tributsch, 2001; Rodríguez et al., 2003).

While the influence of microorganisms on sulfide dissolution has been known for some time, we are now beginning to appreciate how the mere presence of microorganisms also affects the behavior of important elements, including toxic metals. For instance, in the laboratory, both gram-positive and gram-negative cells act as sorbents for aqueous Cd, Cu, Pb, Al, Co, Nd, Ni, Sr, Zn, Fe, and U (Fein et al., 1997; Daughney et al., 1998; Fein et al., 2001; Fowle and Fein, 2001; Haas et al., 2001; Yee and Fein, 2001; Borrok and Fein, 2005; Wightman and Fein, 2005; Guiné et al., 2006). While these studies were conducted at near neutral pH, few studies have focused on acidophilic microorganism-metal interaction at low pH (e.g., Naja et al., 2005; Ginn and Fein, 2008; Kenney and Fein, 2009). Fowle and Fein (2001) observed that 1.1 mg Cu/g biomass sorbed to *Bacillus subtilis* cells at pH 2.6, and 0.2 mg Cu/g biomass sorbed to a river water consortia at pH 2.3 (Johnson et al., 2007). These metal-bacteria interactions have significant implications for mass transport through aqueous systems (Fein et al., 1997).

Metal attenuation in ARD-impacted areas is most often ascribed to inorganic processes such precipitation (e.g., Hammarstrom et al., 2005; Sidenko and Sherriff, 2005; Kumpulainen et al., 2007), sorption of metals onto (oxyhydr)oxide minerals (e.g., Smith, 1999; Schemel et al., 2000; Nimick et al., 2003b; Parker et al., 2007), and dilution by mixing with water at circumneutral pH (e.g., Paulson and Balistrieri, 1999; Balistrieri et al., 2007). Yet because microorganisms can facilitate precipitation and sorption of metals (Ferris et al., 1989), and actively absorb some metals (Bruins et al., 2000; Valls and De Lorenzo, 2002), microbially-mediated processes likely also contribute to metal attenuation to some extent. A better understanding of the microbial role in ARD processes is crucial for efforts to predict the fate and transport of metals in the environment and will aid in future remediation efforts. To this end, this dissertation aims to elucidate the biogeochemical processes affecting Cu mobility in ARD.

Among the transition metals, we chose to focus on Cu for several reasons. First, Cu is a nonrenewable resource that makes up a substantial component of industrialized infrastructure. Copper, along with Al, Fe, and Zn, makes up over 95% of the metal mass mined for human consumption (Rauch and Pacyna, 2009). It is the only metal that is mined at a rate (1.5×10^4 Gt Cu yr^{-1}) greater than any natural global flux (Rauch and Pacyna, 2009). Approximately 1.9×10^3 Gt Cu yr^{-1} wasted onto land during production,

and of the Cu that is discarded, approximately 30% is recycled back into production, with the remaining 70% released to the atmosphere, geosphere, and hydrosphere (Rauch and Pacyna, 2009). The ultimate sink for this anthropogenically cycled Cu is the ocean (Rauch and Graedel, 2007), where it is expected to remain in the dissolved form for 6 to 10 thousand years (Vance et al., 2008). Better understanding how Cu is naturally cycled will improve our ability to abate anthropogenic release of Cu to the environment.

The second reason we focused on Cu is because dissolved Cu is common in ARD, with concentrations typically ranging from 10s of μg/L (e.g., Nimick et al., 2003) to 10s of mg/L (e.g. Runkel et al., 2007; Smuda et al., 2007). Extremely acidic environments can have Cu concentrations up to 5 g/L (e.g. Nordstrom et al., 2000). Copper released by sulfide dissolution is responsible for phytotoxicity in soils (Alva et al., 2000) and aquatic toxicity in nearby receiving waters (Schumbauer-Berigan et al., 1993). Furthermore, the toxicity of dissolved Cu to the sensory systems of fish is well known (e.g., Baldwin et al., 2003; Mcintyre et al., 2008).

The third reason for focusing on Cu is that a new tool has been developed for investigating Cu partitioning. Copper isotope measurements are a novel approach to characterize Cu mobility. Precise measurement of Cu isotope ratios is a decade-old technique that has been applied to the fields of geological, biological, and anthropological sciences as a means of tracking Cu through important processes, such as mineral dissolution (Mathur et al., 2005; Asael et al., 2007; Fernandez and Borrok, 2009; Kimball et al., 2009), nutrient uptake (Zhu et al., 2002; Pokrovsky et al., 2008), and primitive tool making and trading (Klein et al., 2009). As the database for the Cu isotope compositions of environmental samples grows, along with measurement of characteristic isotope fractionation between reservoirs, Cu isotope measurements are becoming an increasingly powerful tool for probing the reactivity of Cu during various (bio)geochemical processes.

Finally, Cu is an important nutrient for life, at least partly because it forms strong bonds with many organic molecules (Fraústo Da Silva and Williams, 2001). Neaman et al. (2005b) and (2005a) showed that release of Cu from basalt under oxic conditions was remarkable when compared to other first row transition metals, particularly in the presence of the organic ligands citrate and gallate. Furthermore, while many soils show that mineral-forming elements are depleted in the upper soil profile relative to the parent

rock (e.g., Brantley et al., 2008), Cu has been shown to sometimes be enriched in upper soil profiles where organic carbon contents are greatest (Teutsch et al., 1999; Latrille et al., 2003). The common association of Cu with organic material makes it appropriate for investigating the (bio)geochemical cycling of metals.

Major advances in ARD science can be credited to the development of new techniques. Measurement of stable metal isotope ratios is such a technique. Because the field of Cu isotope (bio)geochemistry is relatively new, Chapter 2 is a review of published Cu isotope research to date. This review describes the methods developed for making precise Cu isotope measurements, synthesizes the data for natural Cu isotope abundances in rocks, sediments, soils, streams, rivers, and the ocean, and discusses the significant experiments that document isotope fractionation between Cu-bearing reservoirs. Particular attention is given to Cu isotope fractionation during redox reactions and sulfide mineral dissolution, as these processes appear to play the most important role in partitioning Cu isotopes in the environment.

The most common Cu-bearing sulfide mineral, and therefore source of Cu, is chalcopyrite ($CuFeS_2$) (Nesse, 2000). Like pyrite, chalcopyrite can be oxidized by O_2 and Fe(III), releasing sulfuric acid, dissolved Fe(II), and dissolved Cu(II). Chapter 3 is a synthesis and meta-analysis of published chalcopyrite dissolution kinetic data. With the synthesized data, we determined empirical rate laws for nonoxidative chalcopyrite dissolution and oxidation of chalcopyrite by Fe(III). This chapter focuses on one of the primary ways in which Cu is released to solution under abiotic conditions.

Chapter 4 is a survey of Cu isotope compositions in primary chalcopyrite and enargite and leached Cu in an AMD-impacted area in southwestern Colorado, USA. My collaborators and I were among the first to measure Cu isotope compositions of both mineral and water samples from an acidic environment. To aid our interpretation of Cu isotope fractionation measured between field samples, we also conducted chalcopyrite and enargite leach experiments in the absence and presence of *A. ferrooxidans*. The fractionation measured between Cu sulfides and leached Cu in biotic laboratory experiments was smaller than abiotic experiments, and is attributed to preferential incorporation of isotopically heavy Cu into *A. ferrooxidans* cells and/or related precipitates. Despite the fact that microorganisms were present in the field, the Cu

isotope fractionation measured between mineral and water samples from the field was more similar to that measured between chalcopyrite and leached Cu in abiotic, as opposed to biotic, laboratory experiments. Mass balance calculations support the likelihood that partitioning of isotopically heavy dissolved Cu into microbial-associated phases is less significant in the open field system compared to the closed laboratory experiments. Chapter 4 adds to the database of Cu isotope compositions in environmental samples and of Cu isotope fractionation factors. This work also provides the framework needed for transition metal isotope (bio)geochemistry to become an effective tool in understanding the cycling of metals through the environment.

Given our hypothesis that Cu associated with *A. ferrooxidans* and/or related precipicates during biotic Cu sulfide leach experiments (Chapter 4), the research described in Chapter 5 explores how dissolved Cu interacts with *A. ferrooxidans*. This chapter describes the use of Transmission Electron Microscopy (TEM) to image *A. ferrooxidans* cells incubated in varying concentrations of dissolved Cu at pH = 2 and 22 ± 2ºC. We also used Energy Dispersive X-ray Spectroscopy (EDS) to probe the chemistry of subcellular and extracellular features, X-ray Fluorescence Microscopy (μ-XRF) to measure the spatial distribution and concentration of Cu within single cells, and Micro-X-ray Diffraction (μ-XRD) to document the formation of jarosite precipitates during *A. ferrooxidans* growth. This chapter defines where Cu is found within cells and quantifies the amount of Cu associated with single, whole cells. We also document the potential for microbially-mediated precipitation of jarosite through nucleation of jarosite aggregates on *A. ferrooxidans* cell surfaces followed by mineral grain growth. Jarosite is an impurity-rich mineral that commonly entrains toxic trace metals, such as Cu, into an insoluble form. Thus, co-precipitation of Cu with jarosite is a process that can remove dissolved Cu from solution at low pH. By providing published bond length information for the probable solid and liquid Cu-bearing phases in these experiments, and considering that heavy isotopes generally prefer to be in the solid in solid-liquid systems, we argue that preferential incorporation of heavy Cu into jarosite likely caused the differences between abiotic and biotic Cu isotope fractionation observed previously (Chapter 4).

Based on the survey of Cu isotope fractionation factors presented in Chapter 2, abiotic leaching of Cu sulfide minerals produces greater fractionation between the

leachate and minerals during slower leaching than during faster leaching. Thus, an alternative hypothesis for the different abiotic and biotic Cu isotope fractionation observed in Chapter 4 is that the smaller biotic fractionation resulted from faster leaching, which we would expect from the catalytic effects of microbial leaching. The experiments described in Chapter 4 have similar abiotic and biotic leaching rates, however. Using the methods described in Chapter 3 to calculate dissolution rate, the logarithm of the surface area normalized rate for chalcopyrite dissolution was -7.5 for both abiotic and biotic experiments. The logarithm of the surface area normalized rate for enargite dissolution was -9.9 for the abiotic experiment and -9.6 for the biotic experiment. Because the abiotic and biotic rates are the same order of magnitude in these experiments, differing leach rates likely cannot explain the different observed abiotic and biotic Cu isotope fractionation. Instead, we favor the hypothesis that preferential co-precipitation of isotopically heavy Cu with jarosite in biotic experiments caused the remaining Cu in solution to be isotopically depleted relative to abiotoic leachates.

Given that Cu isotope fractionation between leachates and minerals was smaller in experiments with jarosite (and cells) than in experiments without jarosite (abiotic), it follows from our hypothesis that the large Cu isotope fractionation measured between minerals and leachates in the field suggests that no jarosite precipitated in the field. While thermodynamic calculations revealed that the stream was highly supersaturated with respect to jarosite (Chapter 4), the pH of the stream ($2.6 \leq pH \leq 5.2$) was above the pH (2.5) that jarosite generally precipitates (Bigham et al., 1996). Further study of the Cu isotope composition of trace Cu in jarosite is needed to verify our hypothesis.

In summary, this research utilizes kinetic data, Cu isotope measurements, and microscopic and spectroscopic techniques to characterize some of the chemical and microbiological processes affecting Cu cycling in ARD. The determination of rate laws for chalcopyrite dissolution in acidic solutions, the novel use of Cu isotope measurements to characterize abiotic and biotic sulfide dissolution, and the characterization of Cu interaction with acidophilic microbial cells and jarosite precipitates have implications for hydrometallurgical recovery of Cu, remediation of Cu in contaminated environments, and biosignatures of microbial Fe-oxidation on Earth and Mars.

References

Alva A. K., Huang B., and Paramasivam S. (2000) Soil pH affects copper fractionation and phytotoxicity. *Soil Science Society of America Journal* **64**, 955-962.

Baker B. J. and Banfield J. F. (2003) Microbial communities in acid mine drainage. *FEMS Microbiology Ecology* **44**, 139-152.

Baldwin D. H., Sandahl J. F., Labenia J. S., and Scholz N. L. (2003) Sublethal effects of copper on Coho salmon: impacts on nonoverlapping receptor pathways in the peripheral olfactory nervous system. *Environmental Toxicology and Chemistry* **22**, 2266-2274.

Balistrieri L. S., Seal R. R. I., Piatak N. M., and Paul B. (2007) Assessing the concentration, speciation, and toxicity of dissolved metals during mixing of acid-mine drainage and ambient river water dowstream of the Elizabeth Copper Mine, Vermont, USA. *Applied Geochemistry* **22**, 930-952.

Bigham J. M., Schwertmann U., Traina S. J., Winland R. L., and Wolf M. (1996) Schwertmannite and the chemical modeling of iron in acid sulfate waters. *Geochimica Cosmochimica Acta* **60**(12), 2111-2121.

Blowes D. W., Ptacek C. J., Jambor J. L., and Weisener C. G. (2003) The Geochemistry of Acid Mine Drainage. In *Treatise on Geochemistry*, Vol. 9 (ed. H. D. Holland and K. K. Turekian), pp. 149-204. Elsevier.

Bond P. L. and Banfield J. F. (2001) Design and performance of rRNA targeted oligonucleotide probes for *in situ* detection and phylogenetic identification of microorganisms inhabiting acid mine drainage environments. *Microbial Ecology* **41**, 149-161.

Brantley S. L., Bandstra J., Moore J., and White A. F. (2008) Modelling chemical depletion profiles in regolith. *Geoderma* **145**(3-4), 494-504.

Bruins M. R., Kapil S., and Oehme F. W. (2000) Microbial resistance to metals in the environment. *Ecotoxicology and Environmental Safety* **45**, 198-207.

Fein J. B., Daughney C. J., Yee N., and Davis T. A. (1997) A chemical equilibrium model for metal adsorption onto bacterial surfaces. *Geochimica et Cosmochimica Acta* **61**(16), 3319-3328.

Ferris F. G., Schultze S., Witten T. C., Fyfe W. S., and Beveridge T. J. (1989) Metal interactions with microbial biofilms in acidic and neutral pH environments. *Applied and Environmental Microbiology* **55**(5), 1249-1256.

Fowle D. A. and Fein J. B. (2001) Quantifying the effects of *Bacillus subtilis* cell walls on the precipitation of copper hydroxide from aqueous solution. *Geomicrobiology journal* **18**, 77-91.

Fraústo da Silva J. J. R. and Williams R. J. (2001) *The biological chemistry of the elements*. Oxford University Press.

Johnson D. B. (1998) Biodiversity and ecology of acidophilic microorganisms. *FEMS Microbiology Ecology* **27**, 307-317.

Johnson K. J., Szymanowski J. E. S., Borrok D. M., Huynh T. Q., and Fein J. B. (2007) Proton and metal adsorption onto bacterial consortia: Stability constants for metal-bacterial surface complexes. *Chemical Geology* **239**, 13-26.

Klein S., Domergue C., Lahaye Y., Brey G. P., and von Kaenel H.-M. (2009) The lead and copper isotopic composition of copper ores from the Sierra Morena (Spain). *Journal of Iberian Geology* **35**, 59-68.

Kleinmann R. L. P. (1989) Acid mine drainage in the United States--Controlling the impact on streams and rivers. *4th World Congress on the Conservation of the Built and Natural Environments*, 1-10.

Latrille C., Denaix L., and Lamy I. (2003) Interaction of copper and zinc with allophane and organic matter in the B horizon of an Andosol. *European Journal of Soil Science* **54**, 357-364.

McIntyre J. K., Baldwin D. H., Meador J. P., and Scholz N. L. (2008) Chemosensory deprivation in juvenile Coho salmon exposed to dissolved copper under varying water chemistry conditions. *Environmental Science and Technology* **42**, 1352-1358.

Neaman A., Chorover J., and Brantley S. L. (2005a) Element mobility patterns record organic ligands in soils on early Earth. *Geology* **33**(2), 117-120.

Neaman A., Chorover J., and Brantley S. L. (2005b) Implications of the evolution of organic acid moieties for basalt weathering over geological time. *American Journal of Science* **305**, 147-185.

Nesse W. D. (2000) *Introduction to Mineralogy*. Oxford University Press.

Nimick D. A., Gammons C. H., Cleasby T. E., Madison J. P., Skaar D., and Brick C. M. (2003) Diel cycles in dissolved metal concentrations in streams: Occurence and possible causes. *Water Resources Research* **39**(9), 1247-1263.

Nordstrom D. K. and Alpers C. N. (1999) Geochemistry of Acid Mine Waters. In *Reviews in Economic Geology*, Vol. 6A (ed. G. S. Plumblee and M. J. Logsdon), pp. 133-160. Society of Economic Geologists, Inc.

Nordstrom D. K., Alpers C. N., Ptacek C. J., and Blowes D. W. (2000) Negative pH and extremely acidic mine waters from Iron Mountain, California. *Environmental Science and Technology* **34**, 254-258.

Nordstrom D. K. and Southam G. (1997) Geomicrobiology of sulfide mineral oxidation. *Reviews in Mineralogy and Geochemistry* **35**, 361-390.

Olson G. J. (1991) Rate of pyrite bioleaching by *Thiobacillus ferrooxidans*: Results of an interlaboratory comparison. *Applied and Environmental Microbiology* **57**(3), 642-644.

Paulson A. J. and Balistrieri L. (1999) Modeling removal of Cd, Cu, Pb, and Zn in acidic groundwater during neutralization by ambient surface waters and groundwaters. *Environmental Science and Technology* **33**, 3850-3856.

Rauch J. N. and Graedel T. E. (2007) Earth's anthrobiogeochemical copper cycle. *Global Biogeochemical Cycles* **21**, GB2010.

Rauch J. N. and Pacyna J. M. (2009) Earth's global Ag, Al, Cr, Cu, Fe, Ni, Pb, and Zn cycles. *Global Biogeochemical Cycles* **23**, GB2001.

Rodríguez Y., Ballester A., Blazquez M. L., González F., and Muñoz J. A. (2003) Study of bacterial attachment during the bioleaching of pyrite, chalcopyrite, and sphalerite. *Geomicrobiology Journal* **20**, 131-141.

Runkel R. L., Kimball B. A., Walton-Day K., and Verplank P. L. (2007) A simulation-based approach for estimating premining water quality: Red Mountain Creek, Colorado. *Applied Geochemistrty* **22**, 1899-1918.

Schumbauer-Berigan M. K., Dierkes J. R., Monson P. D., and Ankley G. T. (1993) pH-dependent toxicity of Cd, Cu, Ni, Pb, and Zn to *Ceriodaphnia dubia, Pimephales promelas, Hayalella azteca* and *Lumbriculus variegatus*. *Environmental Toxicology and Chemistry* **12**, 1261-1266.

Schwertmann U. and Fitzpatrick R. (1992) Iron Minerals in Surface Environments. In *Biomineralization: Processes of Iron and Manganese: Modern and Ancient Environments* (ed. H. Skinner and R. Fitzpatrick), pp. 7-30. Catena Verlag.

Smith K. S. and Huyck H. L. O. (1999) An overview of the abundance, relative mobility, bioavailability, and human toxicity of metals. In *The Environmental Geochemistry of Mineral Deposits*, Vol. 6A (ed. G. S. Plumblee and M. J. Logsdon), pp. 29-70. Society of Economic Geologists, Inc.

Smuda J., Dold B., Friese K., Morgenstern P., and Glaesser W. (2007) Mineralogical and geochemical study of element mobility at the sulfide-rich Excelsior waste rock dump from the polymetallic Zn-Pb-(Ag-Bi-Cu) deposit, Cerro de Pasco, Peru. *Journal of Geochemical Exploration* **92**, 97-110.

Teutsch N., Erel Y., Halicz L., and Chadwick O. A. (1999) The influence of rainfall on metal concentration and behavior in the soil. *Geochimica et Cosmochimica Acta* **63**, 3499-3511.

Tributsch H. (2001) Direct versus indirect bioleaching. *Hydrometallurgy* **59**, 177-185.

Valls M. and de Lorenzo V. (2002) Exploiting the genetic and biochemical capacities of bacteria for the remediation of heavy metal pollution. *FEMS Microbiology Reviews* **26**, 327-338.

Vance D., Archer C., Bermin J., Perkins J., Statham P. J., Lohan M. C., Ellwood M. J., and Mills R. A. (2008) The copper isotope geochemistry of rivers and the oceans. *Earth and Planetary Science Letters* **274**, 204-213.

Chapter 2
A Review of Copper Isotope (Bio)Geochemistry

2.0. Abstract

The field of Cu isotope biogeochemistry has experienced rapid growth over the past decade due to the advent of multi-collector inductively coupled plasma mass spectrometry (MC-ICP-MS). Early studies focused on measuring the Cu isotope composition of primary Cu(I)-sulfide and secondary Cu(I)/(II) ore minerals. To date, the $\delta^{65}Cu$ values [where $\delta^{65}Cu = (({}^{65}Cu/{}^{63}Cu)_{sample}/({}^{65}Cu/{}^{63}Cu)_{NIST\ 976}) - 1) \times 10^3$] of Cu(I)-sulfide minerals reported in the literature average 0.13 ± 0.94‰ (1σ; n = 561), which is slightly isotopically depleted in ^{65}Cu relative to the average of secondary Cu(I)/(II) minerals (0.26 ± 0.64‰; n = 172). Secondary Cu(I)/(II) minerals display the largest range in isotopic composition ($\Delta^{65}Cu$ = 12‰) among the transition metals contained in environmental samples. Until recently, no Cu isotope measurements existed for natural waters. The average $\delta^{65}Cu$ values reported for water samples increase in the following order: large rivers (0.66 ± 0.34‰; n = 30) < seawater (1.09 ± 0.20‰; n = 25) < acid mine drainage (AMD)-impaced streamwater (1.54 ± 0.14‰; n = 50). Based on many experiments that show enrichment of aqueous Cu(II) in ^{65}Cu realtive to aqueous and solid Cu(I) phases, enrichment of AMD-impacted streams, rivers, and the ocean in ^{65}Cu relative to Cu-bearing minerals is best explained by a redox isotope effect, whereby isotopically heavy Cu(I) in sulfide minerals preferentially oxidizes to Cu(II), which is then released to solution. Alternatively, published experiments show that relatively ^{65}Cu-depleted Cu is preferentially precipitated as Cu(I)-sulfide in reducing environments, causing remaining aqueous Cu(II) to be relatively enriched in ^{65}Cu. Copper isotope fractionation due to a redox isotope effect (up to $\Delta^{65}Cu$ = 4‰) can be overprinted by additional isotope effects identified for Cu-related processes. These include kinetic, biological, and ligand-exchange isotope effects, which, in combination, may account for the large variation in Cu isotope abundances in environmental samples.

2.1. Introduction

Copper is the only metal that is mined at a rate (1.4×10^4 Gt Cu yr^{-1}) greater than it is naturally transported through the geosphere, hydrosphere, and biosphere (Rauch and Pacyna, 2009). Approximately 1.9×10^3 Gt Cu yr^{-1} is wasted onto land during production, and of the Cu currently in use by humans (3.5×10^5 Gg Cu), 70% is released to the environment (Rauch and Pacyna, 2009). The ultimate sink for this anthropogenically cycled Cu is the ocean (Rauch and Graedel, 2007). Better understanding how Cu is naturally cycled will improve our ability to abate anthropogenic release of Cu. Measurement of Cu isotope ratios is a relatively new technique that can be applied to characterizing Cu mobility. Differences in the Cu isotope composition between reactants and products can provide insight into the mechanisms by which reactions proceed.

Two stable Cu isotopes exist: masses 63 (69.174% abundance) and 65 (30.826% abundance). Copper displays the largest range in isotopic composition ($\Delta^{65}Cu = 12‰$) among the transition metals contained in environmental samples. This range is well outside analytical uncertainty when measured using multiple collector inductively coupled plasma mass spectrometry (MC-ICP-MS). For example, in seminal work on precise Cu isotope measurements, Maréchal et al. (1999) achieved a $\pm 2\sigma$ reproducibility of 0.04‰ using MC-ICP-MS. The large isotopic variation in environmental samples and the growing capability to measure $^{65}Cu/^{63}Cu$ precisely makes this isotope system a prime candidate for addressing questions about metal mobility in the environment.

In this work, we review the advances made in Cu isotope (bio)geochemistry over the last decade. These advances were made possible by the development of MC-ICP-MS, as well as innovative sample preparation techniques. We review early Cu isotope work and method development, as well as survey the Cu isotope composition of Earth samples. The reader is directed to Luck et al. (2003) for the Cu isotope composition of the four main groups of carbonaceous chondrites. We also review experimental Cu isotope fractionation during various abiotic and biotic processes, and discuss the possible isotope effects that cause the observed fractionation. We synthesize experimental work in an effort to explain the observed natural Cu isotope variability on Earth.

2.2. Standards and Notation

The field of Cu isotope chemistry relies upon one isotopic standard reference material: the NIST 976 Cu metal. This reference sample of commercial Cu rods has a certified $^{65}Cu/^{63}Cu$ value of 0.4456 ± 4 as measured by thermal ionization mass spectrometry (TIMS) (Shields et al., 1964) and calibration against high-purity Cu isotope separates of known $^{65}Cu/^{63}Cu$ (Maréchal et al., 1999). Nearly every Cu isotope study conducted thus far reports isotopic compositions as the following:

$$\delta^{65}Cu(‰) = \left[\left(\frac{^{65}Cu/^{63}Cu_{sample}}{^{65}Cu/^{63}Cu_{NIST976}}\right) - 1\right] \text{ x } 1000 \qquad (2.1)$$

Samples with positive $\delta^{65}Cu$ values indicate enrichment in ^{65}Cu relative to the standard, and negative $\delta^{65}Cu$ values indicate depletion in ^{65}Cu relative to the standard. Isotopic fractionation refers to measured differences in the isotopic composition between two samples. Isotope fractionation ($\Delta^{65}Cu_{A\text{-}B}$) is calculated by the following:

$$\Delta^{65}Cu_{A\text{-}B} = \delta^{65}Cu_A - \delta^{65}Cu_B \qquad (2.2)$$

where subscripts A and B refer to different reservoirs. Positive $\Delta^{65}Cu_{A\text{-}B}$ values indicate that reservoir A is enriched in ^{65}Cu relative to reservoir B.

At this time, there is no convention for the reporting of uncertainty in $\delta^{65}Cu$ measurements. Some studies report $\delta^{65}Cu$ values with the accompanying 2σ uncertainty determined for replicate measurements of samples, as well as the 2σ for the long-term uncertainty for many NIST 976 Cu measurements for a given instrument. Others report the long-term instrumental 2σ only. As a result, in this work, most $\Delta^{65}Cu_{A\text{-}B}$ values are reported as $\Delta^{65}Cu_{A\text{-}B}$ ± s.d.‰, where s.d. represents the standard deviation for replicate $\delta^{65}Cu$ measurements and $\Delta^{65}Cu_{A\text{-}B}$ calculations. For those experiments where only the long-term instrumental 2σ was reported, we present $\Delta^{65}Cu_{A\text{-}B}$ ± 2σ‰, where 2σ represents the long-term instrumental 2σ propagated through equation 2.2.

2.3. Early Cu Isotope Work

Shields et al. (1965) conducted the first significant exploration of Cu isotope variations in natural materials. Using TIMS, the authors measured the Cu isotope

composition of minerals and compared them to the reference material that later became the NIST 976 standard. Copper was separated from samples of primary ore minerals, secondary ore minerals, oxides, sulfates, native Cu and other Cu-bearing minerals using an acid digestion and electrodeposition technique (Shields et al., 1965). The δ^{65}Cu values of the samples range from -3.3 to 9.1‰. Generally, this study reveals that secondary ore minerals (including bornite, chalcocite, Cu oxides, and Cu carbonates) show a wider variation in isotopic abundance than the primary ore mineral chalcopyrite. Samples of primary ore were reported to not differ from the reference sample beyond analytical uncertainty.

The analytical precision of these early measurements was relatively poor (± 1.5%). This may be due, in part, to the difficulty in using TIMS to analyze elements, including metals, with high ionization potential. Such elements are better ionized using plasma-source methods. Traditional single-collector ICP-MS has been applied to measure stable metal isotope ratios by scanning single ion beams over a small mass range sequentially at high speed (Halliday et al., 1998). This method produces poor peak shape and counting statistics, however (Maréchal and Albarède, 2002). To overcome these problems, as well as the problem of plasma instability, plasma-source magnetic sector mass spectrometers, capable of making simultaneous measurements of multiple ion beams, were developed (Halliday et al., 1998). Thus, major advances in Cu isotope geochemistry did not occur following the Sheilds et al. (1965) study until the advent of the first MC-ICP-MS: the Plasma 54 (VG Elemental). This model was later succeeded by the Micromass IsoProbe, the Nu Instruments Nu Plasma, the ThermoElemental Axiom, and the Thermo Scientific Neptune.

2.4. Development of Plasma-Source Methodologies

2.4.1. Sample Preparation

The purification of Cu from sample matrices using ion exchange chromatography (IEC) reduces the potential for isobaric interferences and matrix effects during measurement of Cu isotope ratios using MC-ICP-MS. Maréchal et al. (1999) were the first to present a method for purifying Cu from environmental samples. Their Cu purification method involves passing acid-digested samples through a strongly basic

anion exchange resin (AG MP-1; Bio Rad®) in 7N HCl. Copper isotope fractionation during IEC is as much as 0.46‰ in 7N HCl (Table 2.1, Maréchal and Albarède, 2002), due to preferential elution of ^{65}Cu. As long as 100% of the original Cu in the sample is recovered during IEC, the isotopic composition of the sample will be preserved.

The Maréchal et al. (1999) purification technique, with little modification, has been used by many researchers to separate Cu from minerals. In order to separate Cu from environmental water samples, however, the technique was significantly modified. Copper in streamwater and seawater can have low trace metal content and high major element content. This requires the processing of large (liters) sample volumes and is subject to external contamination and/or sample impurities (Bermin et al., 2006). The presence of Na in seawater samples can be particularly problematic for Cu isotope measurements because of the $^{40}Ar^{23}Na$ isobar for ^{63}Cu. These obstacles have been overcome by using a larger chromatographic column and a higher volume of resin, and by concentrating Cu from dilute samples. Copper can be concentrated from seawater samples by running samples combined with moderate pH (5-5.5) ammonium acetate solutions through the column, which elutes major elements, followed by elution of metals with low pH solutions (Bermin et al., 2006). The collected metals can then be processed through a second chromatographic column, which yields concentrated Cu with acceptable purity (Bermin et al., 2006). Yet another method for concentrating Cu involves co-precipitating metals from the sample solution by adding $Mg(OH)_2$, acid digesting the precipitates, and then running the digestates through IEC (Bermin et al., 2006). Because Cu can be fractionated at each step, care must be taken to ensure 100% Cu yield through the concentration and separation processes.

To address sample impurity issues associated with river water, Archer and Vance (2004) modified the Maréchal et al. method for Cu separation by reducing the chromatography column size, thereby reducing the resin and eluant acid volume and sample size. The result was a decrease in the concentrations of contaminants in procedural blanks, and the ability to elute Fe, in addition to Cu, from the same sample. Borrok et al. (2007) further modified this separation technique by keeping the same smaller chromatography column geometry and tuning the eluant hydrochoric acid strengths to control the Fe, Cu, and Zn speciation, and therefore, timing of elution. This

allowed elution of Fe, followed by Cu, and then Zn, in separates of high purity, to be extracted from one sample with a single pass through the column. This technique was used succesfully to separate Fe, Cu, and/or Zn from acidic, metal-rich mine drainage (Borrok et al., 2007; Balistrieri et al., 2008; Borrok et al., 2008a; Kimball et al., 2009).

2.4.2. Isotope Ratio Measurement

Multi-collector ICP-MS instruments are ideal for measuring metal isotope ratios because of their high ionization efficiency and nearly constant instrumental mass bias (Albarède and Beard, 2004). Mass bias can be corrected by standard-sample-standard bracketing, or by doping samples and standards with a similar-sized element of known isotopic composition, then observing the instrument mass bias of the dopant (Albarède and Beard, 2004). For example, Maréchal et al. (1999) developed an inter-element standardization technique for Cu isotope measurements, whereby samples and the NIST 976 Cu standard were doped with the Johnson-Mattey Zn solution, which has a known isotopic composition. The mass bias of Zn isotopes during the analytical session was then used to correct that for Cu isotopes using an exponential law (Maréchal et al., 1999):

$$r = R\left(\frac{M_2}{M_1}\right)^f \tag{2.3}$$

where r is the isotope ratio ($^{65}Cu/^{63}Cu$) for the element of interest measured by mass spectrometry, M_2 and M_1 are the masses of the less abundant and more abundant nuclides, respectively, R is the true isotopic ratio (M_2/M_1), and f is the mass fractionation coefficient determined for Zn isotope fractionation. The inherent assumption for this calculation is that the instrument will discriminate against Zn and Cu isotopes similarly.

2.5. Copper Isotope Variation in Environmental Samples

2.5.1. Ore Minerals

Copper ore minerals can be separated into two groups: those that form in the *hypogene* environment and those that form in the *supergene* environment (Fig. 2.1). The term hypogene implies that primary mineralization occurred as a result of ascending or cooling hydrothermal solutions that precipitated pyrite and the common Cu-bearing sulfide mineral chalcopyrite ($CuFeS_2$) (Robb, 2005). Bornite (Cu_5FeS_4) and chalcocite

(Cu_2S) may also be found in hypogene environments. When hypogene minerals are exhumed and exposed to weathering, they oxidize and hydrolyze, and the leachates percolate through the vadose zone. Under oxidizing conditions, the percolating solutions may precipitate Cu oxide minerals, including cuprite (Cu_2O) and tenorite (CuO) and/or carbonate minerals, such as malachite ($Cu_2(OH)_2CO_3$) and azurite ($Cu_3(OH)_2(CO_3)_2$) (Robb, 2005). When percolating solutions reach the water table, where reducing conditions exist, the secondary sulfides bornite, chalcocite, and covellite (CuS) may precipitate. The oxidized and reduced Cu minerals that form from percolating solutions are supergene minerals (Fig. 2.1). Copper sulfides can be found as primary minerals in hypogene deposits and secondary minerals in supergene deposits, but Cu oxides, carbonates, and silicates, such as chrysocolla ($(Cu,Al)_2H_2Si_2O_5(OH)_4 \cdot n(H_2O)$), are strictly secondary minerals found in supergene deposits. Many of the Cu isotope studies conducted thus far report the isotopic composition of Cu minerals from hypogene and supergene environments.

Copper ores can also be found in sedimentary environments. As described by Asael et al. (2009), they form when weathered and eroded clastic sediments containing Cu-bearing igneous rocks further weather under suboxic to oxic conditions, releasing Cu-rich solutions. These solutions eventually circulate into relatively anoxic, pyritiferous or organic-rich sediments and precipitate Cu sulfides, the type commonly found in supergene deposits. These Cu sulfides may then become re-oxidized, releasing acidic solutions that can leach surrounding host rocks and eventually precipitate Cu(II)-bearing secondary minerals such as malachite, chrysocolla, and paratacamite ($(Cu,Zn)_2(OH)_3Cl$).

The $\delta^{65}Cu$ values for primary chalcopyrite and primary/secondary Cu(I)-sulfides span about 9‰, with a mean of 0.13 ± 0.94‰ (1σ) (Maréchal et al., 1999; Zhu et al., 2000; Jiang et al., 2002; Larson et al., 2003; Graham et al., 2004; Rouxel et al., 2004; Mason et al., 2005; Mathur et al., 2005; Markl et al., 2006; Asael et al., 2007; Maher and Larson, 2007; Asael et al., 2009; Kimball et al., 2009; Klein et al., 2009; Mathur et al., 2009). Roughly 80% of the reported values for primary chalcopyrite and primary/secondary Cu(I)-sulfides lie between -0.5‰ and 1‰ (Fig. 2.2). Considering chalcopyrite alone, roughly 94% of the $\delta^{65}Cu$ values lie between -1‰ and 1‰, with a mean of 0.26 ± 0.64‰ (1σ). In general, the Cu isotope composition of primary

chalcopyrite and primary/secondary Cu(I)-sulfides is similar to the NIST 976 Cu standard (Fig. 2.2).

As originally reported in the early Shields et al. (1965) study, secondary Cu minerals, including native Cu, bornite, chalcocite, covellite, malachite, azurite, chrysocolla, tenorite, and cuprite, display a greater Cu isotope variability than primary minerals. The δ^{65}Cu values for secondary minerals span 11.5‰, with a mean of 0.52 ± 1.38‰ (1σ) (Maréchal et al., 1999; Zhu et al., 2000; Larson et al., 2003; Rouxel et al., 2004; Mathur et al., 2005; Markl et al., 2006; Asael et al., 2007; Maher and Larson, 2007; Asael et al., 2009; Klein et al., 2009; Mathur et al., 2009). Most of the reported δ^{65}Cu values (98%) lie between -2‰ and 4‰ (Fig. 2.2). In general, secondary Cu minerals are isotopically enriched in ^{65}Cu relative to primary minerals.

2.5.2. Sediments

Maréchal et al. (1999) measured the Cu isotope composition of marine sediments in the Atlantic Ocean and Mediterranean Sea. The δ^{65}Cu values range from -0.9 to 0.35‰. In contrast, carbon-rich black shales from the 2.7 Ga Belingwe Belt, Zimbabwe, exhibit a δ^{65}Cu of -1.0‰ (Archer and Vance, 2002). These shales have been linked to past sulfate-reducing microbial communities (Archer and Vance, 2002).

2.5.3. Soils

Preliminary measurements of the Cu isotope composition of different soil types show values of 0 ± 1‰, with soil profile gradients varying by up to 1‰ (Bigalke et al., 2009). Additional measurements of Cu in ridgetop soils developed on black shale show δ^{65}Cu values between -0.5‰ and -1‰ in the top 30 – 60 cm of the soil profile, with δ^{65}Cu values increasing with depth toward the parent rock value near 0‰ (Mathur et al., unpublished results). In soils developed on black shale in the valley floor, the δ^{65}Cu values are near -0.5‰ throughout the 0 – 85 cm depth profile (Mathur et al., unpublished results). These weathered samples are depleted in ^{65}Cu relative to the parent rock (δ^{65}Cu ≈ 0‰) (Mathur et al., unpublished results).

2.5.4. Streamwater and Rivers

The δ^{65}Cu values for major world rivers range from 0.02‰ – 1.45‰, with a mean of 0.66 ± 0.34‰ (1σ) (Fig. 2.2)(Vance et al., 2008). In general, the rivers with higher Cu concentration tend to have δ^{65}Cu values closer to 0‰ (Vance et al., 2008). Until recently, little was known about the Cu isotope composition of streams affected by acid mine drainage (AMD). In this dissertation, I report δ^{65}Cu values for AMD-impacted streamwater ranging from 1.28 – 1.79 ± 0.10 (Chapter 4). These values, considered with other recently reported δ^{65}Cu values for AMD streamwater, display a range from -1.01 – 1.79‰ (Balistrieri et al., 2008; Borrok et al., 2008a; Kimball et al., 2009). The data are bimodally distributed, with populations described by means of -0.59 ± 0.27‰ (1σ) and 1.54 ± 0.14‰ (1σ) (Fig. 2.2). Within a single AMD-impacted stream, δ^{65}Cu values do not change over the course of a day (Borrok et al., 2008a) or from upstream to sites that were approximately 1 km downstream (Chapter 4, Kimball et al., 2009).

2.5.5. Seawater

Bermin et al. (2006) were the first to develop a method for measuring the Cu isotope composition of seawater. Their data set includes sea surface measurements of the English Channel and the Southern Pacific Ocean, a depth profile of the Indian Ocean, and two depth profiles of the Northeast Pacific Ocean (Vance et al., 2008). Seawater δ^{65}Cu values range from 0.51‰ – 1.44‰, with a mean of 1.09 ± 0.20‰ (Vance et al., 2008). Most of the reported data (88%) lie between 0.90‰ and 1.30‰ (Fig. 2.2). The seawater depth profiles show that Cu concentrations increase with depth, with no corresponding trend in the δ^{65}Cu values (Vance et al., 2008). These authors also measured the Cu isotope composition of water and particulate matter from two small estuaries in Southeast England and found that the dissolved δ^{65}Cu values averaged 0.65 ± 0.09‰ and particulate δ^{65}Cu values averaged -0.47 ± 0.22‰. The isotopic composition of seawater corresponds to the higher end of that in river water, suggesting that an additional source of Cu, that is isotopically heavier than river water, enters the ocean reservoir (Vance et al., 2008). Alternatively, sorption of dissolved Cu depleted in ^{65}Cu to particulate matter, as observed in estuarine samples, drives residual dissolved Cu to become enriched in ^{65}Cu (Vance et al., 2008).

2.5.6. Biological Material

Copper contained in mussel tissue ($\delta^{65}Cu = 0.08 \pm 0.04‰$) and human blood ($\delta^{65}Cu = 0.30 \pm 0.04‰$) is enriched in ^{65}Cu relative to the Cu standard (Maréchal et al., 1999). Likewise, Cu in octopus haemocyanin has a $\delta^{65}Cu$ value of $0.62 \pm 0.05‰$ (Zhu et al., 2002).

2.6 Experimental Cu Isotope Fractionation

2.6.1 Fractionation among Aqueous Species

Both Zhu et al. (2002) and Maréchal and Albarède (2002) experimented with Cu isotope fractionation during IEC with the AG MP-1 resin. Zhu et al. (2002) used 6M HCl solutions as eluant and found that the $\delta^{65}Cu$ value for the initial eluted Cu was about 6‰. The eluted $\delta^{65}Cu$ values steadily decreased to -8.0‰ during chromatography. Likewise, the $\delta^{65}Cu$ values for the NIST 976 Cu standard eluted in 3M HCl and 7M HCl decreased from 12.6‰ to -11.7‰ and from about 3‰ to -6‰, respectively (Maréchal and Albarède, 2002). This trend of decreasing $\delta^{65}Cu$ values for eluted Cu during chromatography was also found for a chalcopyrite sample in 7M HCl (Maréchal and Albarède, 2002). Fractionation of Cu isotopes in these experiments is reported in Table 2.1 and shown graphically in Figure 2.3. The experimental results were attributed to equilibrium fractionation resulting from reaction among Cu-chloro complexes in solution (Zhu et al., 2002), and the preferential retention of ^{63}Cu by the resin. These results are important for isotopic sample preparation, and support the need to verify 100% Cu yield through chromatographic columns.

2.6.2. Mineral Precipitation

Maréchal and Sheppard (2002) experimented with malachite precipitation from $Cu(NO_3)_2$ and $CuCl_2$ solutions at 30°C and measured fractionation between aqueous and precipitated Cu ($\Delta^{65}Cu_{aq\text{-}min}$) of $0.20 \pm 0.06‰$ (2σ) and $0.38 \pm 0.06‰$, respectively (Table 2.1; Fig. 2.3). The $\Delta^{65}Cu_{aq\text{-}min}$ values were slightly lower ($0.17 \pm 0.06‰$ and $0.31 \pm 0.06‰$) for precipitation from $Cu(NO_3)_2$ and $CuCl_2$ solutions, respectively, at 50°C. As will be seen in the next section, fractionation resulting from precipitation of Cu without a

redox transition is smaller than fractionation due to Cu precipitation accompanied by reduction of aqueous Cu(II) to solid Cu(I).

2.6.3. Redox Processes

Transition metals are oxidized and reduced through a complex array of reactions. To explore the potential for fractionation during reduction of Cu(II), Zhu et al. (2002) precipitated CuI_{solid} from a Cu(II)- and I(-I)-bearing solution at room temperature. Despite different reaction rates, each experiment revealed fractionation between reactant aqueous Cu(II) and product solid Cu(I)I ($\Delta^{65}Cu_{aq\text{-}solid}$) of about 4.03 ± 0.06‰ (2σ) (Table 2.1; Fig. 2.3), reflecting preferential precipitation of ^{63}Cu (Zhu et al., 2002).

A more environmentally relevant redox process is the precipitation of Cu sulfide minerals. Ehrlich et al. (2004) studied the abiotic precipitation of covellite (CuS) from a Cu(II)-bearing solution under anoxic conditions. The average fractionation of seven experiments conducted at 20°C between aqueous Cu(II) and solid Cu(I)S ($\Delta^{65}Cu_{aq\text{-}min}$) was 3.06 ± 0.15‰ (s.d.) (Table 2.1; Fig. 2.3). At 40°C, the $\Delta^{65}Cu_{aq\text{-}min}$ value was 2.72 ± 0.03‰, and at 2°C the $\Delta^{65}Cu_{aq\text{-}min}$ value was 3.47 ± 0.04‰ (Ehrlich et al., 2004). Copper in precipitated covellite was isotopically depleted in ^{65}Cu relative to aqueous Cu(II). In experiments where dissolved Cu(II) was reacted with pyrrhotite ($Fe_{(1-x)}S$) and pyrite (FeS_2) under anoxic conditions, forming chalcopyrite, covellite, and chalcocite, Cu(II) remaining in solution after sulfide formation was enriched in ^{65}Cu relative to sulfides by 3.02 ± 0.14‰ (s.d.) (pyrrhotite; 40°C), 2.67 ± 0.15‰ (pyrrhotite, 100°C), 2.66 ± 0.11‰ (pyrite, 40°C), and 2.69 ± 0.16‰ (pyrite, 100°C) (Asael et al., 2006). Both studies revealed that aqueous Cu(II) tends to be enriched in ^{65}Cu relative to Cu(I) precipitated as sulfides.

The experimental results for Cu redox reactions are consistent with Schauble's (2004) statement that bond strength is greater for higher oxidation states of any given element. Given that, at equilibrium, heavier isotopes tend to concentrate in the chemical environment with the strongest bonds (Bigeleisen and Mayer, 1947; Urey, 1947; Criss, 1999; Schauble, 2004), oxidized Cu phases are expected to be enriched in ^{65}Cu relative to reduced Cu phases. Urey's theory of the partitioning of isotopes at equilibrium (1947) shows that fractionation becomes larger at lower temperatures. The Ehrlich (2004) and

Asael (2006)experiments described previously show increasing fractionation at lower temperatures, supporting the hypothesis that fractionation is due, at least in part, to an equilibrium redox effect.

2.6.4. Fractionation During Abiotic Mineral Dissolution

Dissolution of the Cu(I)-bearing minerals chalcopyrite and chalcocite at pH 2.3 and 25°C was shown to result in fractionation between leached Cu and residual mineral ($\Delta^{65}Cu_{aq\text{-}min}$) of 1.36 ± 0.38‰ (s.d.) and 3.03 ± 0.36‰, respectively(Mathur et al., 2005) (Table 2.1; Fig. 2.3). In similar batch experiments, leached Cu was enriched in ^{65}Cu relative to chalcopyrite (1.37 ± 0.40‰; s.d.) and enargite (Cu_3AsS_4) (0.99 ± 0.10‰) (Chapater 4, Kimball et al., 2009) (Table 2.1; Fig. 2.3). Furthermore, Fernandez and Borrok (2009) measured leached Cu enriched in ^{65}Cu relative to chalcopyrite-bearing rock by 2.04‰ during the initial stages of leaching, but over time $\Delta^{65}Cu_{aq\text{-}min}$ values decreased.

Fractionation of Cu isotopes during abiotic Cu sulfide dissolution is attributed to a redox isotope effect, whereby preferential oxidation of $^{65}Cu(I)$ occurs at the interface of the isotopically homogeneous mineral and a surface oxidized layer, followed by faster solubilization of Cu(II) from the surface layer (Chapter 4, Kimball et al., 2009). Fernandez and Borrok (2009) corroborate this effect, and note that the surface oxidized layer, which is enriched in ^{65}Cu, forms by reaction of Cu sulfides with air prior to experimentation. Those workers also report that after transient release of $^{65}Cu(II)$ from the surface layer, $\Delta^{65}Cu_{aq\text{-}min}$ values decrease as the $\delta^{65}Cu$ values of leached Cu decrease to values closer to that of the undissolved mineral. This trend is documented in the relatively large range of $\Delta^{65}Cu_{aq\text{-}min}$ values determined for abiotic chalcopyrite dissolution (Fig. 2.3). This large range results from variable leaching rates. During fast leaching experiments at pH 2, $\Delta^{65}Cu_{aq\text{-}min}$ values initially near 2‰ decreased to 0.12‰ once 3.5% of the chalcopyrite was leached (Fernandez and Borrok, 2009). During leaching at pH 5, $\Delta^{65}Cu_{aq\text{-}min}$ values initially near 2‰ decreased to only 1.5‰ by 3.5% chalcopyrite leached (Fernandez and Borrok, 2009). Decreasing $\Delta^{65}Cu_{aq\text{-}min}$ values (starting at 3.19 ± 0.14‰) over the course of leaching was also observed during chalcocite leaching (Wall et

al., 2009), suggesting that both redox and kinetic isotope effects are responsible for the isotopic composition of aqueous Cu during sulfide leaching.

2.6.5. Fractionation During Biotic Mineral Dissolution

In Cu sulfide leach experiments run in parallel to the abiotic experiments described above, Mathur et al. (2005) and Kimball et al. (Chapter 4) reacted Cu sulfides with a leach medium containing an inoculum of *Acidithiobacillus ferrooxidans*, an Fe- and S-oxidizing Proteobacterium. The resulting Cu isotope fractionation was smaller, with average $\Delta^{65}Cu_{aq\text{-}min}$ values of 0.38 ± 0.25‰ (s.d.) and 0.87 ± 1.14‰ for chalcopyrite and chalcocite, respectively (Mathur et al., 2005), and of -0.57 ± 0.25‰ (s.d.) and 0.15 ± 0.21‰ for chalcopyrite and enargite, respectively (Chapter 4, Kimball et al., 2009) (Table 2.1; Fig. 2.4). When microorganisms were present, the abiotic fractionation signature was most likely not seen due to preferential association of dissolved ^{65}Cu with *A. ferrooxidans* cells (Mathur et al., 2005) or with a combination of cells and related precipitates (Chapter 4, Kimball et al., 2009). This hypothesis is supported by considering that the volume percent inoculum, containing both cells and precipitates, used by Kimball et al. was 200 times that of Mathur et al. The larger inoculum used by Kimball et al. is consistent with greater association of ^{65}Cu with cells/precipitates and lower $\delta^{65}Cu$ for Cu leached from chalcopyrite relative to the Mathur et al. experiments.

2.6.6. Fractionation During Copper Sorption

Recent experiments show that Cu(II) sorbed to ferrihydrite is 0.73 ± 0.08‰ (s.d.) more enriched in ^{65}Cu than aqueous Cu at pH = 3 (Balistrieri et al., 2008). Likewise, Cu(II) sorbed to goethite and gibbsite at pH 4 – 6 was observed to be 0.78 ± 0.2‰ (s.d.) and 1.0 ± 0.25‰ more enriched in ^{65}Cu than aqueous Cu, respectively (Pokrovsky et al., 2008). Clayton et al. (2005) measured a smaller fractionation between aqueous Cu and Cu sorbed to goethite ($\Delta^{65}Cu_{aq\text{-}sorbed}$ = -0.35 ± 0.11‰). Balistrieri et al. (2008) showed that the extent of fractionation among Fe(II), Zn(II), and Cu(II) isotopes was correlated with the intrinsic equilibrium binding constants for metal sorption onto amorphous Fe(III) oxyhydroxides, with Cu exhibiting the greatest fractionation and the greatest

intrinsic equilibrium binding constant. Pokrovsky et al. (2008) used published EXAFS data to argue that preferential sorption of ^{65}Cu onto metal oxides is consistent with strong, bidentate, inner-sphere complexes of tretrahedrally coordinated Cu on metal oxide surfaces.

Formation of Fe (oxyhydr)oxide minerals is common during sulfide dissolution. Sorption of heavy Cu to Fe (oxyhydr)oxide minerals could explain the net fractionation observed following leaching of chalcocite (Fig. 2.5). The net fractionation measured for Cu(I) oxidation to Cu(II) during Cu-sulfide dissolution is smaller than the maximum experimental fractionation measured during a Cu redox transition ($\Delta^{65}Cu_{Cu(II)-Cu(I)}$ = 4‰) (Zhu et al., 2002). Given that others have observed Cu enriched in ^{65}Cu to sorb to Fe (oxyhydr)oxides (Clayton et al., 2005; Balistrieri et al., 2008; Pokrovsky et al., 2008), and that Fe (oxyhydr)oxide minerals could have formed during chalcocite leaching, since Fe-bearing solutions were used (Mathur et al., 2005; Wall et al., 2009), Fe (oxyhydr)oxide minerals could have sorbed heavy dissolved Cu. This would cause the net fractionation to be smaller than 4‰ (Fig. 2.5).

The redox isotope effect, proposed as causing the fractionation measured during the initial stages of Cu-sulfide leaching, appears to be greatest for chalcocite, followed by chalcopyrite, then enargite (Fig. 2.3, 2.5). The smaller net fractionation observed for chalcopyrite and enargite dissolution can be partially explained by preferential sorption of ^{65}Cu to secondary minerals. For example, Fe originally in chalcopyrite may form jarosite (nominally $KFe_3(SO_4)_2(OH)_6$) on chalcopyrite surfaces during dissolution (Parker et al., 2003; Klauber, 2008). Assuming leached Cu is further fractionated by preferential association of ^{65}Cu with jarosite, leached Cu released to solution would not be as isotopically enriched as would be expected from a redox reaction alone. Likewise, common alteration products of enargite dissolution, such as scorodite ($FeAsO_4 \cdot 2H_2O$) and chenevixite ($Cu_2Fe_2(AsO_4)_2(OH)_4 \cdot H_2O$) (Lattanzi et al., 2008), might also sorb ^{65}Cu preferrentially, leaving dissolved Cu in solution less enriched in ^{65}Cu. While sorption of heavy Cu onto secondary minerals may explain the lower net fractionation during chalcocite dissolution, other fractionating processes, in addition to redox and sorption, are needed to explain the net fractionation measured during enargite and chalcopyrite dissolution (Fig. 2.5).

In addition to mineral sorption, Pokrovsky et al. (2008) also experimented with sorption of Cu(II) onto bacteria and algae. They found that irreversible uptake of Cu by algae at pH 7.5 – 8 did not change the isotopic composition of the remaining dissolved Cu. Additionally, no Cu isotope fractionation was observed when Cu adsorbed to aquatic and soil bacteria and diatoms at pH 4 – 8 ($\Delta^{65}Cu_{aq\text{-}sorbed}$ = -0.05 ± 0.02‰; s.d.) (Table 2.1; Fig. 2.4), even with variable surface loading and experiment duration. In contrast, Cu adsorbed to the soil bacterium *Pseudomonas aureofaciens* at pH 1.8 – 3.5 was depleted in ^{65}Cu relative to solution by 1.16 ± 0.39‰ (Table 2.1; Fig. 2.4) (Pokrovsky et al., 2008). The authors argue that at near neutral pH, Cu was likely bound to carboxyl groups on cell surfaces, and that the bonding environment of Cu in the aqueous phase was similar to that in the sorbed phase, causing $\Delta^{65}Cu_{aq\text{-}sorbed}$ to be near zero. Under acidic conditions, the authors attribute fractionation to outer-sphere, monodentate complexes between Cu and phosphoryl groups on cell surfaces. These complexes are relatively weaker than complexes formed between Cu and aqueous ligands, causing ^{65}Cu to concentrate in the aqueous phase and ^{63}Cu to concentrate in the sorbed phase (Pokrovsky et al., 2008). Thus, the difference in fractionation between neutral and acidic pH is most likely due to differences in the protonation of functional groups on cell surfaces at the different pH conditions.

2.6.7. Fractionation During Biological Uptake

Zhu et al. (2002) grew *E. coli* and *P. aeruginosa* in $Cu(NO_3)_2$ solutions and found that Cu within the protein azurin was depleted in ^{65}Cu relative to remaining dissolved Cu by 1.53 ± 0.07‰ (2σ) and 0.98 ± 0.07‰, respectively (Table 2.1; Fig. 2.4). Likewise, Cu taken up by yeast in metallothionen and Cu-Zn superoxide dismutase was depleted in ^{65}Cu relative to $Cu(SO_4)$ in solution by 1.71 ± 0.07‰ and 1.18 ± 0.07‰, respectively (Zhu et al., 2002) (Table 2.1; Fig. 2.4). Incorporation of isotopically light elements into proteins is commonly observed in more traditional isotope systems (e.g. Hayes, 2001), and is ascribed to a vital isotope effect.

Mathur et al. (2005) measured the Cu isotope composition of Cu after interacting with *A. ferrooxidans* cells for 30 days. The cells caused withdrawal of 19 mg Cu/g dry cell mass from solution. The cell mass also contained mineral precipitates that were

impossible to separate from the cells. The Cu associated with the cell/precipitate mass was enriched in ^{65}Cu relative to the source medium by as much as 2.88‰ ± 0.23‰ (2σ) (Mathur et al., 2005) (Table 2.1; Fig. 2.4). Similarly, Cu(II) adsorbed onto a common soil bacterium was enriched in ^{65}Cu relative to solution by 0.6‰ (Borrok et al., 2008b). Association of heavy Cu with cells and precipitates helps explain why the $\Delta^{65}Cu_{aq\text{-}min}$ values for chalcocite, chalcopyrite, and enargite leaching in the presence of bacteria (Fig. 2.4) were lower than $\Delta^{65}Cu_{aq\text{-}min}$ values for each mineral in the absence of bacteria (Fig. 2.3).

2.7. Summary

The isotopic compositions of primary chalcopyrite and primary/secondary Cu(I)-sulfides have been more thoroughly reported in the literature than those of secondary minerals and natural waters. The average isotopic composition of Cu sulfide minerals (0.13 ± 0.94‰) is slightly isotopically depleted in ^{65}Cu relative to secondary minerals (0.26 ± 0.64‰) (Fig. 2.2). Minerals in general are isotopically depleted relative to water samples, with average values increasing in the following order: large rivers (0.66 ± 0.34‰) < seawater (1.09 ± 0.20‰) < AMD streamwater (1.54 ± 0.14‰). The observed isotopic differences between mineral and natural water samples are consistent with experimental Cu isotope fractionation.

The largest Cu isotope fractionations reported from the literature are based on experiments with sorption and redox reactions (Fig. 2.3). For example, redistribution of isotopes into more stable bonding environments during Cu(II) sorption onto (oxyhydr)oxide minerals results in fractionation of up to 1.25‰ (Fig. 2.3). When redox is involved, however, fractionation can be as much as 4‰ (Fig. 2.3). Figure 2.3 summarizes many reports showing that different redox reactions cause aqueous Cu(II) to be enriched in ^{65}Cu relative to aqueous or solid Cu(I) phases. In addition to experimental evidence for a redox isotope effect, in deposits where Cu(I) and Cu(II) minerals coexist, secondary Cu(II) minerals are isotopically enriched in ^{65}Cu relative to primary Cu(I) minerals (Larson et al., 2003; Mason et al., 2005; Markl et al., 2006; Asael et al., 2007; Mathur et al., 2009). Unlike abiotic systems, in biotic systmes there is less of a distinction between non-redox fractionation and redox fractionation. Fractionation of Cu between the aqueous

phase and biota-associated phases is as much as 2.9‰ for non-redox processes and 1.7‰ for redox processes (Fig. 2.4).

The fractionation between leached Cu and primary minerals in abiotic experiments resembles that measured between AMD and mineral samples from the field, where leached Cu is isotopically enriched in ^{65}Cu relative to sulfide minerals. Enrichment of streams, rivers, and the ocean in ^{65}Cu relative to Cu-bearing minerals is most consistent with a redox isotope effect: where isotopically heavy Cu(I) in sulfide minerals preferentially oxidizes to Cu(II), which is then released to solution. In addition, relatively ^{65}Cu-depleted Cu is preferentially precipitated as Cu(I) sulfide in reducing environments, most likely due to a redox effect between aqueous Cu(II) and Cu(I) species prior to precipitation (Luther, 2002; Ehrlich et al., 2004; Asael et al., 2009). However, the redox isotope effect that causes oxidized aqueous Cu to be enriched in ^{65}Cu relative to aqueous or solid Cu(I) can be overprinted by other isotope effects, such as kinetic or biological isotope effects or those involving ligand exchange. The result is environmental samples with δ^{65}Cu values that span almost 12‰.

Within the field of Cu isotope (bio)geochemistry, there are several areas that would benefit from further study. As is shown in figure 2.2, there are many more Cu isotope measurements for Cu minerals as compared to water samples. Additional measurements of the δ^{65}Cu values of river water, seawater, and impacted streamwater would help complete our understanding of how Cu is fractionated in the environment. Furthermore, the data sets for the Cu isotope composition of sediments and soils are relatively small. Growth of these data sets would provide insights into the fate of Cu in weathering environments. Based on experiments with Cu isotope fractionation, many questions arise. For example, what causes the different overall fractionation during abiotic dissolution of different Cu-sulfides (Fig. 2.3, 2.5)? Why is there no difference in the direction and magnitude of Cu isotope fraction during biological redox and non-redox reactions (Fig. 2.4)? Further experimentation ought to be directed at answering such questions.

Copper isotope fractionation during environmentally relevant processes such as Cu sorption to (oxyhydr)oxide minerals and sulfide mineral dissolution has been measured outside of analytical uncertainty and reproduced by different experimentalists.

Fractionation measured between Cu-bearing reservoirs in laboratory experiments is consistent with the distribution of Cu masses in the environment, where the majority of the earth's Cu in the geosphere is generally isotopically similar to the standard, and the smaller amount of Cu dissolved in the hydrosphere is generally enriched in ^{65}Cu relative to the standard. Additional measurements of the isotopic composition of Cu in secondary minerals, soils, and water will help complete our understanding of the global mass balance of Cu, and future experiments with Cu isotope fractionation will continue to elucidate the isotope effects responsible for Cu isotope abundances in environmental samples. Our understanding of the Cu isotope system has improved greatly over the last decade, and promises to grow in the decades to come.

2.8. References

Albarède, F. and Beard, B. L. (2004) Analytical Methods for Non-Traditional Isotopes. In: Johnson, C. M., Beard, B. L., and Albarede, F. Eds.), *Reviews in Mineralogy and Geochemistry*. Mineralogical Society of America, Washington, D. C.

Archer, C. and Vance, D. (2002) Large fractionations in Fe, Cu, and Zn isotopes associated with Archean microbially-mediated sulphides. *Geochimica et Cosmochimica Acta* **66**, A26.

Archer, C. and Vance, D. (2004) Mass discrimination correction in multiple-collector plasma source mass spectrometry: an example using Cu and Zn isotopes. *Journal of Analytical Atomic Spectroscopy* **19**, 656-665.

Asael, D., Matthews, A., Bar-Matthews, M., and Halicz, L. (2007) Copper isotope fractionation in sedimentary copper mineralization (Timna Valley, Israel). *Chemical Geology* **243**, 238-254.

Asael, D., Matthews, A., Butler, I., Rickard, A. D., Bar-Matthews, M., and Halicz, L. (2006) $^{65}Cu/^{63}Cu$ fractionation during copper sulphide formation from iron sulphides in aqueous solution. *Geochimica Cosmochimica Acta* **70**, A23.

Asael, D., Matthews, A., Oszczepalski, S., Bar-Matthews, M., and Halicz, L. (2009) Fluid speciation controls of low temperature copper isotope fractionation applied to the Kupferschiefer and Timna ore deposits. *Chemical Geology* **262**, 147-158.

Balistrieri, L. S., Borrok, D. M., Wanty, R. B., and Ridley, W. I. (2008) Fractionation of Cu and Zn isotopes during adsorption onto amorphous Fe(III) oxyhydroxide: Experimental mixing of acid rock drainage and ambient river water. *Geochimica Cosmochimica Acta* **72**, 311-328.

Bermin, J., Vance, D., Archer, C., and Statham, P. J. (2006) The determination of the isotopic composition of Cu and Zn in seawater. *Chemical Geology* **226**, 280-297.

Bigalke, M., Weyer, S., and Wolfgang, W. (2009) Isotopic fractionation of copper during soil genesis. *Geochimica Cosmochimica Acta* **73**, A121.

Bigeleisen, J. and Mayer, M. G. (1947) Calculation of equilbrium constants for isotopic exchange reactions. *Journal of Chemical Physics* **15**, 261-267.

Borrok, D. M., Nimick, D. A., Wanty, R. B., and Ridley, W. I. (2008a) Isotopic variations of dissolved copper and zinc in stream waters affected by historical mining. *Geochimica Cosmochimica Acta* **72**, 329-344.

Borrok, D. M., Ridley, W. I., and Wanty, R. B. (2008b) Isotopic fractionation of Cu and Zn during adsorption onto bacterial surfaces. *Geochimica Cosmochimica Acta* **72**, A99.

Borrok, D. M., Wanty, R. B., Ridley, W. I., Wolf, R., Lamothe, P. J., and Adams, M. (2007) Separation of copper, iron, and zinc from complex aqueous solutions for isotopic measurement. *Chemical Geology* **242**, 400-414.

Clayton, R. E., Hudson-Edwards, K. A., and Houghton, S. L. (2005) Isotopic effects during Cu adsorption onto goethite. *Geochimica Cosmochimica Acta* **69**, A216.

Criss, R. E. (1999) *Principles of stable isotope distribution*. Oxford University Press, New York.

Ehrlich, S., Butler, I., Halicz, L., Rickard, D., Oldroyd, A., and Matthews, A. (2004) Experimental study of the copper isotope fractionation between aqueous Cu(II) and covellite, CuS. *Chemical Geology* **209**, 259-269.

Fernandez, A. and Borrok, D. M. (2009) Fractionation of Cu, Fe, and Zn isotopes during the oxidative weathering of sulfide-rich rocks. *Chemical Geology* **264**, 1-12.

Graham, S., Pearson, N., Jackson, S., Griffin, W., and O'Reilly, S. Y. (2004) Tracing Cu and Fe from source to porphyry: in situ determination of Cu and Fe isotope ratios in sulfides from the Grasberg Cu-Au deposit. *Chemical Geology* **207**, 147-169.

Halliday, A. N., Lee, D.-C., Christensen, J. N., Rehkämper, M., Yi, W., Luo, X., Hall, C. M., Ballentine, C. J., Petke, T., and Stirling, C. (1998) Applications of multiple collector-ICPMS to cosmochemistry, geochemistry, and paleoceanography. *Geochimica Cosmochimica Acta* **62**, 919-940.

Hayes, J. M. (2001) Fractionation of the Isotopes of Carbon and Hydrogen in Biosynthetic Processes. *Reviews in Mineralogy and Geochemistry* **43**, 225-278.

Jiang, S., Woodhead, J., Yu, J., Pan, J., Liao, Q., and Wu, N. (2002) A reconnaissance of Cu isotopic compositions of hydrothermal vein-type copper deposit, Jinman, Yunnan, China. *Chinese Science Bulletin* **47**, 247-250.

Kimball, B. E., Mathur, R., Dohnalkova, A. C., Wall, A. J., Runkel, R. L., and Brantley, S. L. (2009) Copper Isotope Fractionation in Acid Mine Drainage. *Geochimica et Cosmochimica Acta* **73**, 1247-1263.

Klauber, C. (2008) A critical review of the surface chemistry of acidic ferric sulphate dissolution of chalcopyrite with regards to hindered dissolution. *International Journal of Mineral Processing* **86**, 1-17.

Klein, S., Domergue, C., Lahaye, Y., Brey, G. P., and von Kaenel, H.-M. (2009) The lead and copper isotopic composition of copper ores from the Sierra Morena (Spain). *Journal of Iberian Geology* **35**, 59-68.

Larson, P. B., Maher, K., Ramos, F. C., Chang, Z., Gaspar, M., and Meinert, L. D. (2003) Copper isotope ratios in magmatic and hydrothermal ore-forming environments. *Chemical Geology* **201**, 337-350.

Lattanzi, P., Da Pelo, S., Musu, E., Atzei, D., Elsener, B., Fantauzzi, M., and Rossi, A. (2008) Enargite oxidation: A review. *Earth-Science Reviews* **86**, 62-88.

Luck, J. M., Ben Othman, D., Barrat, J. A., and Albarède, F. (2003) Coupled ^{63}Cu and ^{16}O excesses in chondrites. *Geochimica Cosmochimica Acta* **67**, 143-151.

Luther, G. W. (2002) Aqueous copper sulphide clusters as intermediates during copper sulphide formation. *Environmental Science and Technology* **36**, 394-402.

Maher, K. C. and Larson, P. B. (2007) Variation in copper isotope ratios and controls on fractionation in hypogene skarn mineralization at Coroccohuayco and Tintaya, Perú. *Economic Geology* **102**, 225-237.

Maréchal, C. N. and Albarède, F. (2002) Ion-exchange fractionation of copper and zinc isotopes. *Geochimica et Cosmochimica Acta* **66**, 1499-1509.

Maréchal, C. N. and Sheppard, S. M. F. (2002) Isotopic fractionation of Cu and Zn between chloride and nitrate solutions and malachite or smithsonite at 30°C and 50°C. *Geochimica Cosmochimica Acta* **66**, A484.

Maréchal, C. N., Télouk, P., and Albarède, F. (1999) Precise analysis of copper and zinc isotopic compositions by plasma-source mass spectrometry. *Chemical Geology* **156**, 251-273.

Markl, G., Lahaye, Y., and Schwinn, G. (2006) Copper isotopes as monitors of redox processes in hydrothermal mineralization. *Geochimica Cosmochimica Acta* **70**, 4215-4228.

Mason, T. F. D., Weiss, D. J., Chapman, J. B., Wilkinson, J. J., Tessalina, S. G., Spiro, B., Horstwood, M. S. A., Spratt, J., and Coles, B. J. (2005) Zn and Cu isotope variability in the Alexandrinka volcanic-hosted massive sulfide (VHMS) ore deposit, Urals, Russia. *Chemical Geology* **221**, 170-187.

Mathur, R., Ruiz, J., Titley, S., Liermann, L., Buss, H., and Brantley, S. L. (2005) Cu isotopic fractionation in the supergene environment with and without bacteria. *Geochimica et Cosmochimica Acta* **69**, 5233-5246.

Mathur, R., Titley, S., Barra, F., Brantley, S. L., Wilson, M., Phillips, A., Munizaga, F., Maksaev, V., Vervoort, J., and Hart, G. (2009) Exploration potential of Cu isotope fractionation in porphyry copper deposits. *Journal of Geochemical Exploration* **102**, 1-6.

Parker, A., Klauber, C., Kougianos, A., Watling, H., and van Bronswijk, W. (2003) An X-ray photoelectron spectroscopy study of the mechanism of oxidative dissolution of chalcopyrite. *Hydrometallurgy* **71**, 265-276.

Pokrovsky, O. S., Viers, J., Emnova, E. E., Kompantseva, E. I., and Freydier, R. (2008) Copper isotope fractionation during its interaction with soil and aquatic microorganisms and metal oxy(hydr)oxides: Possible structural control. *Geochimica Cosmochimica Acta* **72**, 1742-1757.

Rauch, J. N. and Graedel, T. E. (2007) Earth's anthrobiogeochemical copper cycle. *Global Biogeochemical Cycles* **21**, GB2010.

Rauch, J. N. and Pacyna, J. M. (2009) Earth's global Ag, Al, Cr, Cu, Fe, Ni, Pb, and Zn cycles. *Global Biogeochemical Cycles* **23**, GB2001.

Robb, L. (2005) *Introduction to Ore-forming Processes*. Blackwell Publishing, Oxford.

Rouxel, O., Fouquet, Y., and Ludden, J. N. (2004) Copper isotope systematics of the Lucky Strike, Rainbow, and Logatchev sea-floor hydrothermal fields on the Mid-Atlantic Ridge. *Economic Geology* **99**, 585-600.

Schauble, E. A. (2004) Applying stable isotope fractionation theory to new systems. *Reviews in Mineralogy and Geochemistry* **55**, 65-111.

Shields, W. R., Goldich, S. S., Garner, E. L., and Murphy, T. J. (1965) Natural variation in the abundance ratio and atomic weight of copper. *Journal of Geophysical Research* **70**, 479-491.

Shields, W. R., Murphy, T. J., and Garner, E. L. (1964) Absolute isotopic abundance ratio and the atomic weight of a reference sample of copper. *Journal of Research of the National Bureau of Standards* **68A**, 589-592.

Urey, H. C. (1947) The thermodynamic properties of isotopic substances. *Journal of the Chemical Scoiety (London)*, 562-581.

Vance, D., Archer, C., Bermin, J., Perkins, J., Statham, P. J., Lohan, M. C., Ellwood, M. J., and Mills, R. A. (2008) The copper isotope geochemistry of rivers and the oceans. *Earth and Planetary Science Letters* **274**, 204-213.

Wall, A. J., Heaney, P. J., Brantley, S. L., Mathur, R., and Post, J. E. (2009) Copper isotope fractionation during leach layer development on Cu-sulfide minerals. *Geochimica Cosmochimica Acta* **73**, A1202.

Zhu, X. K., Guo, Y., Williams, R. J. P., O' Nions, R. K., Matthews, A., Belshaw, N. S., Canters, G. W., de Waal, E. C., Weser, U., Burgess, B. K., and Salvato, B. (2002) Mass fractionation processes of transition metal isotopes. *Earth and Planetary Science Letters* **200**, 47-62.

Zhu, X. K., O' Nions, R. K., Guo, Y., Belshaw, N. S., and Rickard, D. (2000) Determination of natural Cu-isotope variation by plasma-source mass spectrometry: implications for use as geochemical tracers. *Chemical Geology* **163**, 139-149.

Table 2.1. Experimental Cu isotope fractionation between reservoirs A and B (see equation 2.2) during various abiotic and biotic processes.

Fractionation pair (A-B)	Experiment Description	Solution Matrix	T °C	Δ_{A-B}	Reference	Study Number
Abiotic Systems - No Redox						
$Cu(II)_{aq}$ - $Cu(II)_{aq}$-resin	ion-exchange elution	6 M HCl	20	0.75 ± 0.07	Zhu et al. (2002)	1
$Cu(II)_{aq}$ - $Cu(II)_{aq}$-resin	ion-exchange elution	7 M HCl	20	0.46 ± 0.06	Maréchal and Albarède (2002)	2
$Cu(II)_{aq}$ - $Cu(II)_{aq}$-resin	ion-exchange elution	3 M HCl	20	0.67 ± 0.06	Maréchal and Albarède (2002)	2
$Cu(II)_{aq}$ - Cu(II)malachite	slow precipitation	0.05 - 0.5 M	30	0.20 ± 0.06	Maréchal and Sheppard (2002)	3
		$Cu(NO_3)_2$	50	0.17 ± 0.06		3
$Cu(II)_{aq}$ - Cu(II)malachite	slow precipitation	0.05 - 0.5 M	30	0.38 ± 0.06	Maréchal and Sheppard (2002)	3
		$Cu(Cl)_2$	50	0.31 ± 0.06		3
$Cu(II)_{aq}$ - $Cu(II)_{sorbed}$	sorption onto goethite			-0.35 ± 0.11	Clayton et al. (2005)	4
$Cu(II)_{aq}$ - $Cu(II)_{sorbed}$	sorption onto ferrihydrite	8 mM $NaNO_3$, pH 3	22	-0.73 ± 0.08	Balistrieri et al. (2008)	5
$Cu(II)_{aq}$ - $Cu(II)_{sorbed}$	sorption onto goethite	0.01 M $NaNO_3$, pH 4-5	25	-0.78 ± 0.2	Pokrovsky et al. (2008)	6
$Cu(II)_{aq}$ - $Cu(II)_{sorbed}$	sorption onto gibbsite	0.01 M $NaNO_3$, pH 6	25	-1.0 ± 0.25	Pokrovsky et al. (2008)	7
Biotic Systems - No Redox						
$Cu(II)_{aq}$ - Cu(II) in azurin	in vitro *E. coli* uptake	$Cu(NO_3)_2$	20	1.53 ± 0.07	Zhu et al. (2002)	8
$Cu(II)_{aq}$ - Cu(II) in azurin	in vivo *P. aeruginosa* uptake	$Cu(NO_3)_2$	20	0.98 ± 0.07	Zhu et al. (2002)	9
$Cu(II)_{aq}$ - Cu(II) cells and precipitates	association with *A. ferrooxidans* cells and related precipitates	70 mM $Fe(SO_4)$, pH 2.3 with 50 mM Cu	25	-2.88 ± 0.23	Mathur et al. (2005)	10
$Cu(II)_{aq}$ - $Cu(II)_{sorbed}$	reversible sorption onto *P. aureofaciens* (EPS-rich)	0.1 M $NaNO_3$, pH 1.8-2.9	25	1.39 ± 0.07	Pokrovsky et al. (2008)	11
$Cu(II)_{aq}$ - $Cu(II)_{sorbed}$	reversible sorption onto *P. aureofaciens* (EPS-poor)	0.1 M $NaNO_3$, pH 1.8-3.3	25	0.93 ± 0.06	Pokrovsky et al. (2008)	12
$Cu(II)_{aq}$ - $Cu(II)_{sorbed}$	sorption and incorporation into bacteria and diatoms	4 < pH < 8	20-25	-0.05 ± 0.02	Pokrovsky et al. (2008)	13
Abiotic Systems - Redox						
$Cu(II)_{aq}$ - Cu(I)iodide	reduction and precipitation	0.05 M $Cu(NO_3)_2$ in 0.1 M HNO_3	20	4.03 ± 0.06	Zhu et al. (2002)	14
$Cu(II)_{aq}$ - $Cu(I)_{aq}$	reduction with ascorbic acid and ion-exchange separation	$CuCl_2$ in 0.1 M HCl	20	3.70 ± 0.07	Matthews, A. and Zhu, X-K. unpublished results	15
$Cu(II)_{aq}$ - Cu(I)S	anoxic precipitation of covellite	$CuSO_4.5H_2O$ and $Na_2S.9H_2O$ in pH 4.3-4.45	20	3.06 ± 0.14	Ehrlich et al. (2004)	16
$Cu(II)_{aq}$ - $Cu(I)_2S$	oxidative chalcocite dissolution by O_2/Fe^{3+} in ferrous sulfate	70 mM $Fe(SO_4)$, pH 2.3	25	3.03 ± 0.36	Mathur et al. (2005)	17
$Cu(II)_{aq}$ - $Cu(I)_2S$	oxidative chalcocite dissolution by Fe^{3+} in ferric sulfate	$Fe_2(SO_4)_3$	25	3.19 ± 0.14	Wall et al. (2009)	18
$Cu(II)_{aq}$ - Cu(I) sulfide	reduction by reaction with pyrite or pyrrhotite, anoxic	$CuSO_4.5H_2O$	40	2.84 ± 0.09	Asael et al. (2006)	19
$Cu(II)_{aq}$ - Cu(I) sulfide	reduction by reaction with pyrite or pyrrhotite, anoxic	$CuSO_4.5H_2O$	100	2.68 ± 0.11	Asael et al. (2006)	19
$Cu(II)_{aq}$ - Cu(I)FeS_2	oxidative chalcopyrite dissolution by O_2/Fe^{3+} in ferrous sulfate	70 mM $Fe(SO_4)$, pH 2.3	25	1.36 ± 0.38	Mathur et al. (2005)	20
$Cu(II)_{aq}$ - Cu(I)FeS_2	oxidative chalcopyrite dissolution by O_2/Fe^{3+} in ferrous sulfate	70 mM $Fe(SO_4)$, pH 2.0	25	1.37 ± 0.40	Kimball et al. (2009)	21
$Cu(II)_{aq}$ - Cu(I)FeS_2	oxidative chalcopyrite dissolution by O_2/Fe^{3+} in acid	water pH 5	25	1.91 ± 0.26	Fernandez & Borrok (2009)	22
$Cu(II)_{aq}$ - Cu(I)FeS_2	oxidative chalcopyrite dissolution by O_2/Fe^{3+} in acid	HCl pH 2	25	0.12-2.04	Fernandez & Borrok (2009)	23
$Cu(II)_{aq}$ - Cu(I)AsS_4	oxidative enargite dissolution by O_2/Fe^{3+} in ferrous sulfate	70 mM $Fe(SO_4)$, pH 2.0	25	0.99 ± 0.10	Kimball et al. (2009)	24
Biotic Systems - Redox						
$Cu(II)_{aq}$ - Cu(I)metallothionen	Cu uptake by yeast	$Cu(SO_4)$	20	1.71 ± 0.07	Zhu et al. (2002)	25
$Cu(II)_{aq}$ - Cu(I/II)-Zn superoxide dismutase	Cu uptake by yeast	$Cu(SO_4)$	20	1.18 ± 0.07	Zhu et al. (2002)	26
$Cu(II)_{aq}$ - $Cu(I)_2S$	oxidative chalcocite dissolution by O_2/Fe^{3+} in ferrous sulfate with 0.05% inoculum *A. ferrooxidans*	70 mM $Fe(SO_4)$, pH 2.3	25	0.87 ± 1.14	Mathur et al. (2005)	27
$Cu(II)_{aq}$ - Cu(I)FeS_2	oxidative chalcopyrite dissolution by O_2/Fe^{3+} in ferrous sulfate with 0.05% inoculum *A. ferrooxidans*	70 mM $Fe(SO_4)$, pH 2.3	25	0.38 ± 0.25	Mathur et al. (2005)	28
$Cu(II)_{aq}$ - Cu(I)FeS_2	oxidative chalcopyrite dissolution by O_2/Fe^{3+} in ferrous sulfate with 10% inoculum *A. ferrooxidans*	70 mM $Fe(SO_4)$, pH 2.0	25	-0.57 ± 0.25	Kimball et al. (2009)	29
$Cu(II)_{aq}$ - Cu(I)AsS_4	oxidative enargite dissolution by O_2/Fe^{3+} in ferrous sulfate with 10% inoculum *A. ferrooxidans*	70 mM $Fe(SO_4)$, pH 2.0	25	0.15 ± 0.21	Kimball et al. (2009)	30

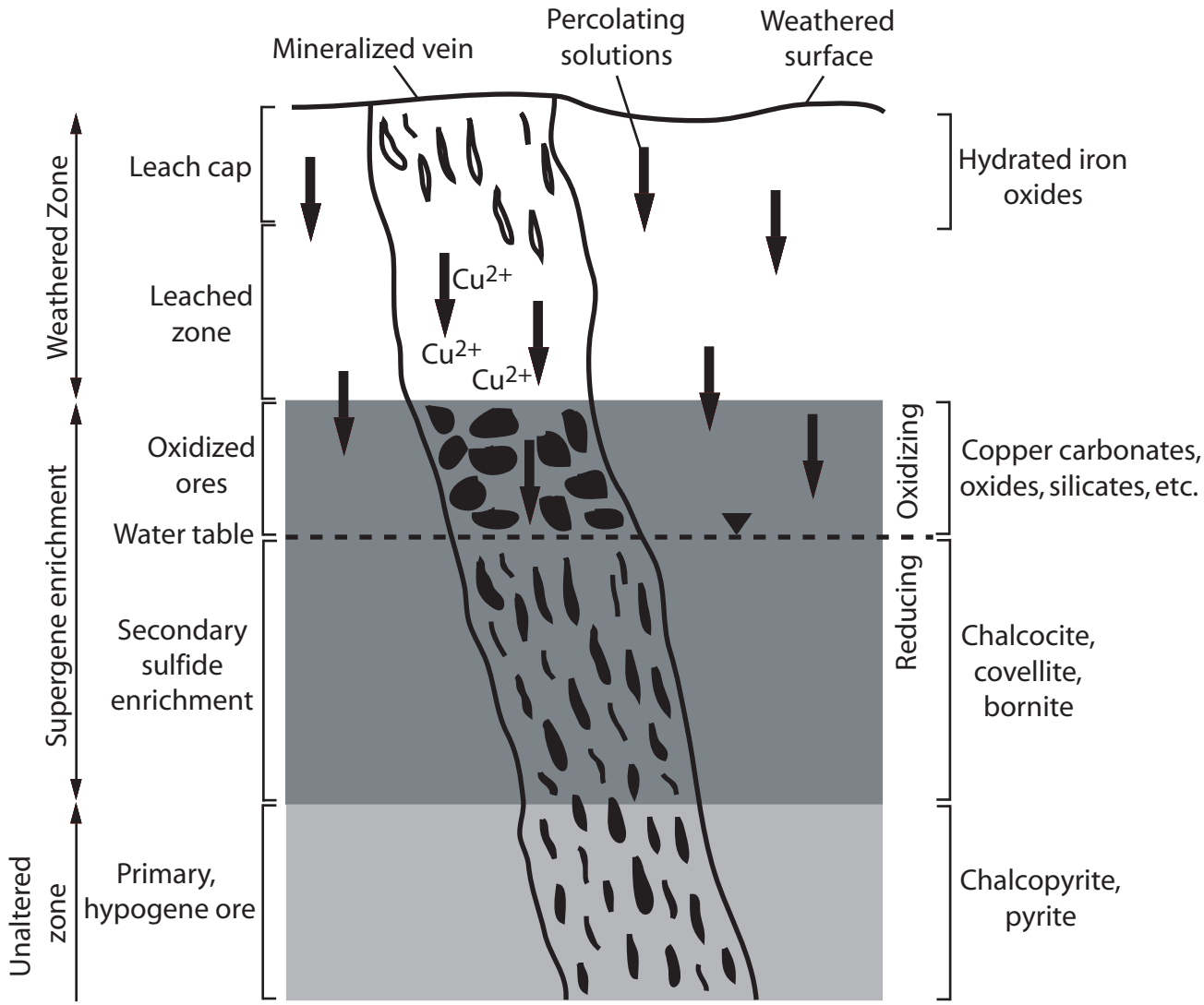

Figure 2.1. Schematic cross section through a weathered hydrothermal deposit showing an oxidized weathered zone, supergene enrichment of Cu minerals at the vadose zone-groundwater interface, and the reduced, unaltered zone, where primary hypogene ores (i.e., chalcopyrite and pyrite) exist. Oxidized Cu minerals can be found in the upper oxidizing portion of the supergene environment, and secondary sulfide ores are found in the lower reducing portion of the supergene environment (after Robb, 2005).

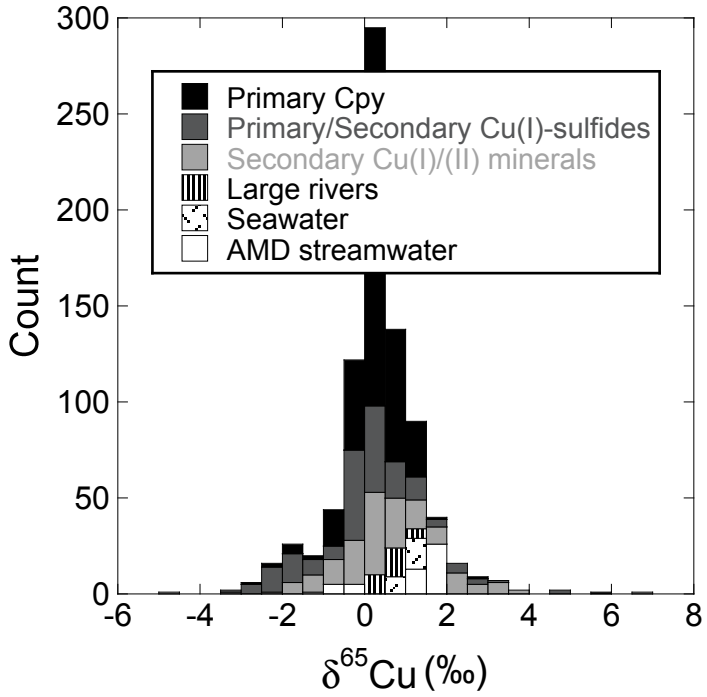

Figure 2.2. Histogram of the Cu isotope composition of environmental samples. The δ^{65}Cu values of primary chalcopyrite, other Cu(I)-sulfides, and secondary Cu(I),(II) minerals are shown, as well as the δ^{65}Cu values of dissolved Cu in large rivers, seawater, and acid mine drainage (AMD) streamwater. While the number of measurements on mineral samples far outweighs those for water samples, waters are generally isotopically enriched in ^{65}Cu relative to most Cu minerals.

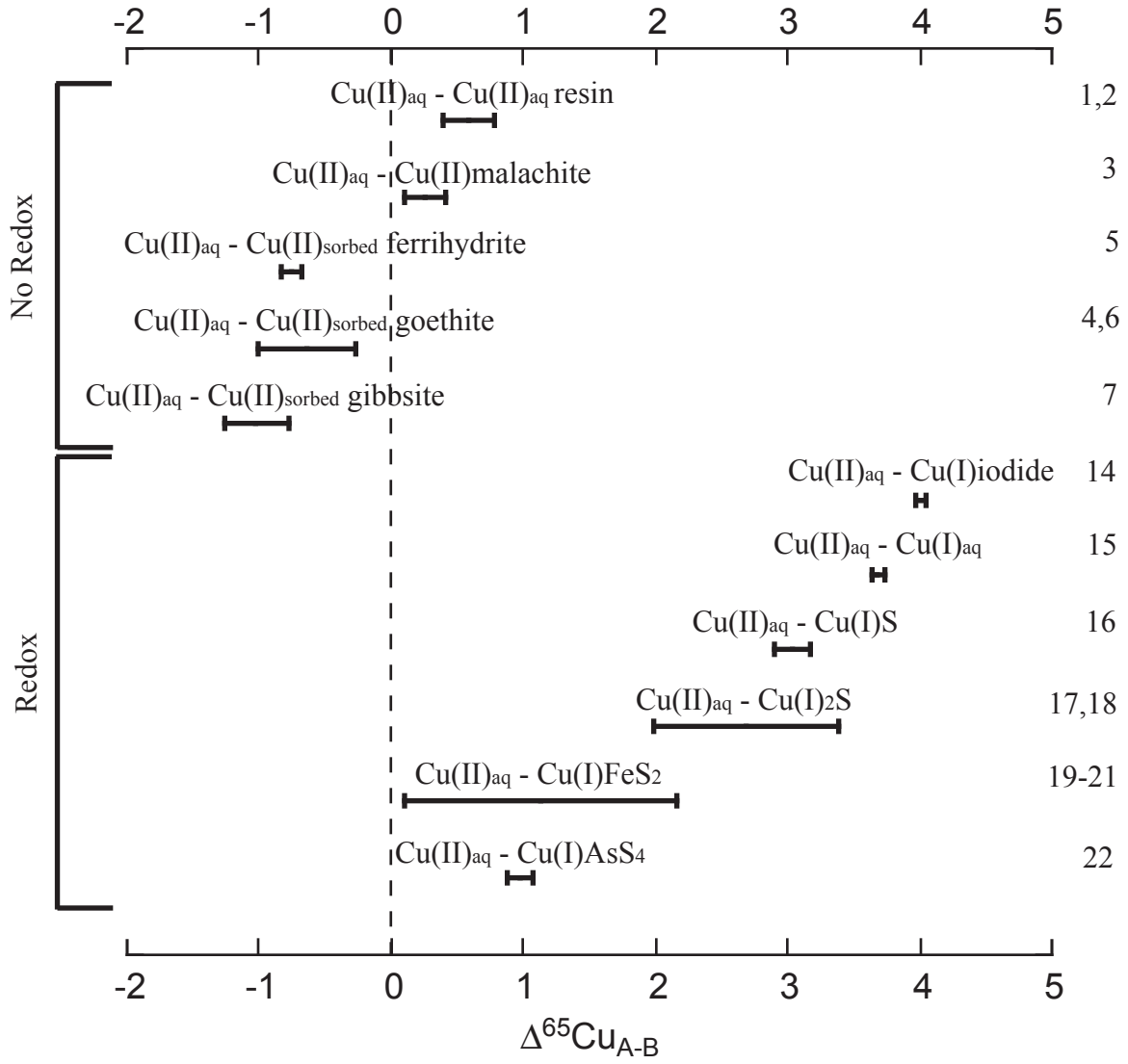

Figure 2.3. Copper isotope fractionation ($\Delta^{65}Cu_{A-B} = \delta^{65}Cu_A - \delta 65Cu_B$) for abiotic laboratory experiments without and with Cu redox transitions. The numbers on the right-hand side refer to the study number noted in Table 2.1.

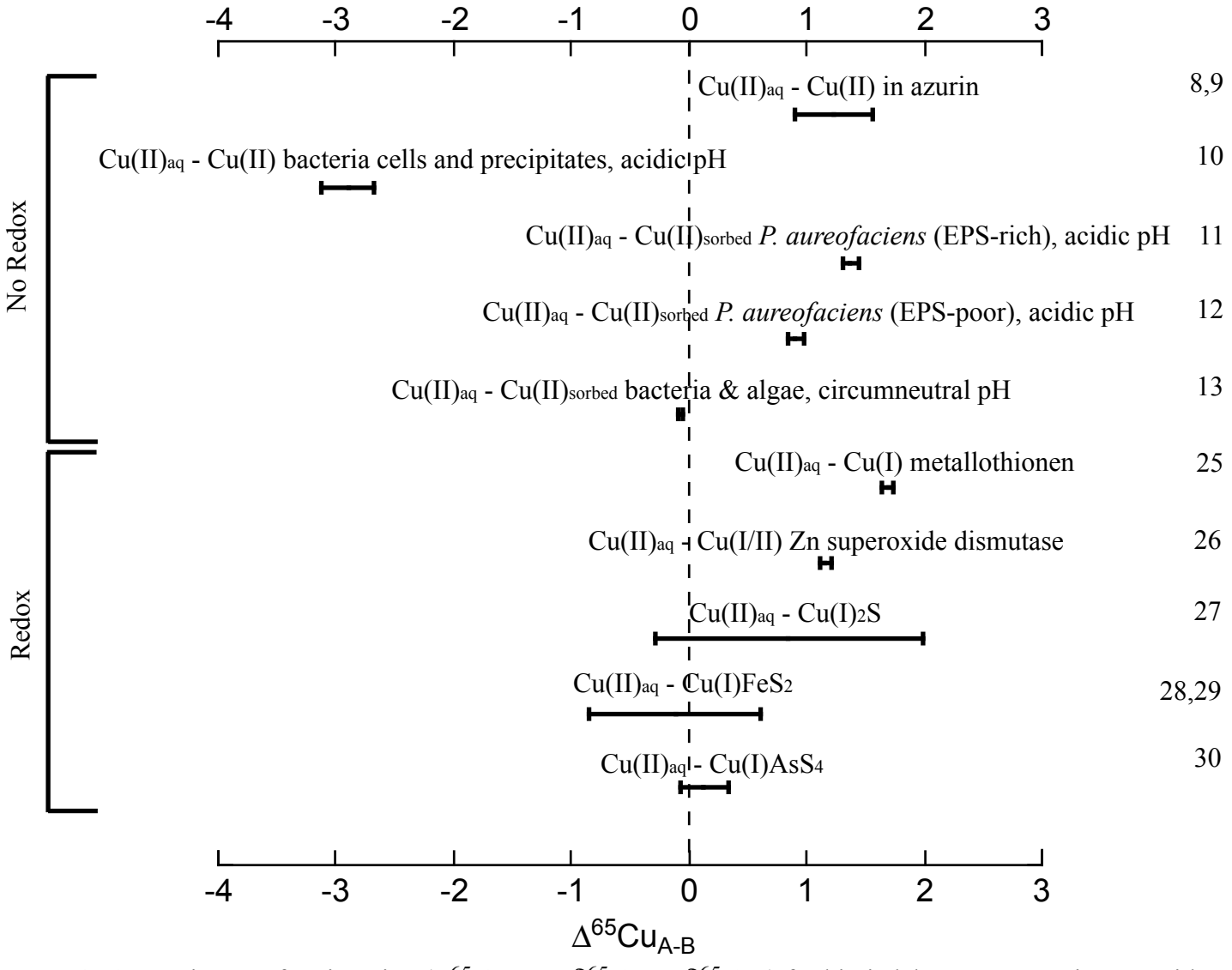

Figure 2.4. Copper isotope fractionation ($\Delta^{65}Cu_{A-B} = \delta^{65}Cu_A - \delta^{65}Cu_B$) for biotic laboratory experiments without and with Cu redox transitions. The numbers on the right-hand side refer to the study number noted in Table 2.1.

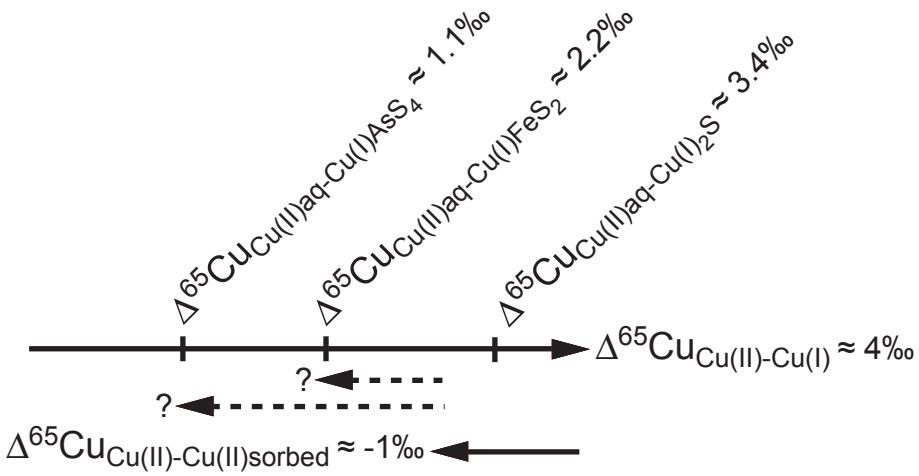

Figure 2.5. Schematic showing the maximum experimental fractionation measured during Cu(II) reduction to Cu(I) ($\Delta^{65}Cu \approx 4‰$; Zhu et al., 2002) and sorption of Cu(II) to goethite ($\Delta^{65}Cu \approx -1‰$; Pokrovsky et al., 2008). Along the redox fractionation vector, the maximum extents of fractionation measured during enargite (Kimball et al., 2009), chalcopyrite (Fernandez & Borrok, 2009), and chalcocite (Mathur et al., 2005) dissolution are shown. While sorption of heavy Cu onto Fe (oxyhydr)oxides may explain the lower net fractionation during chalcocite dissolution, other fractionating processes, in addition to redox and sorption, are needed to explain the net fractionation measured during enargite and chalcopyrite dissolution.

Chapter 3
Chalcopyrite Dissolution Rate Laws

3.0. Abstract

Meta-analysis of 171 rate measurements from 21 publications was used to develop rate laws for chalcopyrite dissolution under environmentally relevant conditions. Multiple linear regression analysis of 30 data for nonoxidative chalcopyrite dissolution in the presence of O_2 and Cl^- produced the following rate law:

$$r = 10^{-2.35} e^{-22100/RT} m_{H^+}^{2.00}$$

Here, r is the rate of chalcopyrite destruction in units of mol m^{-2} s^{-1} where the surface area is expressed on a geometric basis. Multiple linear regression analysis of 38 data for chalcopyrite dissolution caused by reaction with Fe(III) in the presence and absence of O_2 and Cl^- produced the following rate law:

$$r = 10^{1.28} e^{-44300/RT} m_{H^+}^{0.74} m_{Fe(III)}^{0.43}$$

Some data were excluded from these rate law models because they were inconsistent with the overall dataset and/or were relatively unconstrained. There were no published rate data that could be clearly identified as representing chalcopyrite dissolution caused by O_2 oxidation alone. Although there are numerous reports that suggest that chalcopyrite dissolution rates are increased by the presence of Cl^- in solution, our regression models found the effect of Cl^- to be insignificant for our selected datasets.

3.1. Introduction

Chalcopyrite ($CuFeS_2$) is the most common Cu-bearing mineral on earth (Nesse, 2000). This primary mineral most often precipitates from hydrothermal fluids in association with other sulfides, but also occurs as an accessory mineral in mafic igneous rocks. Dissolution of chalcopyrite releases dissolved metals and acid to the environment, thereby contributing to the problem of acid rock drainage (ARD). There are two situations where the release rate of Cu from chalcopyrite is particularly important. Chalcopyrite is often the most abundant Cu-bearing mineral in mine wastes and Cu released by its dissolution is responsible for significant phytotoxicity in soils (Alva et al., 2000) and aquatic toxicity in nearby receiving waters (Schumbauer-Berigan et al., 1993). In this case, we seek to minimize the natural rate of chalcopyrite dissolution, so researchers design experiments that closely match the pH, Eh, and temperature conditions typical of surface weathering environments. On the other hand, chalcopyrite is often the most abundant Cu-bearing mineral in sulfide ores and we often seek to maximize its dissolution rate during hydrometallurgical recovery of Cu (Bartlett, 1997). For this purpose, experiments often involve dissolution at $pH < 0$ and $T > 100^{\circ}C$, which are conditions generally less relevant to the environment. Regardless of the conditions, however, solutions reacting with chalcopyrite tend to evolve towards low pH and high sulfate and dissolved Fe(III) concentrations.

The purpose of this work is to compile the published kinetic data for chalcopyrite dissolution from all fields in order to conduct a meta-analysis that will allow the determination of rate laws for chalcopyrite dissolution that are applicable to environmentally relevant conditions. The kinetic data used to derive empirical rate laws were critically selected in order to maintain statistical validity and chemical reality. To our knowledge, collection and meta-analysis of chalcopyrite dissolution rate data has not been attempted previously. Although microbial bioleaching of sulfides is important, we chose to limit our scope to abiotic experiments because of the relatively few number of quantitative studies of microbiological rates.

3.2. Background

3.2.1. Chalcopyrite Dissolution Reactions

The difficulty in understanding and analyzing published rate data is determining which of several possible reactions was responsible for the observed rate. We limited our data gathering and data analysis to consider the three reactions that are likely to be important at ambient conditions.

The simplest reaction that can liberate Cu from chalcopyrite is nonoxidative dissolution:

$$CuFeS_{2(s)} + 4H^{+}_{(aq)} = Cu^{2+}_{(aq)} + Fe^{2+}_{(aq)} + 2H_2S_{(aq)} \quad (3.1)$$

Although debated, overwhelming evidence now shows that the valences of Cu and Fe in chalcopyrite are +1 and +3, respectively (Boekema et al., 2004; Goh et al., 2006; Pearce et al., 2006; Wincott and Vaughan, 2006). Because sulfide surfaces readily oxidize upon exposure to air and water (Yin et al., 1995; Rosso and Vaughan, 2006), Cu on the chalcopyrite surface is likely to be a mixture of intermediate Cu(I) and Cu(II) phases. O'Malley and Liddell (1986) measured the oxidation state of Cu during chalcopyrite dissolution in batch experiments and found that initially, the released Cu was predominantly Cu(II). After about 35% of the total Cu had dissolved, however, the reaction rate increased and nearly all released Cu was Cu(I). This experiment is consistent with release of Cu(II) from oxidized chalcopyrite grain surfaces, followed by release of Cu(I) from unoxidized chalcopyrite surfaces after a significant reduction in grain size and extent of reaction. Regardless of the valences of Cu and Fe in the mineral, oxidation of Cu(I) by Fe(III) in solution is rapid under acidic conditions (Orth and Liddell, 1990):

$$Cu^{+}_{(aq)} + Fe^{3+}_{(aq)} = Cu^{2+}_{(aq)} + Fe^{2+}_{(aq)} \quad (3.2)$$

so we expect Cu(II) and Fe(II) to be the predominant aqueous products even if Cu(I) and Fe(III) are the species that are initially liberated from the chalcopyrite. Because reaction (3.1) involves only the interaction of hydrogen ions and chalcopyrite, we can assume the reaction rate depends only upon the chalcopyrite surface area and the solution pH.

In the environment, dissolved oxygen (DO) is a frequent electron acceptor so we expect chalcopyrite to oxidize and release Cu by a reaction that involves DO.

$$CuFeS_{2(s)} + 4O_{2(aq)} = Cu^{2+}_{(aq)} + Fe^{2+}_{(aq)} + 2SO_4^{2-}{}_{(aq)} \quad (3.3)$$

Because DO concentrations are relatively low (< ~10 mg/kg) in ARD and heap leaching liquors and because the reduction of O_2 is a complex, multi-step reaction, the rate of this reaction is expected to be relatively slow. Furthermore, based on the stoichiometry of the reaction we expect little or no pH dependence of the rate, so the rate should depend mostly on the chalcopyrite surface area and the DO concentration.

Usually, the most important reaction in ARD and heap leaching is the oxidation of chalcopyrite by Fe(III).

$$CuFeS_{2(s)} + 16Fe^{3+}_{(aq)} + 8H_2O = Cu^{2+}_{(aq)} + 17Fe^{2+}_{(aq)} + 2SO_4^{2-}_{(aq)} + 16H^{+}_{(aq)} \quad (3.4)$$

Because Fe(III) is relatively soluble in the low pH solutions that are characteristic of ARD and heap leach liquor and because it is rapidly regenerated from Fe(II) oxidation by microorganisms at low pH (Schwertmann and Fitzpatrick, 1992; Nordstrom and Southam, 1997), dissolved Fe(III) concentrations can be high in these settings. In addition, like pyrite oxidation, the rate determining step for reaction (3.4) is likely the simple and fast transfer of one electron from the chalcopyrite to an adsorbed Fe(III) (Rimstidt and Vaughan, 2003). As a result, reaction (3.4) is expected to dominate chalcopyrite dissolution in most low pH settings. Based on the stoichiometry of the reaction we expect the rate law to contain a term for Fe(III) concentration. Because Fe(III) oxyhydroxide solubility, which is very pH dependent, tends to control Fe(III) concentrations, we expect chalcopyrite dissolution rates to be relatively high at low pH and to decrease with increasing pH.

3.2.2. Chemical Reactors

Many rates of chalcopyrite dissolution have been reported for experiments under controlled temperature, pH, and solution composition. The most common experimental set-up is the batch reactor (BR), which is a flask containing mineral and solution, open or closed to the atmosphere, that is stirred or agitated without flow (Brantley, 2003; Lengke et al., 2009). The reaction is monitored by measuring the change in product concentrations over time. Care must be taken to correct for sample removal over time, if applicable, and to account for possible back-reactions such as precipitation of secondary phases (Brantley, 2003).

The second most common reactor used in this compilation was the mixed flow-through reactor (MFR). In a MFR, a mineral sample is placed within a reactor of a given volume, then solution is pumped through the reactor at a known rate while the solution within the reactor is stirred. One study utilized a flow reactor (FR) without any mixing; it was analyzed as if it were a MFR. Determination of rates from flow-through reactors is more straightforward than from batch reactors, and is calculated by comparing the inlet concentration (C_i) to the outlet concentration (C_o) of a component of the mineral sample (Brantley and Chen, 1995):

$$r = \frac{Q(C_o - C_i)}{v_i A m} \tag{3.5}$$

Here r is the rate of dissolution (mol m^{-2} s^{-1}), Q is the flow rate (L s^{-1}), v_i is the stoichiometric coefficient of component i in the mineral, A is the specific surface area of the mineral sample (m^2 g^{-1}), and m is the initial mineral mass (g). The rate is determined from equation (3.5) when C_o has reached steady-state.

The third type of reactor used by many investigators is the plug-flow reactor (PFR). Plug-flow reactors are columns packed with mineral sample through which fluid is pumped or drained. In an ideal PFR, every packet of fluid is assumed to have had the same contact time with the mineral sample (Hill, 1977). The calculation of rate from the PFR is more complex than that for flow-through reactors (see Brantley, 2003), and the set-up is more time-consuming. However, the results can be more representative of water-rock interaction in the environment (Brantley and Conrad, 2008).

3.2.3. Data Acquisition

In this study, our goal was to determine the rate of chemical reaction at the chalcopyrite surface under environmentally relevant conditions, so we did not include data from experiments conducted at high temperatures and oxidant concentrations. In many previous experiments, chalcopyrite dissolution was measured in the presence of high oxidant concentrations (e.g., Palmer et al., 1981; Lin et al., 1986), in the presence of environmentally unrealistic oxidants (e.g., Antonijević et al., 2004; Aydogan et al., 2006), or at high temperatures (e.g., Yu et al., 1973; Habashi and Toor, 1979; Hackl et al., 1995; Qui et al., 2007). These types of experiments often proceeded to large extents

of reaction and developed product layers (e.g., elemental sulfur (S^0) or jarosite) on the grain surfaces. In such experiments, the thickness and density of product layers usually acted as a diffusion barrier that caused the rates to be controlled by the rate of diffusive transport of reactants from solution to the chalcopyrite surface. For example, Majima et al. (1985) leached chalcopyrite in acidic $Fe_2(SO_4)_3$ and $FeCl_3$ solutions and found that S^0 formed on chalcopyrite grain surfaces in both experiments, but the S^0 formed in $Fe_2(SO_4)_3$ was denser than that formed in $FeCl_3$. This likely contributed to the slower oxidation rate determined for $Fe_2(SO_4)_3$ leaching compared to that for $FeCl_3$ leaching (Majima et al., 1985). To reduce the potential for rates affected by surface product layers, we only considered data from experiments conducted at T < 100ºC, $P_{O2} \leq 1.7$ atm, and $m_{Fe(III)} \leq 1$ M. In total, we compiled 171 rates for low-temperature chalcopyrite dissolution from 21 publications (Fig. 3.1a; Appendix 3A).

3.2.4. Data Quality

Prosser (1996) identified over 30 variables and phenomena that affect the leaching rate of sulfide minerals, each of which has an associated uncertainty. Among the variables included in this compilation, time and temperature are likely known with the most certainty (Prosser, 1996). Solution pH or log m_{H+} is known with reasonable certainty at the beginning of experiments, but is subject to change over the course of the reaction. Few studies monitored changes in pH over time. Likewise, when Fe(III) was added as an oxidant, the initial $m_{Fe(III)}$ was known with some certainty, but only one study observed changes in this variable with time. The P_{O2} was more stable than $m_{Fe(III)}$ in oxidation experiments.

The extent of reaction commonly reported in sulfide mineral dissolution experiments is calculated as the total moles of element *i* released to solution divided by the total moles of element *i* in the starting material ($\alpha = \text{moles}_{i\ \text{solution}}/\text{moles}_{i\ \text{total}}$). The reaction progress variable (RPV) most often used to describe chalcopyrite leaching is α calculated for Cu. While m_{Cu}, and thus moles of Cu, can be measured with reasonable certainty, calculated α values can have large errors due to the uncertain composition of the solid. Sulfide mineral specimens are rarely pure, and often contain minor quantities of other sulfides or minerals (Prosser, 1996). Most studies report the bulk composition of

the solids used in experiments based on mineral digestion and spectrometry or quantitative x-ray diffraction (XRD) analysis. When possible, we used the results from such techniques to estimate the total Cu in an experimental system in order to calculate α as accurately as possible. The calculated α values, and rates based on these values, are likely the most uncertain parameters included in this meta-analysis. We assume that the uncertainty associated with α is smaller than the meta-effects observed when considering multiple studies simultaneously, and therefore does not detract from detecting the control that certain variables have on dissolution rates.

3.3. Methods

3.3.1. Data Conversion and Analysis

The physiochemical conditions (e.g., pH, temperature, oxygen partial pressure, etc.) as well as the reactor type (e.g., batch, plug flow reactor, etc.) for experiments included in this compilation are listed in Table 3.1. Although some experiments were conducted under anoxic conditions, and others were carried out under controlled atmospheres, many experiments were open to the atmosphere, so we assumed a P_{O2} = 0.21 atm if not otherwise stated. We only considered the initial Fe(III) concentrations in leach solutions in our compilation, as most studies did not measure changes in Fe(III) during the reaction. Some data sets included intial pH, and others only the initial acid concentration. To be consistent, we assumed the following:

$$-\text{pH} = \log m_{H+} \tag{3.6}$$

$$\log m_{acid} = \log m_{H+} \tag{3.7}$$

We used the normality of acid to represent log m_{acid} and assumed that HCl and HNO_3 dissociated completely, and that H_2SO_4 dissociated to H^+ and HSO_4^- at pH < 2 and to $2H^+$ and SO_4^{2-} at pH $\geq$ 2.

To normalize dissolution rates by surface area, we collected available data describing the initial specific surface area of the chalcopyrite starting material. However, only 3 of the 21 studies included in this compilation report initial specific surface area measured by BET sorption analysis (A_{BET}), so we calculated initial geometric surface area (A_{geo}) for all experiments and used A_{geo} to normalized rate calculations to be consistent. The A_{geo} was calculated with the following relationship:

$$A_{\text{geo}} = \frac{6V_m}{W_m d_e} \tag{3.8}$$

where V_m is the molar volume of chalcopyrite (4.39 x 10^{-5} m^3/mol), W_m is the molar weight of chalcopyrite (183.5 g/mol), and d_e is the effective grain diameter of particles in a given sieved fraction (m). Most studies reported a range of grain sizes obtained from sieving. Assuming that grain sizes are evenly distributed between the maximum (d_{max}) and minimum (d_{min}) mesh size, d_e is approximated (Tester et al., 1994) by:

$$d_e = \frac{d_{\text{max}} - d_{\text{min}}}{\ln\left(\frac{d_{\text{max}}}{d_{\text{min}}}\right)} \tag{3.9}$$

A few studies only reported d_{max}, so we assumed smaller particles were at least the size of colloidal material with a d_{min} of 1 nm in order to use equation (3.9). In the few cases where both A_{BET} and A_{geo} were reported, it was observed that $A_{\text{BET}} > A_{\text{geo}}$. Therefore, the geometric surface area-normalized rates are expected to be larger than BET-normalized rates. Experimental conditions for each data source are given in Table 3.1.

Most studies used the concentration of Cu in solution as the RPV. A few studies (Table 3.1) reported the RPV in terms of production of dissolved Fe(II) or sulfate. These rates were converted to rates of chalcopyrite destruction in units of mol m^{-2} s^{-1}, based on the assumption that the mineral dissolved congruently.

When chalcopyrite dissolution rates where not tabulated, we extracted rate data from graphs using digitizing software (Data Thief III©). We calculated rates using both the standard initial rate method (IRM) (Rimstidt and Newcomb, 1993) and the shrinking particle model (SPM). A derivation of the SPM can be found in Appendix 3B, and compiled rates can be found in Appendix 3A.

To calculate rates using the IRM we plotted Cu concentration (in moles) versus time (s) for the initial linear portion of the experiment, then found the best-fit linear function:

$$m_{\text{Cu}} = a_1 + b_1 t \tag{3.10}$$

where a_1 and b_1 are constants. The derivative of (3.10) is:

$$r'_{\text{Cu}} = \frac{dm_{\text{Cu}}}{dt} = b_1 \tag{3.11}$$

where r'_{Cu} is the apparent rate of production of Cu (in mol s^{-1}), which can be converted to the surface area normalized rate of production (r_{Cu}; mol m^{-2} s^{-1}):

$$r_{Cu} = \frac{r'_{Cu}}{A_{geo}} \tag{3.12}$$

Here A_{geo} is the total surface area of the reacting mineral (m^2). The rate of release of Cu is equal to the rate of destruction of chalcopyrite based on stoichiometry.

With the SPM, the dissolution rate was calculated from the shrinking particle rate constant, k_p (s^{-1}), by assuming the reaction is pseudozeroth order. The SPM is most appropriate for experiments where the specific surface area and extent of reaction has changed significantly. In this case, the extent of reaction is the fraction of mineral that has dissolved away (α = $moles_{Cu\ dissolved}$/$moles_{Cu\ total}$). Among the studies included in this compilation, α values range from approximately 0.000002 to 0.98. We applied the SPM to all calculated α and found that for many experiments, rates calculated using the initial rate method and the shrinking particle method were within ± 0.5 log units. Unless otherwise stated (Table 3.1), for those rates that were calculated, SPM rates are reported (Appendix 3A).

We assumed that the dissolution rate could be described by an empirical dissolution rate law of the form:

$$r = A\left(e^{E_a/RT}\right)\prod m_i^{n_i} \tag{3.13}$$

Here A represents the pre-exponential in the Arrhenius rate law, E_a is the activation energy (J mol^{-1}), R is the gas constant (J mol^{-1} K^{-1}), T is temperature (Kelvins), m_i represents the concentration of appropriately chosen reactants (H^+, Fe(III), $O_{2(g)}$, and Cl^-), and n_i is the rate order with respect to that reactant. Equation (3.13) can be log transformed to:

$$\log r = \log A + \frac{E_a}{2.303R}\left(1/T\right) + \sum n_i\left(\log m_i\right) \tag{3.14}$$

We found values for A, E_a, and n_i with multiple linear regression models using JMP© software. Multiple regression involves fitting a dependent variable with a linear combination of independent variables using least squares analysis. We considered log m_{H+}, log P_{O2}, log $m_{Fe(III)}$, log m_{Cl-}, and 1/T as the regressors (or independent variables) and log r as the response (or dependent variable). Regressors had a significant effect on

the response when the significance level, or *p*-value, was < 0.0001. When the *p*-value for a certain regressor was > 0.0001, it was excluded from the regression. Thus, the values for A, E_a, and n_i were determined iteratively.

As will be seen below, chalcopyrite can dissolve oxidatively and nonoxidatively, depending upon the conditions. Based on previous experiments with chalcopyrite, and other sulfides, we expected some combination of pH, P_{O2}, $m_{Fe(III)}$, m_{Cl-}, and temperature to act as rate-controlling variables depending upon which reaction was fastest at a given set of conditions. We attempted to identify which reaction predominated at each set of conditions, and included the data that reflected the given reaction type and conditions in the regression. When inclusion of specific datasets in the regression caused violations of statistical validity or of chemical reality, such as a decreasing rate with increasing temperature or increasing oxidant concentration, we inferred that there was either a problem with those data or that the data were not consistent with the overall dataset, so we excluded them from the regression model.

3.4. Results

3.4.1. Nonoxidative Chalcopyrite Dissolution

We collected 68 rate measurements for chalcopyrite dissolution in the presence of O_2, with or without Cl^- present, of which 30 were used to determine the rate law (Fig. 3.2). Multiple linear regression yielded:

$$\log r = -2.35(0.44) - 1153(152)/T + 2.00(0.04) \log m_{H+} \quad (3.15)$$

where the numbers in parentheses are 1 standard error of the regression coefficient. The R^2 for this model is 0.995, and the empirical rate law is:

$$r = 10^{-2.35} e^{-22100/RT} m_{H^+}^{2.00} \quad (3.16)$$

The activation energy for this reaction is 22 ± 3 kJ mol^{-1}.

We obtained a best-fit model by excluding the rates of An04, Ca05, Co09, Do02, Li87, and Sa06 (these abbreviations refer to published studies as referenced in Table 3.1) from the regression. These data were excluded for the following reasons. The ore sample used in the An04 study contained other sulfides and oxides, in addition to chalcopyrite, which may have caused the rates to be much slower than most others. Additionally, the effective grain diameter (d_e) of the particles used in that experiment was larger than all

other experiments conducted in the presence of O_2. The larger grain size in the An04 experiments may have also contributed to the slower rates, given that smaller particles tend to dissolve quicker (e.g., Dutrizac, 1981; Palmer et al., 1981). The Ca05 rate measurement is from an experiment with pyritic sludge containing only 0.6 wt. % chalcopyrite, as well as other sulfide, sulfate, and silicate minerals. This rate is much faster than all others at similar conditions. Inclusion of the Ca05 rate in the regression causes the rate to be independent of temperature, which is unlikely. Two of the Co09 rates are slower than others at similar conditions. In these experiments, S^0 and jarosite formed on chalcopyrite grains during dissolution (Córdoba et al., 2009), which could account for the slower rates. The residuals for the Do02 rates varied over an order of magnitude, perhaps because the chalcopyrite samples were contaminated by other sulfides, quartz, gypsum, and clays. The Li87 rate was about 2 orders of magnitude faster than the others, likely because the experiment was conducted under P_{O2} of 1.7 atm, while most of the other experiments were conducted under P_{O2} of 0.21 atm. This rate may have been influenced by the chalcopyrite-DO reaction. The Sa06 rates were from experiments conducted on mill tailings with mixed mineralogy. The residuals of these rates vary over 2 orders of magnitude, and so many of them are much faster or much slower than rates measured at similar experimental conditions.

The remaining rates were nearly all based on experiments carried out in Cl^--bearing solutions. For consistency, we therefore excluded the Lu00 and Ac07 rates (3 total) that were from experiments without Cl^-. In a separate analysis, we regressed all the rates for experiments conducted in the presence of O_2 and found that temperature was the only variable that significantly affected the rate. The rate did not depend on P_{O2}, likely because most measurements were from experiments at P_{O2} of 0.21 atm. Over half of these rates were calculated for experiments conducted at 25ºC. At this temperature the rates varied over 2 orders of magnitude. This suggests that an additional variable (not included in this analysis) affected the rates for chalcopyrite dissolution in the presence of O_2.

3.4.2. Chalcopyrite Oxidation by Fe(III)

We collected 103 rate measurements for chalcopyrite oxidation by Fe(III), of which 38 were used to determine the rate law (Fig. 3.3). Multiple linear regression yielded:

$$\log r = 1.28(1.29) - 2316(459)/T + 0.74(0.08)\log m_{H+} + 0.43(0.06)\log m_{Fe(III)} \quad (3.17)$$

The R^2 for this model is 0.95, and the empirical rate law is:

$$r = 10^{1.28} e^{-44300/RT} m_{H^+}^{0.74} m_{Fe(III)}^{0.43} \quad (3.18)$$

Preliminary models showed that the log m_{Cl-} parameter was not a significant predictor of rate so we combined data for chalcopyrite oxidation by Fe(III) in the presence and absence of Cl^- to obtain the rate law. The activation energy for chalcopyrite oxidation by Fe(III) is 44 ± 9 kJ mol^{-1}.

To obtain the best fit, the An04, Du81, Ha95, Hi01, Li76, Pa81, and Sa92 (Table 3.1) rates were excluded from the regression. We consider the following as valid reasons for excluding those data. Issues with the An04 rates are given above. A few of the Du81 rates are much slower than all other rates. This may have resulted from formation of jarosite on chalcopyrite surfaces, which has been observed before in $Fe_2(SO_4)_3$ solutions like that used in the Du81 study (e.g., Córdoba et al., 2008; Córdoba et al., 2009). Regardless, inclusion of the Du81 data causes the rate law to be independent of temperature. The Ha95 rates are generally faster than most others. These rates are faster despite observed S^0 coatings on the chalcopyrite grains (Havlík et al., 1995). When the Ha95 rates are included, the rate law shows no dependence on temperature. The Hi01 data were excluded because one rate was much slower than the others, and some experiments included Fe(II) and Cu(II) in the leach solution, unlike other studies. The Li76 rates are much faster than all other rates, which likely resulted from leaching in HNO_3 solutions. Nitrate might have acted as an additional oxidant. The Pa81 rates vary over an order of magnitude, and inclusion of this data in the regression model causes temperature to have no significant affect on the rate. The Sa92 study did not report the pH of the initial leach solution or the pH during dissolution, so we did not include these rates in the regression model.

3.5. Discussion

3.5.1 Identifying the Predominant Reaction

The most difficult task in this study was identifying the reaction that was the main cause of the reported rate of chalcopyrite dissolution. Most experiments contained more than one species that was capable of reacting to cause chalcopyrite dissolution. For example, most of the reactions involving Fe(III) contained relatively high hydrogen ion activities and were carried out in contact with air so they contained some DO. We developed the following guidelines to help identify which of these possible reactants caused the predominant (fastest) reaction: 1) if an experiment containing a possible reactive species showed reaction rates that were comparable to an experiment without that reactive species, we concluded that the possible reactive species did not contribute to the rate; 2) if the regression coefficient for a possible reactive species did not appear to be significant in our regression models, we concluded that the species did not contribute to the rate. As a result of these guidelines, we determined that none of the experiments considered here gave rates that we could assign to chalcopyrite dissolution resulting from oxidation by DO alone.

3.5.2. Nonoxidative Chalcopyrite Dissolution

The rate law calculated for nonoxidative dissolution of chalcopyrite (3.15 and 3.16) shows that the rate depends only on temperature and m_{H+} (Fig. 3.2). Even though all of the experiments were performed with solutions that contained DO, the regression model showed that the effect of increased P_{O2} on the rate was not significant, so this variable therefore does not appear in the rate law. Lin et al. (1986) showed that leaching rates increased when P_{O2} was raised from 1.7 to 30.6 atm at 90ºC, but at 25ºC and lower P_{O2}, chalcopyrite dissolution rates were the same at P_{O2} of 0.21, 0.05, and 0.005 atm (Acero et al., 2007). Likewise, chalcopyrite-bearing pyritic sludge leached in Cl^--bearing solution showed no change in dissolution rate under P_{O2} atmospheres ranging from 0.00074 to 0.20 atm at 22ºC (Domènech et al., 2002).

The positive dependence of the dissolution rate on pH (Fig. 3.2c) is consistent with nonoxidative dissolution (reaction 3.1). When the solution contains high hydrogen ion activities a number of complicated parallel reactions also occur. For example, the

Fe(III) produced presumably reacts quickly with H_2S to form sulfur species with intermediate oxidation states. This reaction is evident in previous experiments where elemental sulfur (S^0) formed a porous product layer on dissolving grains (Dutrizac, 1990; Havlík et al., 1995; Lu et al., 2000). Others have observed sulfate, polysulfides, and sulfides, in addition to S^0, on chalcopyrite surfaces reacted with acidic, Cl-bearing solutions (Abraitis et al., 2004; Acero et al., 2007). Acero et al. (2007) did not observe a passivating effect due to the formation of various S phases on chalcopyrite surfaces in long-term leach experiments. In this context, 'passivation' refers to a decrease in chalcopyrite dissolution over time due to the eventual formation of an armoring layer (Klauber, 2008).

3.5.3. Chalcopyrite Oxidation by Fe(III)

Most of the rate measurements for chalcopyrite oxidation by Fe(III) were based on experiments conducted at relatively high $m_{Fe(III)}$ and m_{H+} (Fig. 3.1). The rate law calculated for chalcopyrite oxidation by Fe(III) (3.17 and 3.18) indicates that the rate depends significantly upon temperature, m_{H+}, and $m_{Fe(III)}$ (Fig. 3.3). If the rates calculated by equation (3.18) represent the total reaction rate (r_{total}), due to both nonoxidative dissolution and oxidation by Fe(III), and the rates calculated by equation (3.16) represent nonoxidative rates (r_{H+}) only, we might expect the rate of oxidation by Fe(III) only ($r_{Fe(III)}$) to be $r_{Fe(III)} = r_{total} - r_{H+}$ if the r_{total} rate represents parallel r_{H+} and $r_{Fe(III)}$ rates. According to this calculation, at a given temperature, pH, and $m_{Fe(III)}$, $r_{Fe(III)}$ is essentially the same as r_{total} because r_{H+} is 2 orders of magnitude slower than r_{total}. Thus, r_{total} resulting from parallel r_{H+} and $r_{Fe(III)}$ rates is not valid, and $r_{Fe(III)}$ shows a dependence on pH for some other reason, such as a lowered activation barrier for $r_{Fe(III)}$ with increasing m_{H+}. Further work is needed to characterize the pH dependence of $r_{Fe(III)}$.

X-ray photoelectron spectroscopy (XPS) and scanning electron microscopy (SEM) show that when chalcopyrite grains react with solutions containing high concentrations of Fe(III) they develop a leach layer that is enriched in sulfate (a jarosite-like phase) (Parker et al., 2003; Klauber, 2008), disulfide (a metal-S^{2-} phase) (Klauber et al., 2001; Parker et al., 2003), and/or S^0 (Rimstidt et al., 1994; Klauber et al., 2001; Parker et al., 2003; Klauber, 2008). Thus, although chalcopyrite dissolution by Fe(III)

likely follows reaction (3.4) for relatively low Fe(III) concentrations, it seems to have a stoichiometry that approaches

$$CuFeS_{2(s)} + 4Fe^{3+}_{(aq)} = Cu^{2+}_{(aq)} + 5Fe^{2+}_{(aq)} + 2S^{0}_{(s)} \quad (3.19)$$

for high Fe(III) concentrations.

3.5.4 Effect of Cl^-

There are numerous reports of enhanced chalcopyrite dissolution rates with increasing Cl^- concentrations (e.g., Muñoz-Ribadeneira and Gomberg, 1971; Palmer et al., 1981; Majima et al., 1985; Lu et al., 2000; Al-Harahsheh et al., 2008). Improved leaching in Cl^--bearing, oxygenated, acid solutions is believed to result from the formation of intermediate mixed-ligand (e.g., Cu(OH)Cl, $Cu_2(Cl(OH_3))$ complexes on mineral surfaces (Senanayake, 2009), which are conducive to ligand-promoted dissolution. While increased m_{Cl^-} in leaching solutions has been shown to increase chalcopyrite dissolution rates in individual studies, log m_{Cl^-} was found to have an insignificant affect on the rate for the reactions considered in this meta-analysis. This may have resulted from using rate measurements that were from experiments conducted at pH ≤ 3. At low pH, nonoxidative dissolution may predominate over ligand-promoted dissolution. Additional experiments with chalcopyrite leaching by Cl^--bearing solutions, conducted at higher pH, might reveal more of a rate dependence on m_{Cl^-}.

3.5.5. Comparison of Chalcopyrite and Pyrite Dissolution Rates

The chalcopyrite dissolution rate laws determined in this compilation and meta-analysis can be compared to those for pyrite oxidation by O_2 only and by Fe(III) in the presence of O_2 (Williamson and Rimstidt, 1994) (Fig. 3.4). At pH ≤ 4, pyrite oxidation by Fe(III) in the presence of O_2 is 4 orders of magnitude faster than Fe(III)-oxidative chalcopyrite dissolution (Fig. 3.4). Sulfide oxidation by Fe(III) is fast at low pH, and is enhanced when O_2 is present. This is likely due to the combined effects of Fe(III) and O_2 oxidation, as well as nonoxidative dissolution.

During chalcopyrite and pyrite dissolution, Fe is released to solution and is cycled between the reduced and oxidized states by microbial Fe(II)-oxidation and consumption of oxidant Fe(III) during sulfide oxidation (e.g., reactions 3.4 and 3.19). Given the

characteristic presence of Fe(II)/(III) in acidic leaching solutions near sulfide deposits, Fe(III)-oxidative sulfide dissolution is likely to predominate over sulfide oxidation by O_2 at low pH. This is reflected in the slower calculated rates for nonoxidative chalcopyrite dissolution where Fe(III) was not initially present in leach solutions relative to Fe(III)-oxidative chalcopyrite dissolution (Fig. 3.4). With increasing pH, Fe(III) becomes less soluble, and tends to precipitate into various Fe(III) (oxyhydr)oxide minerals. As a result, sulfide oxidation by O_2 is likely to become more important at higher pH, as shown by the increasing pyrite oxidation by O_2 with increasing pH (Fig. 3.4). Assuming the rate law for pyrite oxidation by Fe(III) applies to pH values beyond the experimental maximum of about 3, and that the activity of Fe(III) is controlled by ferrihydrite solubility (log Keq (25ºC) = 4.89, Drever, 1997), the rate of oxidation of pyrite by O_2 overtakes that for oxidation of pyrite by Fe(III) between pH 4 and 5 at 25°C (Fig. 3.4). The rate of oxidation of chalcopyrite by O_2 is likely to be faster at higher pH as well. Future work is needed that focuses on chalcopyrite dissolution in the presence of O_2 at pH $\geq$ 3. Such experiments would provide the data needed to determine the dependence of the rate of chalcopyrite dissolution on DO.

The activation energies determined for nonoxidative chalcopyrite dissolution (22 ± 3 kJ mol^{-1}) and Fe(III)-oxidative chalcopyrite dissolution (44 ± 9 kJ mol^{-1}) are within the range of activation energies reported previously for chalcopyrite dissoluion (15 – 95 kJ mol^{-1}; Table 3.2). The wide range of reported activation energies (Table 3.2) likely results from differences in experimental design, leach solutions, preparation of starting materials, and starting mineral samples among the different studies. The chalcopyrite dissolution rates included in this compilation come from experiments conducted at temperatures ranging from 3.5 – 95°C, with most experiments conducted at 25°C or between 65 and 95°C (Fig. 3.1b). Inhomogeneous distribution of the data over the given temperature range likely contributes to the relatively large uncertainty associated with the activation energy estimates.

3.5.6 Future Work

Figure 3.1a shows the reported and calculated rate measurements (log r) plotted versus log m_{H+} and log P_{O2} or log $m_{Fe(III)}$. Dissolution experiments were mostly

conducted at pH ≤ 3; thus, the rate laws derived in this work will apply most approporiately to acidic conditions. Future experiments should focus on chalcopyrite dissolution at higher pH in order to generate the kinetic data needed to derive rate laws for dissolution under such conditions. Furthermore, for those experiments where Fe(III) was initially present in the leach medium, the oxidant concentrations were relatively high in a majority of the studies (Fig. 3.1a). Additional experiments with leach solutions containing lower $m_{Fe(III)}$, like those of (Rimstidt et al., 1994), may provide rate measurements that will allow us to better characterize the rate dependence of chalcopyrite oxidation by Fe(III).

3.5.7. Summary

Using published kinetic data for chalcopyrite dissolution, we compiled rates of dissolution, then conducted a meta-analysis in order to determine rate laws for chalcopyrite dissolution. Chalcopyrite dissolution rates were taken directly from the literature or were calculated with the initial rate method and the shrinking particle model using data available in the literature. We performed multiple linear regression analysis to determine the dependence of log rate on the independent variables 1/T, log m_{H+}, log P_{O2}, log $m_{Fe(III)}$, and log m_{Cl-}.

The regression models for experiments that did not contain Fe(III) showed that chalcopyrite dissolution in acidic solutions with a pH less than 3.5 is influenced only by temperature and hydrogen ion activity. From this we conclude that the experiments considered in our model produced data for the nonoxidative dissolution reaction (3.1), even though most studies were carried out at oxygen partial pressures of 0.21 atm. Future measurements of the rate of chalcopyrite dissolution in oxic solutions at higher pH are necessary in order to determine a rate law for chalcopyrite oxidation by DO. Interestingly, we found that m_{Cl-} (ranging from 0 – 5.5 M) also does not affect the rate at pH ≤ 3, despite the conventional practice of leaching with acidic Cl^- solutions as a means of increasing metal extraction efficiency (e.g., Muñoz-Ribadeneira and Gomberg, 1971). Experimenting with chalcopyrite dissolution in oxic, Cl^--bearing solutions at higher pH may also reveal a rate dependence on m_{Cl-}.

The regression model for experiments that contained Fe(III) showed that the rates were influenced by temperature, hydrogen ion activity, and Fe(III) activity. Although these results give strong support for the reaction stoichiometry given in equation (3.4), the cause of the positive correlation between rate and hydrogen ion activity is at present unclear. Figure 3.4 shows that predicted chalcopyrite dissolution rates are about 4 orders of magnitude slower than pyrite rates in ARD settings where Fe(III) is the predominant oxidant.

This chalcopyrite dissolution rate synthesis and meta-analysis has provided insights into the mechanisms by which chalcopyrite dissolves in low pH, O_2- and/or Fe(III)-bearing solutions. The determined rate laws will benefit those concerned with predicting Cu concentrations during ARD and during hydrometallurgical leaching. This compilation has also highlighted gaps in the chalcopyrite dissolution rate database. Future experimentation with chalcopyrite dissolution at pH > 3 and at lower oxidant concentrations will help close these gaps and complete our understanding of chalcopyrite dissolution over a wider range of conditions.

3.6. References

Abraitis P. K., Pattrick R. A. D., Kelsall G. H., and Vaughan D. J. (2004) Acid leaching and dissolution of major sulphide ore minerals: process and galvanic effects in complex systems. *Mineralogical Magazine* **68**(2), 343-351.

Acero P., Cama J., and Ayora C. (2007) Kinetics of chalcopyrite dissolution at pH 3. *European Journal of Mineralogy* **19**, 173-182.

Adebayo A., Ipinmoroti K., and Ajayi O. (2003) Dissolution kinetics of chalcopyrite with hydrogen peroxide in sulphuric acid medium. *Chemical and Biochemical Engineering Q* **17**, 213-218.

Al-Harahsheh M., Kingman S., and Al-Harahsheh A. (2008) Ferric chloride leaching of chalcopyrite: Synergistic effect of CuCl2. *Hydrometallurgy* **91**, 89-97.

Alva A. K., Huang B., and Paramasivam S. (2000) Soil pH affects copper fractionation and phytotoxicity. *Soil Science Society of America Journal* **64**, 955-962.

Antonijević M. M. and Bogdanović G. D. (2004) Investigation of the leaching of chalcopyrite ore in acidic solutions. *Hydrometallurgy* **73**, 245-256.

Antonijević M. M., Janković Z. D., and Dimitrijević M. D. (2004) Kintetics of chalcopyrite dissolution by hydrogen peroxide in sulphuric acid. *Hydrometallurgy* **71**, 329-334.

Ammou-Chokroum M., Cambazoglu M., and Steinmetz D. (1977) Oxidation menagee de la chalcopyrite en solution acide: analyse cinetique des reactions. *Bulletin de la Societe Françise de Mineralogie et de Cristallophraphie* **100**, 149-161.

Aydogan S., Ucar G., and Canbazoglu M. (2006) Dissolution kinetics of chalcopyrite in acidic potassium dichromate solution. *Hydrometallurgy* **81**, 45-51.

Bartlett R. W. (1997) Metal extraction from ores by heap leaching. *Metallurgical and Materials Transactions B* **28B**, 529-545.

Brantley S. L. (2003) Reaction kinetics of primary rock-forming minerals under ambient conditions. In *Treatise on Geochemistry*, Vol. 5 (ed. H. D. Holland and K. K. Turekian), pp. 73-117. Elsevier.

Brantley S. L. and Chen Y. (1995) Chemical weathering rates of pyroxenes and amphiboles. In *Reviews in Mineralogy and Geochemistry*, Vol. 31 (ed. A. F. White and S. L. Brantley), pp. 119-172.

Brantley S. L. and Conrad C. F. (2008) Analysis of rates of geochemical reactions. In *Kinetics of Water-Rock Interaction* (ed. S. L. Brantley, J. D. Kubicki, and A. F. White), pp. 1-37. Springer.

Burkin A. R. (2001) *Chemical Hydrometallurgy*. Imperial College Press.

Cama J. and Acero P. (2005) Dissolution of minor sulphides present in a pyritic sludge at pH 3 and 25C □□□. *Geologica Acta* **3**(1), 15-26.

Córdoba E. M., Muñoz J. A., Blázquez M. L., González F., and Ballester A. (2008) Leaching of chalcopyrite with ferric ion. Part II. Effect of redox potential. *Hydrometallurgy* **93**, 88-96.

Córdoba E. M., Muñoz J. A., Blázquez M. L., González F., and Ballester A. (2009) Passivation of chalcopyrite during its chemical leaching with ferric ion at 68C. *Minerals Engineering* **22**, 229-235.

Domènech C., de Pablo J., and Ayora C. (2002) Oxidative dissolution of pyritic sludge from the Aznalcóllar mine (SW Spain). *Chemical Geology* **190**, 339-353.

Drever J. I. (1997) *The Geochemistry of Natural Waters: Surface and Groundwater Environments*. Prentice Hall.

Dutrizac J. E. (1978) The kinetics of dissolution of chalcopyrite in ferric ion media. *Metallurgical Transactions B* **9**, 431-439.

Dutrizac J. E. (1981) The dissolution of chalcopyrite in ferric sulfate and ferric chloride media. *Metallurgical Transactions B* **12B**, 371-378.

Ermilov V. V., Tkachenke O. B., and Tseft A. L. (1969) Kinetics of the dissolution of chalcopyrite in ferric chloride. *Trudy Instituta Metallov Obogashch* **30**, 3-14.

Ferreira R. C. H. and Burkin A. R. (1975) Acid leaching of chalcopyrite. In *Leaching and Reduction in Hydrometallurgy* (ed. A. R. Burkin), pp. 54-66. Institution of Mining and Metalllurgy.

Havlík T. and Kammel R. (1995) Leaching of chalcopyrite with acidified ferric chloride and carbon-tetrachloride addition. *Minerals Engineering* **8**, 1125-1134.

Havlík T., Škrobian M., Baláž P., and Kammel R. (1995) Leaching of chalcopyrite concentrate with ferric chloride. *International Journal of Minerals Processing* **43**, 61-72.

Hill C. G. (1977) *An Introduction to Chemical Engineering Kinetics and Reactor Design*. John Wiley & Sons, Inc.

Hirato T., Kinoshita M., Awakura Y., and Majima H. (1986) The leaching of chalcopyrite with ferric-chloride. *Metallurgical Transactions B* **17**, 19-28.

Hiroyoshi N., Miki H., Hirajima T., and Tsunekawa M. (2001) Enhancement of chalcopyrite leaching by ferrous ions in acidic ferric sulfate solutions. *Hydrometallurgy* **60**, 185-197.

Klauber C. (2008) A critical review of the surface chemistry of acidic ferric sulphate dissolution of chalcopyrite with regards to hindered dissolution. *International Journal of Mineral Processing* **86**, 1-17.

Klauber C., Parker A., van Bronswijk W., and Watling H. (2001) Sulphur speciation of leached chalcopyrite surfaces as determined by X-ray photoelectron spectroscopy. *International Journal of Mineral Processing* **62**, 65-94.

Le Houillier R. and Ghali E. (1982) Contribution to the study of the leaching of chalcopyrite. *Hydrometallurgy* **9**(2), 169-194.

Lengke M. F., Sanpawanitchakit C., and Tempel R. N. (2009) The oxidation and dissolution of arsenic-bearing sulfides. *The Canadian Mineralogist* **47**, 593-613.

Levenspiel O. (1972) *Chemical reaction engineering*. Wiley.

Lin H. and Sohn H. (1987) Mixed-control kinetics of oxygen leaching of chalcopyrite and pyrite from porous primary ore materials. *Metallurgical Transactions B* **18**, 497-503.

Lin H. K., Sohn H. Y., and Wadsworth M. E. (1986) The kinetics of leaching of chalcopyrite and pyrite grains in primary copper ore by dissolved oxygen. In *Hydrometallurgical Reactor Design and Kinetics* (ed. R. G. Bautista, R. J. Wesely, and G. W. Warren), pp. 149-168. The Metallurgical Society, Inc.

Linge H. G. (1976) A study of chalcopyrite dissolution in acidic ferric nitrate by potentiometric titration. *Hydrometallurgy* **2**, 51-64.

Lu Z. Y., Jeffrey M. I., and Lawson F. (2000) The effect of chloride ions on the dissolution of chalcopyrite in acidic solutions. *Hydrometallurgy* **56**, 189-202.

Majima H., Awakura Y., Hirato T., and Tanaka T. (1985) The leaching of chalcopyrite in ferric chloride and ferric sulfate solutions. *Canadian Metallurgical Quarterly* **24**(4), 283-291.

Maurice D. and Hawk J. A. (1998) Ferric chloride leaching of mechanically activated chalcopyrite. *Hydrometallurgy* **49**, 103-123.

Munoz P., Miller J., and Wadsworth M. (1979) Reaction-mechanism for the acid ferric sulfate leaching of chalcopyrite. *Metallurgical Transactions B* **10**, 149-158.

Muñoz-Ribadeneira F. J. and Gomberg H. J. (1971) Leaching of chalcopyrite ($CuFeS_2$) with sodium chloride sulfuric acid solutions. *Nuclear Technology* **11**, 367-371.

Nesse W. D. (2000) *Introduction to Mineralogy*. Oxford University Press.

Ngoc N. V., Shamsuddin M., and Prasad P. M. (1990) Oxidative leaching of an offgrade/complex copper concentrate in chloride lixiviants. *Metallurgical Transactions B* **21**, 611-619.

Nordstrom D. K. and Southam G. (1997) Geomicrobiology of sulfide mineral oxidation. *Reviews in Mineralogy and Geochemistry* **35**, 361-390.

O'Malley M. L. and Liddell K. C. (1986) A rate equation for the initial stage of the leaching of $CuFeS_2$ by aqueous $FeCl_3$, HCl and NaCl. In *Hydrometallurgical Reactor Design and Kinetics* (ed. R. G. Bautista, R. J. Wesely, and G. W. Warren), pp. 67-73. The Metallurgical Society, Inc.

Orth R. J. and Liddell K. C. (1990) Rate law and mechanism for the oxidation of copper(I) by iron(III) in hydrochloric acid solutions. *Industrial Engineering and Chemistry Research* **29**, 1178-1183.

Palmer B. R., Nebo C. O., Rau M. F., and Fuerstenau M. C. (1981) The phenomena involved in the dissolution of chalcopyrite in chloride-bearing lixiviants. *Metallurgical Transactions B* **12B**, 595-601.

Parker A., Klauber C., Kougianos A., Watling H., and van Bronswijk W. (2003) An X-ray photoelectron spectroscopy study of the mechanism of oxidative dissolution of chalcopyrite. *Hydrometallurgy* **71**, 265-276.

Prosser A. P. (1996) Review of uncertainty in the collection and interpretation of leaching data. *Hydrometallurgy* **41**, 119-153.

Rimstidt J. D., Chermak J. A., and Gagen P. M. (1994) Rates of reaction of galena, sphalerite, chalcopyrite, and arsenopyrite with Fe(III) in acidic solutions. In *Environmental geochemistry of sulfide oxidation*, Vol. 550 (ed. C. N. Alters and D. W. Blowes), pp. 2-13. American Chemical Society.

Rimstidt J. D. and Newcomb W. D. (1993) Measurement and analysis of rate data: The rate of reaction of ferric iron with pyrite. *Geochimica Cosmochimica Acta* **57**, 1919-1934.

Rimstidt J. D. and Vaughan D. J. (2003) Pyrite oxidation: a state-of-the-art assessment of the reaction mechanism. *Geochimica Cosmochimica Acta* **67**, 873-880.

Rosso K. M. and Vaughan D. J. (2006) Reactivity of sulfide mineral surfaces. *Reviews in Mineralogy and Geochemistry* **61**, 557-607.

Salmon S. U. and Malmström M. E. (2006) Quantification of mineral dissolution rates and applicability of rate laws: Laboratory studies of mill tailings. *Applied Geochemistry* **21**, 269-288.

Saxena N. N. and Mandre N. R. (1992) Mixed control kinetics of copper dissolution for copper ore using ferric chloride. *Hydrometallurgy* **28**, 111-117.

Schumbauer-Berigan M. K., Dierkes J. R., Monson P. D., and Ankley G. T. (1993) pH-dependent toxicity of Cd, Cu, Ni, Pb, and Zn to *Ceriodaphnia dubia, Pimephales promelas, Hayalella azteca* and *Lumbriculus variegatus*. *Environmental Toxicology and Chemistry* **12**, 1261-1266.

Schwertmann U. and Fitzpatrick R. (1992) Iron Minerals in Surface Environments. In *Biomineralization: Processes of Iron and Manganese: Modern and Ancient Environments* (ed. H. Skinner and R. Fitzpatrick), pp. 7-30. Catena Verlag.

Senanayake G. (2009) A review of chloride assisted copper sulfide leaching by oxygenated sulfuric acid and mechanistic considerations. *Hydrometallurgy* **98**, 21-32.

Tester J. W., Worley G., Robinson B. A., Grisby C. O., and Feerer J. L. (1994) Correlating quartz dissolution kinetics in pure water from 25 to 625°C. *Geochimica Cosmochimica Acta* **58**, 2407-2420.

Williamson M. A. and Rimstidt J. D. (1994) The kinetics and electrochemical rate-determining step of aqueous pyrite oxidation. *Geochimica Cosmochimica Acta* **58**(24), 5443-5454.

Yin Q., Kelsall G. H., Vaughan D. J., and England K. E. R. (1995) Atmospheric and electrochemical oxidation of the surface of chalcopyrite ($CuFeS_2$). *Geochimica Cosmochimica Acta* **59**, 1091-1100.

Table 3.1. Identification, experimental conditions, and rate calculation method used for studies included in this compilation.

Identifier-Reference	Experimental Conditions	Rate Calculation Method (RPV)	Notes (data source)
Ab04-(Abraitis et al., 2004)	pH = 2.5 (HCl); T = 298K; P_{O2} = 0.21 atm, m_{Cl-} = 0.1; grainsize = 45 – 150 μm; A_{geo} = 0.02 m^2/g; BR	SPM (Cu)	(graph)
Ac07-(Acero et al., 2007)	pH = 3 (HCl); T = 298K; P_{O2} = 0.21 atm; m_{Cl-} = 0.001; A_{BET} = 0.71 m^2/g; grainsize = 10 – 100 μm; A_{geo} = 0.04 m^2/g; MFR	Reported in article (Fe)	(table)
Al08-(Al-Harahsheh et al., 2008)	m_{H+} = 0.5 (HCl); 343 ≤ T ≤ 363K; P_{O2} = 0.21 atm; m_{Cl-} = 1.5; $m_{Fe(III)}$ = 0.5; grainsize ≤ 38 μm; A_{geo} = 0.038, 1.4 m^2/g; BR	SPM (Cu)	(graph)
An04-(Antonijević and Bogdanović, 2004)	pH = 0.5, 0.7, 1.0, 1.3, 2.0 (H_2SO_4); T = 298K; P_{O2} = 0.21 atm; $m_{Fe(III)}$ = 0, 0.02, 0.09, 0.18, 0.27, 0.36; grainsize ≤ 5 mm; A_{geo} = 0.008 m^2/g; PFR	SPM (Cu)	(graph)
Ca05-(Cama and Acero, 2005)	pH = 3.0 (HCl); T = 298K; P_{O2} = 0.21 atm; grainsize = 10 – 100 μm; A_{BET} = 0.44 m^2/g; FR	Reported in article (Cu)	Pyritic sludge (table)
Co09-(Córdoba et al., 2009)	pH = 0.5, 1, 1.5, 1.8, 2 (H_2SO_4); T = 341K; P_{O2} = 0, 0.21 atm; $m_{Fe(III)}$ = 0.02; A_{BET} = 0.07 m^2/g; grainsize ≤ 70 μm; A_{geo} = 0.51 m^2/g; BR	SPM = IRM (Cu)	(graph)
Do02-(Domènech et al., 2002)	2.53 ≤ pH ≤ 4.75; T = 295K; P_{O2} = 0.20, 0.09, 0.0044, 0.00074 atm; m_{Cl-} = 7.2 x 10^{-5} – 2.4 x 10^{-3}; grainsize average = 12 μm; A_{BET} = 1.2 m^2/g; A_{geo} = 0.12 m^2/g; FR	Reported in article (SO_4)	Pyritic sludge (table)
Du81-(Dutrizac, 1981)	m_{H+} = 0.3 (H_2SO_4); T = 363K; P_{O2} ≤ 0.21 atm; $m_{Fe(III)}$ = 0, 0.1, 0.3, 0.5, 1.5; grainsize = 10 – 152 μm; A_{geo} = 0.01, 0.04, 0.06, 0.08, 0.12 m^2/g; BR	SPM = IRM (Cu)	(graph)
Fe75-(Ferreira and	pH = 1 (H_2SO_4); T = 323, 338,	SPM = IRM (Cu)	(graph)

Burkin, 1975)	353, 368K; $m_{Fe(III)}$ = 0.001, 0.03; grainsize = 53 – 153 μm; A_{geo} = 0.011, 0.016, 0.023 m^2/g; BR		
Ha95-(Havlík et al., 1995)	m_{H+} = 0.25, 0.5, 0.75 (HCl); T = 276.5, 293, 313, 323, 333, 343, 353K; P_{O2} = 0 atm; $m_{Fe(III)}$ = 0.5, 1.0; m_{Cl-} = 1.5, 3.0; grainsize = 200 – 315 μm; A_{geo} = 0.006 m^2/g; BR	SPM = IRM (Cu)	(graph)
Hi01-(Hiroyoshi et al., 2001)	m_{H+} = 0.1 (H2SO4); T = 303K; P_{O2} = 0 atm; $m_{Fe(III)}$ = 0.25; A_{geo} = 0.48 m^2/g (BR); $m_{Fe(III)}$ = 0.03; grainsize ≤ 75 μm; A_{geo} = 0.01 m^2/g (PFR)	SPM = IRM (BR); SPM (PFR) (Cu)	(graph)
Li76-(Linge, 1976)	m_{H+} = 0.01 (HNO_3); T = 298K; P_{O2} = 0 atm; $m_{Fe(III)}$ = 0.0002; grainsize = 390 – 460 mm; A_{geo} = 0.0003 m^2/g; BR	IRM (Cu)	(graph)
Li86-(Lin et al., 1986)	pH = 1.78 (H_2SO_4); T = 363K; P_{O2} = 1.7 atm; grainsize = 53 – 75 μm; A_{geo} = 0.023 m^2/g; BR	SPM = IRM (Cu)	(graph)
Lu00-(Lu et al., 2000)	m_{H+} = 0.8 (H_2SO_4); T = 303K; P_{O2} = 0.21, 1 atm; m_{Cl-} = 0, 0.5, 1, 2; grainsize not reported; A_{geo} = 0.10, 0.36 m^2/g; BR	SPM = IRM (Cu)	(graph)
Ma85-(Majima et al., 1985)	m_{H+} = 0.2 (HCl, H_2SO_4); T = 343K; m_{Cl-} = 0, 3.2; $m_{Fe(III)}$ = 1; grainsize not reported; BR	Reported in article (Cu)	(graph)
Mu71-(Muñoz-Ribadeneira and Gomberg, 1971)	m_{H+} = 1 (H_2SO_4); T = 298K; P_{O2} = 0.21 atm; m_{Cl-} = 0, 0.05, 0.10, 0.25, 0.5, 0.75, 1; grainsize = 74 – 105 μm; A_{geo} = 0.02 m^2/g; BR	SPM = IRM (Cu)	(graph)
Om87-(O'Malley and Liddell, 1986)	m_{H+} = 0.4, 3 (HCl); T = 368K; P_{O2} = 0 atm; m_{Cl-} = 3.7; $m_{Fe(III)}$ = 0.1; grainsize = 45 – 53 μm; A_{geo} = 0.03 m^2/g; BR	SPM = IRM (Cu)	(graph)
Pa81-(Palmer et al., 1981)	m_{H+} = 0.2, 1 (HCl); T = 348, 353, 355.5, 359.5, 363, 365.5, 369K; P_{O2} = 0 atm; m_{Cl-} = 0.8, 1.2, 1.8, 2.8, 3.8, 4.06, 4.15, 4.3, 4.75, 5.5; $m_{Fe(III)}$ = 0.02, 0.05, 0.1, 0.2, 0.25, 0.5; grainsize = 37 – 53 μm; A_{geo} =	SPM = IRM (Cu)	(graph)

	0.03, 0.04 m^2/g; BR		
Ri94-(Rimstidt et al., 1994)	$1.86 \leq pH \leq 1.93$; T = 313, 333K; P_{O2} = 0.21 atm; A_{BET} = 0.049 m^2/g; grainsize = 152 – 251 μm; A_{geo} = 0.0073 m^2/g; MFR	Reported in article (Fe)	(table)
Sa92-(Saxena and Mandre, 1992)	T = 303, 323, 343, 363K; P_{O2} = 0.21 atm; m_{Cl-} = 0.6; $m_{Fe(III)}$ = 0.2; grainsize = 74 – 104 μm; A_{geo} = 0.02 m^2/g; BR	SPM = IRM (Cu)	(graph)
Sa06-(Salmon and Malmström, 2006)	$2 \leq pH \leq 3.5$ (H_2SO_4, HNO_3); T = 296K; P_{O2} = 0.21 atm; grainsize not reported; BR	Reported in article (Cu)	Mill tailings (table)

RPV = reaction progress variable, BR = batch reactor, MFR = mixed flow reactor, PFR = plug flow reactor, SPM = shrinking particle model, IRM = initial rate model

Table 3.2. Reported activation energies for chalcopyrite dissolution in acidic, Cl- and/or SO_4-bearing solutions.

Reference	Solution Description	T(ºC)	Ea (kJ mol^{-1})
Saxena & Mandre (1992)	Iron(III) chloride	30-90	15-28
Aydogan et al. (2006)	Potassium dichromate in sulfuric acid	50-97	24
Acero et al. (2007)	Hydrochloric acid pH 3	25-70	32 ± 5
Le Houillier & Ghali (1982)	Sulfuric acid pH 1	70-110	30
Ammou-Chokroum et al. (1977)	Iron(III) chloride	25-75	38 ± 4
Dutrizac (1978)	Iron(III) sulfate	30-95	38-63
Adebayo et al. (2003)	Hydrogen peroxide in sulfuric acid	30-80	39
Ngoc et al. (1990)	Iron(III) chloride + hydrochloric acid	65-110	38
Dutrizac (1978)	Iron(III) chloride	30-100	44 ± 3
Dutrizac (1981)	Iron(III) chloride	30-100	42-46
Ferreira and Burkin (1975)	Iron(III) sulfate	30-100	42
Lu et al. (2000)	Mixed hydrochloric-sulfuric acid	60-95	48
Ermilov et al. (1969)	Iron(III) chloride	60-106	50
Havlik et al. (1995)	Iron(III) chloride	3.5-80	55 ± 5
Antonijevic et al. (2004)	Hydrogen peroxide in sulfuric acid	25-50	60
Palmer et al. (1981)	Iron(III) chloride + hydrochloric acid	80-100	62
Lin & Sohn (1987)	Hydrochloric acid pH 2	75-97	64
Maurice and Hawk (1998)	Iron(III) chloride + hydrochloric acid + NaCl	60-90	68
Majima et al. (1985)	Iron(III) chloride	55-85	69
Havlik and Kammel (1995)	Iron(III) chloride	45-80	69
Hirato et al. (1986)	Iron(III) chloride + hydrochloric acid	52-85	69
Palmer et al. (1981)	Iron(III) chloride + hydrochloric acid + NaCl	82.5-96	83
Munoz et al. (1979)	Iron(III) sulfate	20-112	83.7
Linge et al. (1976)	Iron(III) nitrate	25-40	95

Appendix 3A. *Compiled Chalcopyrite Oxidation Rate Data*
Physiochemical conditions for chalcopyrite dissolution in the presence of O_2 and absence of Cl^-. Temperature is in Kelvins, and rates are in units of mol m^{-2} s^{-1}.

Identifier	$\log m_{H+}$	T	$\log P_{O2}$	r	$\log r$
Ac07	-3.00	298	-0.678	5.81E-13	-12.2
An04	-1.00	298	-0.678	1.42E-11	-10.8
An04	-1.00	298	-0.678	1.05E-11	-11.0
An04	-1.00	298	-0.678	2.13E-11	-10.7
An04	-0.50	298	-0.678	1.32E-12	-11.9
An04	-0.70	298	-0.678	1.81E-12	-11.7
An04	-1.00	298	-0.678	2.33E-12	-11.6
An04	-1.30	298	-0.678	1.79E-12	-11.7
An04	-2.00	298	-0.678	1.58E-12	-11.8
Ca05	-3.00	298	-0.678	2.21E-11	-10.7
Co09	-0.50	341	-0.678	6.06E-09	-8.22
Co09	-1.00	341	-0.678	7.97E-09	-8.10
Co09	-1.50	341	-0.678	1.05E-08	-7.98
Co09	-2.00	341	-0.678	1.08E-08	-7.97
Co09	-1.80	341	-0.678	6.91E-09	-8.16
Co09	-1.80	341	-0.678	6.94E-09	-8.16
Co09	-1.80	341	-0.678	9.48E-09	-8.02
Co09	-1.80	341	-0.678	2.52E-08	-7.60
Co09	-1.80	341	-0.678	2.52E-08	-7.60
Li87	-1.78	363	0.231	1.64E-07	-6.78
Lu00	-0.10	368	0	7.63E-07	-6.12
Lu00	-0.10	368	0	1.77E-07	-6.75
Sa06	-2.30	296	-0.678	6.52E-13	-12.2
Sa06	-2.70	296	-0.678	8.54E-13	-12.1
Sa06	-2.30	296	-0.678	2.03E-12	-11.7
Sa06	-2.90	296	-0.678	6.29E-12	-11.2
Sa06	-3.80	296	-0.678	3.23E-12	-11.5
Sa06	-3.80	296	-0.678	2.67E-13	-12.6

Appendix 3A. (Continued)
Physiochemical conditions for chalcopyrite dissolution in the presence of O_2 and Cl^-.

Identifier	$\log m_{H+}$	T	$\log P_{O2}$	$\log m_{Cl-}$	r	$\log r$
Ab04	-1	298	-0.678	-1	1.66E-08	-7.78
Ac07	-3	298	-0.678	-3	4.25E-13	-12.4
Ac07	-3	323	-0.678	-3	9.38E-13	-12.0
Ac07	-3	343	-0.678	-3	3.38E-12	-11.5
Ac07	-3	298	-1.301	-3	5.06E-13	-12.3
Ac07	-3	298	-2.301	-3	4.19E-13	-12.4
Ac07	-3	298	-0.678	-3	5.88E-13	-12.2
Ac07	-3	298	-1.301	-3	5.19E-13	-12.3
Ac07	-3	298	-2.301	-3	4.69E-13	-12.3
Ac07	-3	323	-0.678	-3	1.31E-12	-11.9
Do02	-3.04	295	-0.699	-3.04	8.48E-11	-10.1
Do02	-3.79	295	-0.699	-3.79	1.67E-10	-9.78
Do02	-3.77	295	-0.699	-3.77	2.27E-10	-9.64
Do02	-4.33	295	-0.699	-4.33	7.80E-11	-10.1
Do02	-3.06	295	-1.046	-3.06	5.45E-11	-10.3
Do02	-4.14	295	-1.046	-4.14	1.77E-10	-9.75
Do02	-2.61	295	-2.357	-2.61	9.19E-11	-10.0
Do02	-3.94	295	-2.357	-3.94	1.07E-11	-11.0
Do02	-2.53	295	-3.131	-2.53	6.70E-11	-10.2
Do02	-4.75	295	-3.131	-4.75	8.57E-11	-10.1
Lu00	-0.1	368	0	0	1.19E-06	-5.92
Lu00	-0.1	368	0	0	7.23E-07	-6.14
Lu00	-0.1	368	0	0	1.20E-06	-5.92
Lu00	-0.1	368	0	0	1.19E-06	-5.92
Lu00	-0.1	368	0	0	3.28E-06	-5.48
Lu00	-0.1	368	-0.678	0	2.08E-06	-5.68
Lu00	-0.1	368	0	0	3.29E-06	-5.48
Lu00	-0.1	333	0	0	8.80E-07	-6.06
Lu00	-0.1	343	0	0	1.42E-06	-5.85
Lu00	-0.1	358	0	0	2.69E-06	-5.57
Lu00	-0.1	368	0	0	3.28E-06	-5.48
Lu00	-0.1	368	0	-0.301	3.09E-06	-5.51
Lu00	-0.1	368	0	0	3.29E-06	-5.48
Lu00	-0.1	368	0	0.301	3.01E-06	-5.52
Mu71	-1	298	-0.678	0	6.33E-09	-8.20
Mu71	-1	298	-0.678	-0.12	5.95E-09	-8.23
Mu71	-1	298	-0.678	-0.30	5.14E-09	-8.29
Mu71	-1	298	-0.678	-0.60	4.08E-09	-8.39
Mu71	-1	298	-0.678	-1.00	4.21E-09	-8.38
Mu71	-1	298	-0.678	-1.30	3.47E-09	-8.46

Appendix 3A. (Continued)
Physiochemical conditions for chalcopyrite oxidation by Fe(III) without Cl^-.

Identifier	$\log m_{H+}$	T	$\log P_{O2}$	$\log m_{Fe(III)}$	r	$\log r$
An04	-1	298	-0.678	-1.747	9.84E-13	-12.0
An04	-1	298	-0.678	-1.048	1.39E-12	-11.9
An04	-1	298	-0.678	-0.747	1.17E-12	-11.9
An04	-1	298	-0.678	-0.571	1.49E-12	-11.8
An04	-1	298	-0.678	-0.446	1.87E-12	-11.7
Co09	-1.8	341	-0.678	-1.8	2.75E-09	-8.56
Co09	-1.8	341	-0.678	-1.8	3.05E-08	-7.52
Co09	-1.8	341	-0.678	-1.8	1.83E-08	-7.74
Co09	-1.8	341	-0.678	-1.8	1.16E-08	-7.93
Co09	-1.8	341	-0.678	-1.8	9.98E-09	-8.00
Co09	-1.8	341	-0.678	-1.7	2.76E-08	-7.56
Co09	-1.8	341	-	-1.7	5.80E-09	-8.24
Du81	-0.523	363	-0.824	-0.699	2.23E-07	-6.65
Du81	-0.523	363	-0.823	-0.699	1.68E-07	-6.77
Du81	-0.523	363	-0.823	-0.699	1.52E-07	-6.82
Du81	-0.523	363	-0.823	-0.699	1.60E-07	-6.80
Du81	-0.523	363	-0.823	-0.699	1.59E-07	-6.80
Du81	-0.523	363	-0.823	-1	3.49E-08	-7.46
Du81	-0.523	363	-0.823	-1	7.77E-08	-7.11
Du81	-0.523	363	-0.823	-1	1.94E-07	-6.71
Du81	-0.523	363	-0.823	-1	3.11E-07	-6.51
Du81	-0.523	363	-0.823	-1	5.85E-07	-6.23
Du81	-0.523	363	-0.823	-1	2.02E-07	-6.69
Du81	-0.523	363	-0.823	-1	2.66E-07	-6.57
Du81	-0.523	363	-0.823	-1	3.88E-07	-6.41
Du81	-0.523	363	-0.823	-1	4.80E-07	-6.32
Du81	-0.523	363	-0.823	-1	5.85E-07	-6.23
Fe75	0	323	-	-1.222	3.30E-07	-6.48
Fe75	0	338	-	-1.222	5.25E-07	-6.28
Fe75	0	353	-	-1.222	8.94E-07	-6.05
Fe75	0	368	-	-1.222	1.57E-06	-5.80
Fe75	0	368	-	-1.222	3.06E-06	-5.51
Fe75	0	368	-	-1.222	5.37E-06	-5.27
Fe75	0	368	-	-1.222	4.67E-06	-5.33
Fe75	0	368	-	-1.222	1.82E-06	-5.74
Fe75	0	368	-	-1.222	2.34E-06	-5.63
Fe75	0	353	-	-1.222	2.68E-06	-5.57
Fe75	0	353	-	-1.699	2.66E-06	-5.58
Hi01	-1	303	-	-0.602	1.41E-09	-8.85
Hi01	-1	303	-	-0.602	1.59E-08	-7.80
Hi01	-1	303	-	-0.602	2.33E-08	-7.63
Hi01	-1	303	-	-1.523	1.95E-08	-7.71
Hi01	-1	303	-	-1.523	1.38E-08	-7.86
Li76	-2	298	-	-4	3.85E-05	-4.41
Li76	-2	298	-	-4	6.71E-05	-4.17
Li76	-2	298	-	-4	1.34E-04	-3.87
Ma85	0	343	-	0	1.43E-06	-5.85

Appendix 3A. (Continued)
Physiochemical conditions for chalcopyrite oxidation by Fe(III) with Cl^-.

Identifier	$\log m_{H+}$	T	$\log P_{O2}$	$\log m_{Fe(III)}$	$\log m_{Cl-}$	r	$\log r$
Al08	-0.301	363	-0.678	-0.301	0.301	5.27E-06	-5.28
Al08	-0.301	363	-0.678	-0.301	0.301	6.73E-06	-5.17
Al08	-0.301	363	-0.678	-0.301	0.301	3.05E-06	-5.52
Al08	-0.301	363	-0.678	-0.301	0.301	4.67E-06	-5.33
Al08	-0.301	343	-0.678	-0.301	0.301	1.84E-06	-5.73
Al08	-0.301	353	-0.678	-0.301	0.301	3.30E-06	-5.48
Al08	-0.301	363	-0.678	-0.301	0.301	5.40E-06	-5.27
Al08	-0.301	363	-0.678	-0.301	0.301	2.90E-06	-5.54
Al08	-0.301	363	-0.678	-0.301	0.301	1.96E-06	-5.71
Al08	-0.301	363	-0.678	-0.301	0.301	4.02E-06	-5.40
Ha95	0	276.5	-	0	0.477	8.28E-06	-5.08
Ha95	0	293	-	0	0.477	1.03E-05	-4.99
Ha95	0	313	-	0	0.477	1.45E-05	-4.84
Ha95	0	323	-	0	0.477	1.41E-05	-4.85
Ha95	0	333	-	0	0.477	1.93E-05	-4.71
Ha95	0	343	-	0	0.477	1.99E-05	-4.70
Ha95	0	353	-	0	0.477	2.78E-05	-4.56
Ha95	-0.60	343	-	-0.301	0.176	1.98E-05	-4.70
Ha95	-0.30	343	-	-0.301	0.176	1.84E-05	-4.74
Ha95	-0.12	343	-	-0.301	0.176	1.95E-05	-4.71
Ma85	0	343	-	0	0.505	5.25E-06	-5.28
Ma85	0	343	-	0	0.505	3.31E-06	-5.48
Ma85	0	343	-	0	0.505	1.80E-06	-5.74
Ma85	0	343	-	0	0.505	3.75E-06	-5.43
Ma85	0	343	-	0	0.505	5.89E-06	-5.23
Om87	-0.398	368	0	-1	0.568	2.13E-06	-5.67
Om87	0.477	368	0	-1	0.568	3.55E-06	-5.45
Pa81	0	369	-	-1	0.633	1.66E-06	-5.78
Pa81	0	369	-	-1	0.633	1.65E-06	-5.78
Pa81	0	369	-	-1	0.633	1.58E-06	-5.80
Pa81	0	369	-	-1	0.633	1.60E-06	-5.80
Pa81	0	369	-	-1.699	0.609	6.59E-07	-6.18
Pa81	0	369	-	-1.301	0.618	1.23E-06	-5.91
Pa81	0	369	-	-1	0.633	1.53E-06	-5.82
Pa81	0	369	-	-0.602	0.677	2.36E-06	-5.63
Pa81	0	369	-	-0.301	0.740	3.01E-06	-5.52
Pa81	-0.699	369	-	-0.699	-0.097	1.07E-06	-5.97
Pa81	-0.699	369	-	-0.699	0.079	1.17E-06	-5.93
Pa81	-0.699	369	-	-0.699	0.255	1.28E-06	-5.89
Pa81	-0.699	369	-	-0.699	0.447	1.33E-06	-5.88
Pa81	0	355.5	-	-1	0.633	5.60E-07	-6.25
Pa81	0	359.5	-	-1	0.633	7.72E-07	-6.11
Pa81	0	365.5	-	-1	0.633	1.19E-06	-5.92
Pa81	0	369	-	-1	0.633	1.56E-06	-5.81
Pa81	-0.699	348	-	-0.699	0.580	1.58E-07	-6.80
Pa81	-0.699	353	-	-0.699	0.580	2.07E-07	-6.68
Pa81	-0.699	363	-	-0.699	0.580	3.63E-07	-6.44
Pa81	-0.699	369	-	-0.699	0.580	5.21E-07	-6.28
Ri94	-1.89	313	-0.678	-4.850	-1.89	2.65E-10	-9.58
Ri94	-1.88	333	-0.678	-4.310	-1.87	1.76E-09	-8.75
Sa92	-	303	-0.678	-0.699	-0.222	4.67E-06	-5.33
Sa92	-	323	-0.678	-0.699	-0.222	7.68E-06	-5.11
Sa92	-	343	-0.678	-0.699	-0.222	9.61E-06	-5.02
Sa92	-	363	-0.678	-0.699	-0.222	1.32E-05	-4.88

Appendix 3B. *Derivation of Rates with the Shrinking Particle Model*

Notation

A	Surface area of spherical particle (m^2)
n	Number of moles
α	Fraction of substance reacted away
p	Fraction remaining
r	Radius of spherical particle (m)
r_o	Initial radius of spherical particle (m)
k_p	Rate constant for particle rate law (s^{-1})
k_+	Specific rate constant (mol m^{-2} s^{-1})
r_+	Rate of release of a component (mol s^{-1})
t	Time (s)
V	Volume of spherical particle (m^3)
V_m	Molar volume of substance (m^3 mol^{-1})

When the extent of mineral dissolution is such that a significant portion of the mineral grain surface area has reacted away, the shrinking particle model (SPM) can be used to calculate the surface area normalized rate of reaction. Following models developed by Burkin (2001) and Levenspiel (1972), this derivation of the SPM relates particle grain diameter, dissolution rate, and fraction reacted to time. The model assumes that the specific rate constant (k_+) is constant over time, following pseudozeroth order kinetics, and that the mineral particles are spheres and leach uniformly.

The dissolution rate of a sphere is

$$r_+ = -Ak_+ = -4\pi r^2 k_+ \tag{3B.1}$$

and the rate of volume loss of the particle is

$$\frac{dV}{dt} = r_+ V_m = -4\pi r^2 k_+ V_m \tag{3B.2}$$

Alternately, the rate of volume loss can be represented by the time derivative of the volume formula for a sphere

$$\frac{dV}{dt} = 4\pi r^2 \frac{dr}{dt} \tag{3B.3}$$

Setting (3B.3) equal to (3B.2) gives

$$\frac{dr}{dt} = -k_+ V_m \tag{3B.4}$$

The fraction of material reacted away at any time is

$$\alpha = 1 - \left(\frac{r^3}{r_o^3}\right) \tag{3B.5}$$

thus

$$r = r_o\left(1-\alpha\right)^{1/3} \tag{3B.6}$$

The time derivative of (3B.6) is

$$\frac{d\alpha}{dt} = -3\left(\frac{r^2}{r_o^3}\right)\frac{dr}{dt} \tag{3B.7}$$

Substituting (3B.4) for dr/dt and (3B/6) for r gives

$$\frac{d\alpha}{dt} = \frac{3k_+ V_m}{r_o}\left(1-\alpha\right)^{2/3} \tag{3B.8}$$

The particle rate constant (k_p) is defined as

$$k_p = \frac{k_+ V_m}{r_o} \tag{3B.9}$$

which is substituted into (3B.8) to get the differential rate law

$$\frac{d\alpha}{dt} = 3k_p\left(1-\alpha\right)^{2/3} \tag{3B.10}$$

that can be integrated

$$\int_o^\alpha \frac{d\alpha}{\left(1-\alpha\right)^{2/3}} = 3k_p \int_0^t dt \tag{3B.11}$$

and evaluated to give

$$1-\left(1-\alpha\right)^{1/3} = k_p t \tag{3B.12}$$

A graph of $1-\left(1-\alpha\right)^{1/3}$ versus t has a slope of k_p and the specific rate can be found by rearranging (3B.9) to get

$$k_+ = \frac{r_o k_p}{V_m} \tag{3B.13}$$

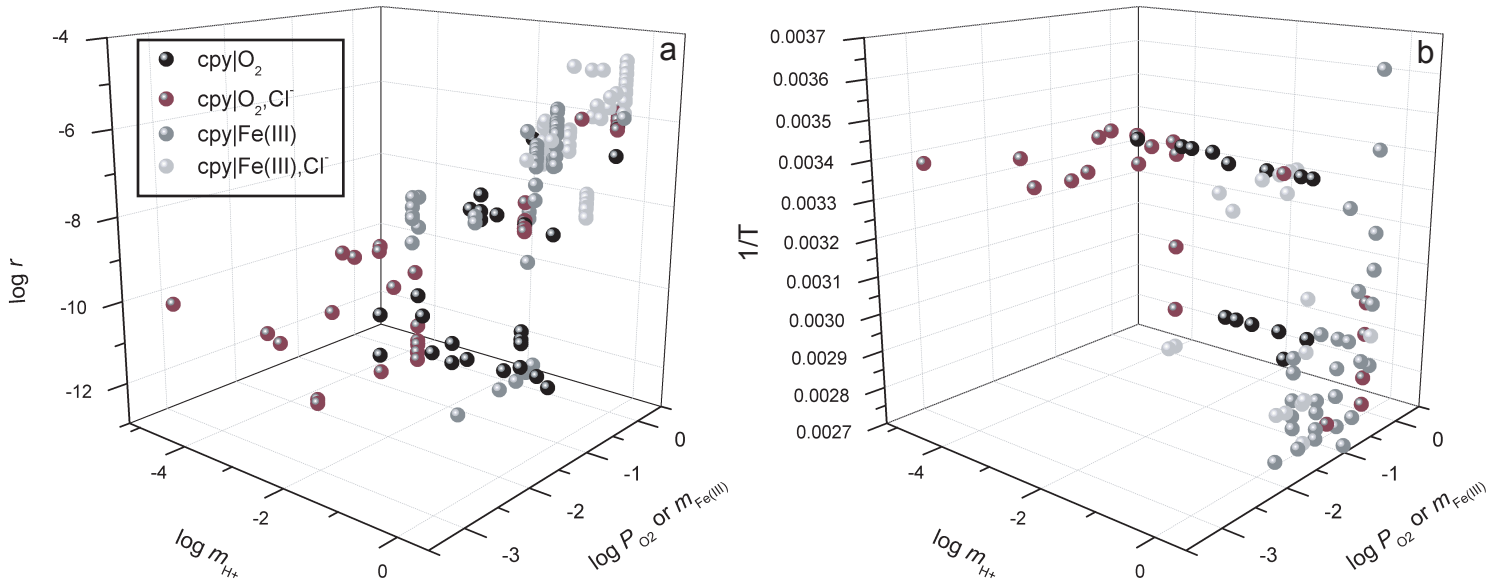

Figure 3.1. Reported and calculated rate measurements (log r) are plotted versus log m_{H+} and log P_{O2} or log $m_{Fe(III)}$ (a). Rates for chalcopyrite dissolution in the presence of O_2 (black spheres), in the presence of both O_2 and Cl^- (dark grey spheres), in the presence of Fe(III) (grey spheres), and in the presence of both Fe(III) and Cl^- (light grey spheres) are shown. The log m_{H+} and log P_{O2} or log $m_{Fe(III)}$ data are also plotted against 1/T (b). All data are given in Appendix 3A.

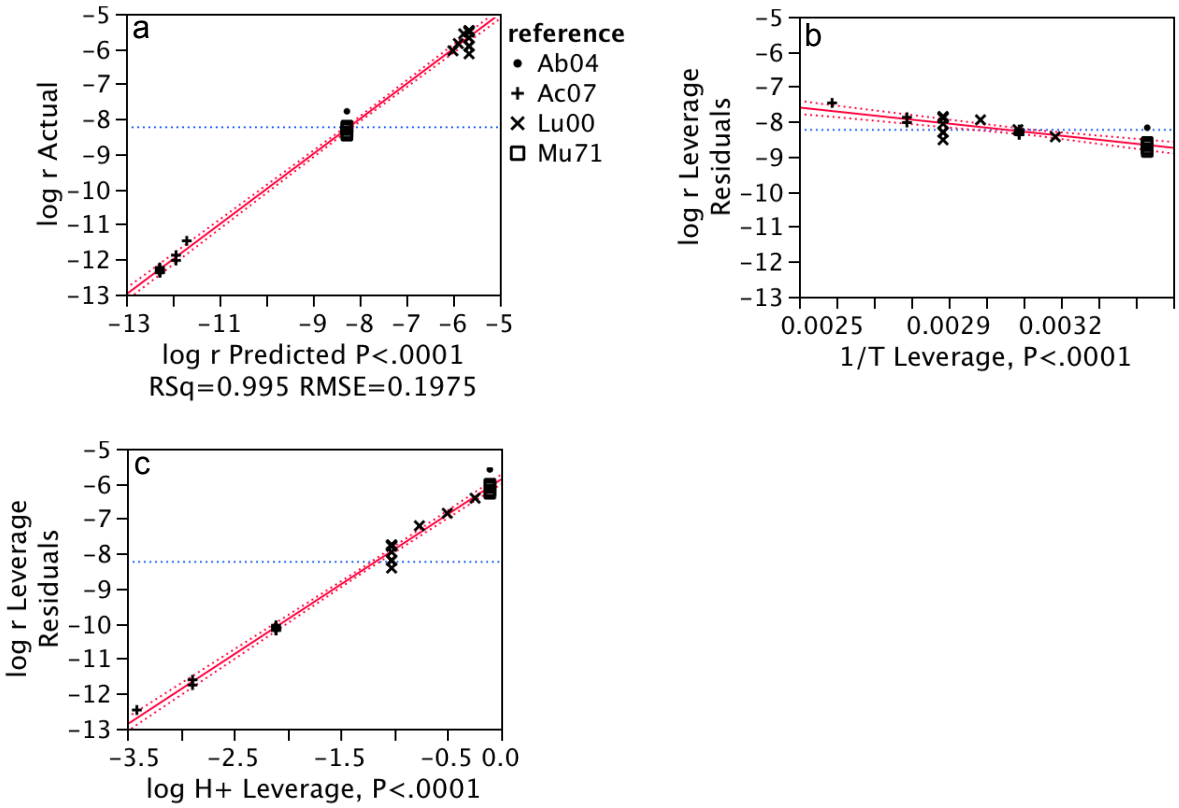

Figure 3.2. The whole-model leverage plot for the multiple linear regression of chalcopyrite dissolution in the presence of O_2 and Cl^- (a). The 45º line is where the actual response and predicted response are equal, and the accompanying dashed lines represent the 5% and 95% confidence curves. The vertical distance from data points to the 45º line represents the residual error. The horizontal line represents the actual mean log *r* value. In this regression, log *r* was regressed against $1/T$ (b) and log m_{H+} (c). The references correspond to those in Table 3.1.

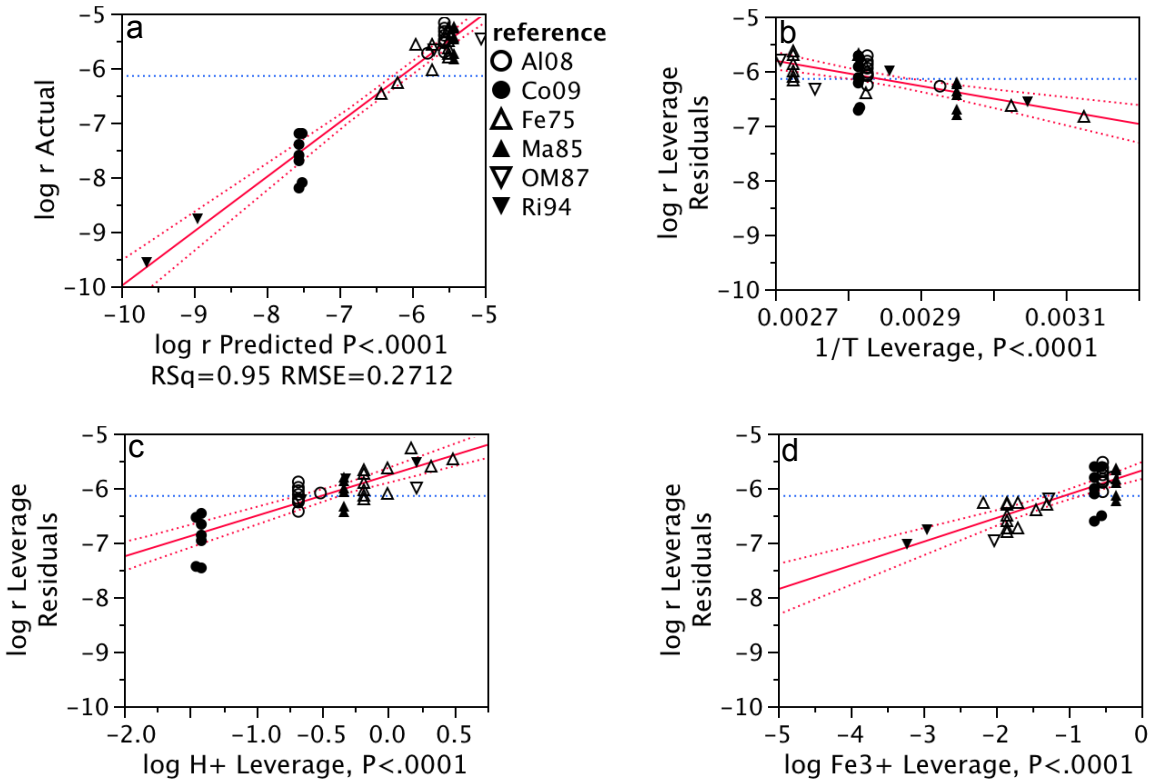

Figure 3.3. The whole-model leverage plot for the multiple linear regression of chalcopyrite oxidation by Fe(III) ± O_2 ± Cl^- (a). See figure 3.2 caption for description of plot features. In this multiple regression, log r was regressed against $1/T$ (b), log m_{H^+} (c), and log $m_{Fe(III)}$ (d). The references correspond to those in Table 3.1.

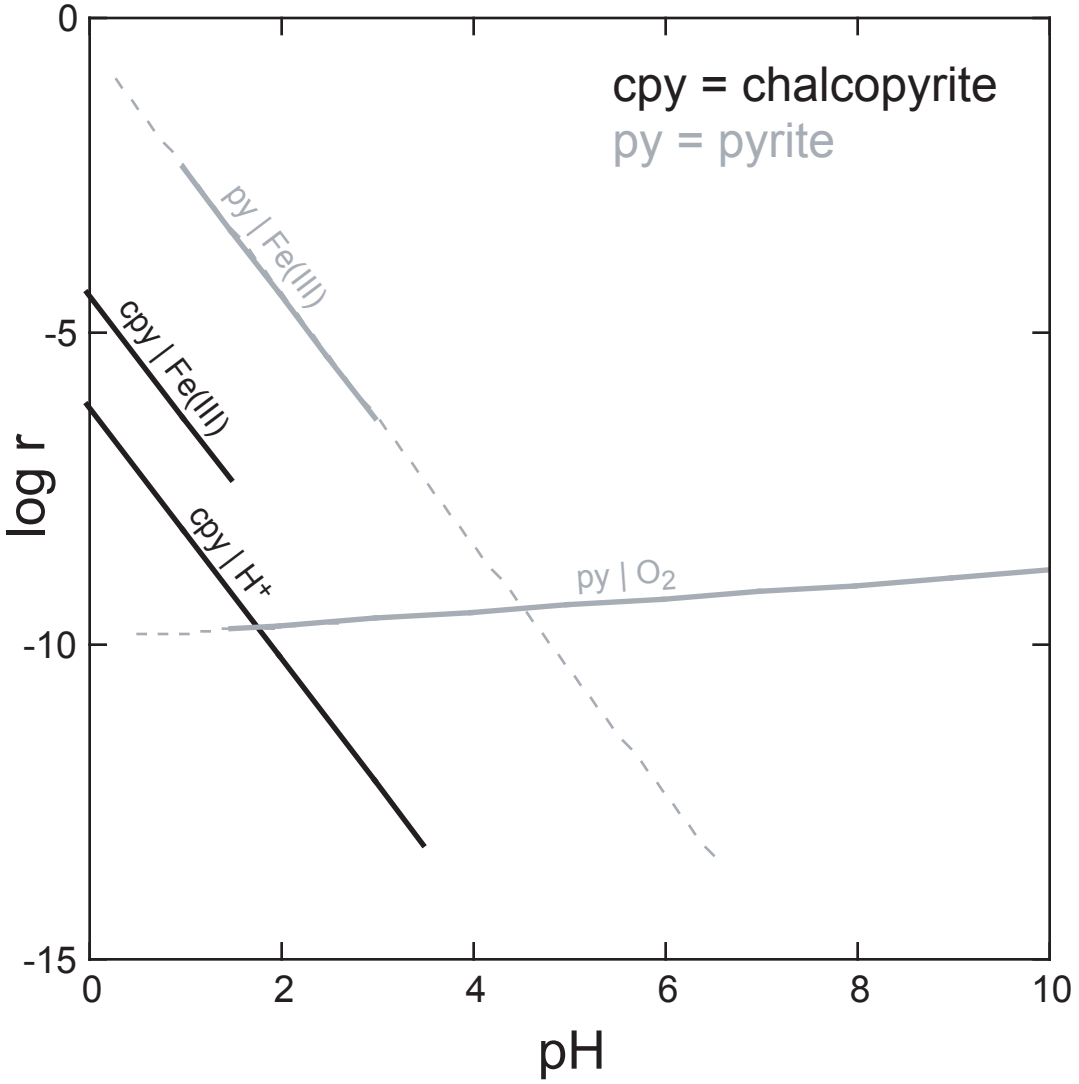

Figure 3.4. A plot of log rate versus pH for chalcopyrite and pyrite dissolution. The rate laws used to estimate log rate for chalcopyrite are from this study, and the rate laws for estimating log rate for pyrite are from Williamson and Rimstidt (1994). For those rates that depend on O_2, m_{DO} of 0.3 mM (i.e., equilibrium with P_{O2} = 0.21 atm) was assumed. For those rates that depend on Fe(III), the activity of Fe(III) was assumed to be controlled by ferrihydrite solubility using log K_{eq} (25ºC) = 4.89 (Drever, 1997). A temperature of 298K was assumed for all rate calculations. Heavy solid lines cover the pH range over which the rate laws were calculated. The lighter dashed line for pyrite oxidation by Fe(III) (py|Fe(III)) extends beyond the experimental pH range in order to show where the rate is equal to that for pyrite oxidation by O_2 (py|O_2) at higher pH. Note that the rates for nonoxidative chalcopyrite dissolution (cpy|H^+) and Fe(III)-oxidative chalcopyrite dissolution (cpy|Fe(III)) are fast at low pH, but are likely overtaken by chalcopyrite oxidation by O_2 at higher pH.

Chapter 4
Copper Isotope Fractionation in Acid Mine Drainage

4.0. Abstract

We measured the Cu isotopic composition of primary minerals and stream water affected by acid mine drainage in a mineralized watershed (Colorado, USA). The $\delta^{65}Cu$ values (based on $^{65}Cu/^{63}Cu$) of enargite ($\delta^{65}Cu = -0.01 \pm 0.10‰$; 2σ) and chalcopyrite ($\delta^{65}Cu = 0.16 \pm 0.10‰$) are within the range of reported values for terrestrial primary Cu sulfides ($-1‰ < \delta^{65}Cu < 1‰$). These mineral samples show lower $\delta^{65}Cu$ values than stream waters ($1.38‰ \leq \delta^{65}Cu \leq 1.69‰$). The average isotopic fractionation ($\Delta_{aq\text{-}min} = \delta^{65}Cu_{aq} - \delta^{65}Cu_{min}$, where the latter is measured on mineral samples from the field system), equals $1.43 \pm 0.14‰$ and $1.60 \pm 0.14‰$ for chalcopyrite and enargite, respectively. To interpret this field survey, we leached chalcopyrite and enargite in batch experiments and found that, as in the field, the leachate is enriched in ^{65}Cu relative to chalcopyrite ($1.37 \pm 0.14‰$) and enargite ($0.98 \pm 0.14‰$) when microorganisms are absent. Leaching of minerals in the presence of *Acidithiobacillus ferrooxidans* results in smaller average fractionation in the opposite direction for chalcopyrite ($\Delta_{aq\text{-}min}{}^{o} = -0.57 \pm 0.14‰$, where min^{o} refers to the starting mineral) and no apparent fractionation for enargite ($\Delta_{aq\text{-}min}{}^{o} = 0.14 \pm 0.14‰$). Abiotic fractionation is attributed to preferential oxidation of $^{65}Cu^{+}$ at the interface of the isotopically homogeneous mineral and the surface oxidized layer, followed by solubilization. When microorganisms are present, the abiotic fractionation is most likely not seen due to preferential association of $^{65}Cu_{aq}$ with *A. ferrooxidans* cells and related precipitates. In the biotic experiments, Cu was observed under TEM to occur in precipitates around bacteria and in intracellular polyphosphate granules. Thus, the values of $\delta^{65}Cu$ in the field and laboratory systems are presumably determined by the balance of Cu released abiotically and Cu that interacts with cells and related precipitates. Such isotopic signatures resulting from Cu sulfide dissolution should be useful for acid mine drainage remediation and ore prospecting purposes.

4.1. Introduction

Measurement of stable metal isotope ratios is a new tool for understanding the biogeochemical cycling of metals through contaminated environments. The mechanisms involved in mineral dissolution and precipitation at low temperatures (e.g., Bullen et al., 2001; Brantley et al., 2004; Ehrlich et al., 2004; Mathur et al., 2005; Wiederhold et al., 2006), in microbial metabolism of metals (e.g., Beard et al., 1999; Beard et al., 2003; Brantley et al., 2004), in redox reactions (e.g., Ehrlich et al., 2004; Markl et al., 2006; Asael et al., 2007), and in sorption of aqueous metals onto mineral and bacterial surfaces (e.g., Icopini et al., 2004; Pokrovsky et al., 2005; Balistrieri et al., 2008; Pokrovsky et al., 2008) may be highlighted by taking inventory of the isotopic fractionation between metal reservoirs. Copper isotope ratios are particularly promising among the transition metals because they vary over 3‰ in stream, river, and ocean samples (Archer et al., 2008; Balistrieri et al., 2008; Borrok et al., 2008) and 9‰ in solid samples (Shields et al., 1965; Larson et al., 2003). Copper isotope fractionation between samples is well outside analytical uncertainty, making Cu isotope measurements an attractive tool for understanding Cu mobility in metal contaminated environments.

Metal contamination is particularly pronounced in areas where sulfide mineral dissolution proceeds, forming acid rock drainage (ARD) or acid mine drainage (AMD). Primary Cu minerals in sulfide deposits dissolve upon reaction with an oxidant such as aqueous O_2 or Fe^{3+}, releasing aqueous Cu that is either transported downstream or precipitated into secondary minerals. The valences of Cu and Fe in chalcopyrite, the most abundant Cu sulfide mineral, are +1 and +3, respectively (Boekema et al., 2004; Goh et al., 2006; Pearce et al., 2006; Wincott and Vaughan, 2006), so either Cu^{+} or S^{2-} can be oxidized. For example, when S^{2-} is oxidized, the reaction for chalcopyrite oxidized by Fe^{3+} can be written:

$$CuFeS_{2(s)} + 15Fe^{3+}_{(aq)} + 8H_2O \rightarrow Cu^{+}_{(s)} + 16Fe^{2+}_{(aq)} + 2SO_4^{2-}{}_{(aq)} + 16H^{+} \quad (4.1)$$

Here $Cu^{+}_{(s)}$ represents a metastable reactive intermediate in the mineral that can be oxidized by Fe^{3+} in the chalcopyrite and then released to solution:

$$Cu^{+}_{(s)} + Fe^{3+}_{(s)} \rightarrow Cu^{2+}_{(aq)} + Fe^{2+}_{(aq)} \quad (4.2)$$

Combining (4.1) and (4.2) gives an overall reaction for chalcopyrite dissolution:

$$CuFeS_{2(s)} + 15Fe^{3+}_{(aq)} + Fe^{3+}_{(s)} + 8H_2O \rightarrow Cu^{2+}_{(aq)} + 17Fe^{2+}_{(aq)} + 2SO_4^{2-}{}_{(aq)} + 16H^{+} \quad (4.3)$$

The isotopic composition ($\delta^{65}Cu$; based on $^{65}Cu/^{63}Cu$) of primary Cu sulfide minerals is generally 0 ± 1‰ (Maréchal et al., 1999; Zhu et al., 2000; Larson et al., 2003; Graham et al., 2004; Rouxel et al., 2004; Mason et al., 2005; Mathur et al., 2005; Markl et al., 2006; Asael et al., 2007), but most fall within the range 0 ± 0.5‰ (Markl et al., 2006; Asael et al., 2007). Excursions from this range are attributed to low-temperature secondary processes (Rouxel et al., 2004; Mathur et al., 2005; Markl et al., 2006).

For example, in previous work in our laboratory, abiotic oxidative dissolution of the Cu^{+}-bearing minerals chalcopyrite ($CuFeS_2$) and chalcocite (Cu_2S) at pH 2.3 and 25°C was shown to result in fractionation between leached Cu (Cu_{aq}) and residual mineral (Cu_{min}). This fractionation, defined as:

$$\Delta_{aq\text{-}min} = \delta^{65}Cu_{aq} - \delta^{65}Cu_{min} \quad (4.4)$$

was found to average 1.36 ± 0.23‰ and 3.00 ± 0.23‰ for chalcopyrite and chalcocite, respectively (Mathur et al., 2005). Fractionation was inferred to be related to preferential sorption or precipitation of ^{63}Cu onto the dissolving chalcopyrite surface, leaving isotopically enriched Cu in solution.

Interestingly, in that previous work, leaching in the presence of *Acidithiobacillus ferrooxidans* under the same conditions resulted in Cu isotope fractionation that was smaller, averaging 0.38 ± 0.23‰ and 0.87 ± 0.23‰ for chalcopyrite and chalcocite, respectively. *A. ferrooxidans* is an Fe- and S-oxidizing Proteobacterium known to colonize many acidic environments (López-Archilla et al., 2001; Baker and Banfield, 2003; Johnson and Hallberg, 2003). Microorganisms such as *A. ferrooxidans* dissolve Fe-bearing sulfides through: 1) indirect bioleaching (Fe^{2+}_{aq} leached from minerals is microbially oxidized to Fe^{3+}_{aq}, which then attacks sulfide at the surface to release more Fe^{2+}_{aq} and reduced S), and 2) contact bioleaching (attachment of cells to minerals creates a microenvironment optimized for electron extraction from reduced elements) (Tributsch, 2001; Rodríguez et al., 2003a). Given the characteristic presence of ferrous ions in natural solutions near sulfide deposits, mechanism (1) presumably can occur for Fe-bearing as well as Fe-deficient minerals.

A. ferrooxidans has been grown on pyrite (e.g., Yu et al., 2001; Sharma et al., 2003; Garcia et al., 2007), chalcopyrite (Bevilaqua et al., 2002; Rodríguez et al., 2003b), covellite (Falco et al., 2003), chalcocite (Nielsen and Beck, 1972), enargite (Ehrlich,

1964; Escobar et al., 1997), and other sulfide mineral substrates. This microorganism is known to be able to oxidize Fe^{2+}, elemental S (S^0), and sulfide (S^{2-}) (Sharma et al., 2003), but we have seen no reports of its ability to oxidize Cu^+. Furthermore, microorganisms are expected to oxidize sulfide before Cu, given that more energy is harvested from S^{2-} oxidation than Cu^+ oxidation. The Gibbs free energy yield for oxidation of Cu^+ (to Cu^{2+}) and S^{2-} (to S^0), coupled with O_2 reduction, is -106 kJ/mol e^- and -165 kJ/mol e^-, respectively, at pH = 0 (references within Bertocci and Wagman, 1985; Hoare, 1985; Ross, 1985; Zhdanov, 1985).

Mathur et al. (2005) conducted additional biotic experiments where *A. ferrooxidans* grown in Cu-rich medium without minerals accumulated Cu on their cells (based on microscopic and spectroscopic observations). Cu associated with whole cells and related precipitates was on average 2.20 ± 0.23‰ greater than the starting medium after 30 days (Mathur et al., 2005). They inferred that the mineral-free biotic experiments provided evidence for preferential association of $^{65}Cu_{aq}$ with *A. ferrooxidans* cells in experiments with Cu sulfides, resulting in depletion of ^{65}Cu in the remaining Cu_{aq} relative to the abiotic experiments.

Predicting that we would find evidence for abiotic and/or biotic Cu isotope fractionation in natural acidified systems, we surveyed the Cu isotope composition of rocks and stream waters impacted by ARD and AMD in Mineral Creek (MC), located in southwestern Colorado, USA. Others have conducted intensive investigation of the acidic drainage in MC (e.g., Bove et al., 2000; Schemel et al., 2000; Runkel and Kimball, 2002). This is the first survey of the Cu isotopic composition of both minerals and stream water in a natural acidic environment. To interpret the field survey, we simulated Cu sulfide leaching in batch experiments at pH 2.0 under abiotic and biotic (in the presence of *A. ferrooxidans*) conditions. The experimental design was similar to earlier experiments (Mathur et al., 2005), but the volume percent cell inoculum we used was 200 times that used in previous experiments, and we tested both live and heat-killed inocula. We also tested leaching of enargite (Cu_3AsS_5) along with chalcopyrite, since these were the primary sulfides we found in the study area. Understanding enargite dissolution is of great importance due to the hazardous potential of mobile As (Smith and Huyck, 1999).

4.2. Study Area

The San Juan Mountains in southwestern Colorado, USA, contain many abandoned metal mines as a result of mining from 1871 to 1991 (Jones, 2007). The Silverton caldera was a particularly productive area. Ore deposits associated with this caldera were emplaced by three major magma-induced mineralization and hydrothermal alteration events from 26 to 10 Ma (Bove et al., 2001), resulting in one of the largest acid-sulfate hydrothermal systems in the western United States (Bove et al., 2007). Our study focuses on the Red Mountain area, which hosts breccia-pipe acid-sulfate alteration from 23 Ma (Bove et al., 2007). Published descriptions of a mineralogical reconnaissance conducted in the 1880s reported unoxidized primary ore including enargite, galena, chalcopyrite, pyrite, chalcocite, bornite, tetrahedrite-tennantite, sulfobismuthites, and stromeryite (Schwarz, 1883). These sulfides have presumably been weathering naturally since exposure and since the onset of mining. As a result, acidic, metal-rich ARD and AMD now impact the area (Wirt et al., 1999; Bove et al., 2000).

In the Red Mountain area, several mines impact the MC drainage. For example, the Koehler Tunnel drainage joins drainage emanating from the Longfellow mine adit near Red Mountain pass (3,375 m), and eventually meets MC (Fig. 4.1). We sampled the Koehler Tunnel drainage at its emergence, an acidic pond slightly downstream, a small reach in the Koehler Tunnel drainage transected by a mineralized fault, and a small reach in MC near the Silverledge mine tailings (Fig. 4.1). We collected sulfide samples from the Silverledge mine tailings (Fig. 4.1), the Carbon Lakes mine tailings about 600 m southeast of the Koehler Tunnel (see figure 13 in Bove et al., 2007), and the Idarado mine tailings about 2.2 km northeast of the Koehler Tunnel (see figure 13 in Bove et al., 2007). These sample sites flank Red Mountains No. 2 and 3, which host acid-sulfate alteration assemblages that are expansive and genetically linked (Bove et al., 2007).

4.3. Methods

4.3.1. Field Sample Collection and Analysis

We measured the in-stream pH and conductivity at each site while collecting samples. At each MC stream site (Fig. 4.1), both filtered (0.22 μm) and unfiltered samples were collected and acidified. Rock samples from MC were cut, polished, and

carbon-coated in preparation for scanning electron microscopy (SEM; JEOL 6460 at 20 kev) and energy dispersive x-ray spectroscopy (EDS), and ground and sieved (to < 45 μm) for micro-x-ray diffractometry (micro-XRD; Rigaku, DMAX-Rapid Microdiffractometer). The primary Cu sulfides collected (chalcopyrite and enargite) were hand-picked, from the field samples, crushed, sieved (to < 75 μm), and digested with heated aqua regia in Teflon bombs (Savillex®). Concentrations of major (Al, Ca, Fe, K, Mg, Na, Si), minor (Ba, Mn, Sr), and trace (Cu, Ni, Zn) elements in stream water and Cu concentrations in mineral digestates were measured using inductively coupled plasma atomic emission spectrometry (ICP-AES; Leeman Labs, PS3000UV) to a precision of ± 3%. Stream sample F, Cl, NO_3, PO_4, SO_4, formate and propionate, and acetate concentrations were measured using ion chromatography (IC; Dionex, ICS-2500).

Additional stream samples were collected to measure tracer-dilution, dissolved ferrous ion, total dissolved Fe, and total dissolved Cu concentrations. Following the procedure for an earlier tracer injection into MC (Runkel and Kimball, 2002), we measured dilution of an injected LiBr tracer to estimate stream flow. For further explanation of the tracer-dilution method, see Kilpatrick and Cobb (1985). Stream samples from selected sites were filtered (0.45 μm) and acidified with HNO_3 in clear HPDE bottles (dissolved metal concentrations) or with HCl in amber bottles (ferrous ion and total dissolved Fe concentrations). Dissolved metal concentrations were determined using inductively coupled plasma mass spectrometry (ICP-MS; Thermo Scientific, Element II). We used colorimetric methods (Brown et al., 1970) to measure total dissolved Fe and ferrous ion concentrations.

4.3.2. Batch Leach Experiments

In addition to the field survey, we conducted abiotic and biotic batch leach experiments with chalcopyrite and enargite-bearing rock samples. For biotic experiments, a pure strain of *Acidithiobacillus ferrooxidans* (ATCC® 13598) was continuously subcultured in an $FeSO_4$-based medium with the following composition: (in g/L) 3.5 $(NH_4)_2SO_4$, 0.116 KCl, 0.058 K_2HPO_4, 0.028 $MgSO_4$, 0.0024 $Ca(NO_3)_2 \cdot 4H_2O$, and 20.0 $FeSO_4 \cdot 7H_2O$, with the pH adjusted to 2.0 with concentrated H_2SO_4 (Barron and Lueking, 1990). Cultures were maintained at 25ºC on a shaker set to 200 rpm.

Two mineral samples were used for dissolution experiments: chalcopyrite (Wards's) and enargite-bearing rock (Butte, MT). These samples were ground in a porcelain mortar and pestle and sieved to a size range of 45 to 75 μm. The grains were then sterilized by soaking in 100% ethanol till dryness (overnight) in a laminar hood prior to use. Compositions of the mineral samples were analyzed by complete digestion in aqua regia followed by analysis using ICP-AES (Perkin Elmer, Optima 5300 DV). Based on digestate metal and S contents and mineral stoichiometry, these samples were 100% chalcopyrite and ~25% enargite + 75% sphalerite.

For the leaching experiments, 2 g of sterilized mineral were added to sterile, polycarbonate 250 ml Erlenmeyer flasks. Sterile $FeSO_4$-based medium at pH ≈ 2.0 was added to flasks to make three different treatments: 1) 100 mL medium + mineral, 2) 90 mL medium + mineral + 10 mL *A. ferrooxidans* inoculum (containing ≈ 2.5×10^7 cells), and 3) 90 mL medium + mineral + 10 mL autoclaved (>120 ºC for 45 min.) *A. ferrooxidans* inoculum. The experimental pH was lower than the values measured at our stream sites ($2.6 \leq pH \leq 5.2$) in order to be closer to the optimal pH for *A. ferrooxidans* growth and the low pH values expected near dissolving sulfide mineral surfaces. The only difference between conditions (2) and (3) was that the latter experiments included cells that had been autoclaved: this experiment was designed to test the effect of nonliving cells on leaching. Henceforth, we will refer to the nonautoclaved culture and autoclaved culture as nonautoclaved biotic and autoclaved biotic experiments, respectively. The flasks were shaken at 200 rpm at 25ºC for 1, 7, or 14 days. The nonautoclaved and autoclaved biotic inocula contained cells and ferric precipitates that form upon chemical and biological oxidation of Fe^{2+} in the medium; these precipitates could not be separated from the cells. No precipitates were observed in the abiotic experiments.

At the experiment termination, supernatants were filtered (0.22 μm) and set aside and the remaining solids were rinsed with deionized water. The solid/deionized water solution was centrifuged at 4500 rpm for 20 min., and the liquid was decanted. This process was repeated once more before the solids were dried in an oven at 60ºC. Subsamples of the filtered experimental liquid were separated for pH and [Fe^{2+}] measurements. Ultrapure HCl was added to samples for [Fe^{2+}] measurements using a

ferrozine assay (Lovely and Phillips, 1986). Two mLs of ultrapure HNO_3 were added to the remaining filtered experimental liquid prior to analysis by ICP-AES (Perkin Elmer, Optima 5300 DV). The solutions were then prepared for isotopic analysis following the same procedure used for the field samples.

4.3.3. Copper Isotope Preparation and Analysis

Prior to isotope analysis, aliquots of liquid and mineral digestate samples were evaporated (at ~60ºC) to prepare at least 2 μg Cu. The salts were resuspended in 2% (v/v) HNO_3 and then the solution was halved; one half was set aside and the other was re-evaporated. The salts were then resuspended in 1 mL of 10 M HCl in preparation for ion-exchange chromatography (IEC). All acids were ultrapure reagent grade (J. T. Baker) and water was deionized (18.2 MΩ/cm; Millipore).

Modified, acid-rinsed 3 mL transfer pipettes were used as chromatography columns following Borrok et al. (2007). The anion exchange resin AG MP-1 (Bio-Rad®) was rinsed in 50% (v/v) HNO_3, followed by five sequences of decanting and addition of water. Acid rinsed [50% (v/v) HNO_3] frits were placed in the tips of the columns and 0.65 to 0.75 mL resin was added. We conducted IEC in a clean hood (NuAire; NU-156) following the protocol developed by Borrok et al. (2007). Briefly, resin loaded onto the columns was rinsed with 3 mL of deionized water, followed by 4 mL of 10 M HCl for resin conditioning. Next, the 1 mL of 10 M HCl bearing sample was loaded. We then eluted the sample matrix with 4 mL of 10 M HCl. Copper was eluted with another 6 mL of 5 M HCl. For all steps, eluant was added in 1 mL increments. The total eluted Cu portion was evaporated and resuspended in 2% (v/v) HNO_3 twice. Using ICP-MS (Thermo Scientific, Element I), we verified complete recovery of Cu, since IEC is known to fractionate Cu isotopes (Maréchal and Albarède, 2002), and tested for eluant purity.

We measured $^{65}Cu/^{63}Cu$ using multi-collector inductively coupled plasma mass spectrometry (MC-ICP-MS; Thermo Scientific, Neptune) at Washington State University. To correct for instrumental mass fractionation, our samples and the NIST 976 Cu standard were spiked with an internal standard of known isotopic composition: the Johnson-Mattey Zn solution. Using standard-sample-standard bracketing and sample correction with the exponential law of mass fractionation of the internal standard

(following Maréchal et al., 1999), Cu isotopic composition was determined with the following equation:

$$\delta^{65}\mathrm{Cu}(‰) = \left[\left(\frac{{}^{65}\mathrm{Cu}/{}^{63}\mathrm{Cu}_{\mathrm{sample}}}{{}^{65}\mathrm{Cu}/{}^{63}\mathrm{Cu}_{\mathrm{NIST976}}}\right) - 1\right] \times 1000 \qquad (4.5)$$

The exponential correction was used only when there was enough data spread on a $\ln({}^{65}\mathrm{Cu}/{}^{63}\mathrm{Cu})$ vs. $\ln({}^{68}\mathrm{Zn}/{}^{64}\mathrm{Zn})$ plot of standard analyses (e.g., Maréchal et al., 1999; Archer and Vance, 2004). During some sessions, the standard measurements were too replicable (i.e., not linear) on such a plot. In this case, only standard-sample-standard bracketing was used. The $\delta^{65}\mathrm{Cu}$ values for samples corrected using both techniques are the same, within long-term analytical uncertainty. For all NIST 976 measurements taken over the course of 1.5 years, the average value equaled 0.05 ± 0.10‰ (2σ). For replicate measurements on a single sample, 2σ values are also within 0.10‰. The few samples that showed lower reproducibility ($2\sigma \leq 0.14‰$) are noted in Tables 4.1 and 4.2.

4.3.4. TEM and EDS on Copper-incubated Cells

To investigate $\mathrm{Cu}_{\mathrm{aq}}$ association with the bacteria cells, we grew *A. ferrooxidans* in the same $\mathrm{FeSO_4}$-based medium described above, but with Cu added to make concentrations of 0, 0.1, 1, and 10 mM. We used transmission electron microscopy (TEM) and EDS to image and characterize cells grown for 5 days at room temperature. Aliquots of each culture were centrifuged (4,000 – 8,000 × *g*; 1 – 2 min.), the supernatant discarded, and the cell/precipitate pellet was fixed in 2.5% glutaraldehyde. The pellet was washed several times in PBS buffer, dehydrated in solutions of water + ethanol of increasing concentration, embedded in LR White resin and cured at 60ºC overnight. Hardened resin blocks were sectioned to ~70 nm with a Diatome 45-degree diamond knife using a Leica UCT ultramicrotome (Leica Microsystems) and mounted on 200 mesh copper grids with formvar support film coated with carbon. Unstained sections were examined at 120 kV using a Tecnai T-12 TEM (FEI Company). Images were digitally collected and analyzed using DigitalMicrograph software (Gatan Inc.). The grids prepared for high-resolution TEM were also analyzed on a separate JEOL 2010 high-resolution TEM equipped with an Oxford ISIS X-ray EDS microanalysis system for quantitative spectroscopy of elemental abundance.

4.3.5. Thermodynamic Calculations

To calculate the speciation of aqueous Cu species in MC samples and in experimental solutions, we used the chemical equilibrium-solving program PHREEQC and the minteq.v4 thermodynamic database (Parkhurst and Appelo, 1999). We also used PHREEQC to determine the saturation indices of minerals in field and experimental solutions. Enthalpy of formation and stability constants for schwertmannite ($\sim FeO(OH)_{3/4}(SO4)_{1/8}$) (Majzlan et al., 2004) were added to the minteq.v4 thermodynamic database. For the field and laboratory calculations, we assumed that the redox potential was maintained at equilibrium with the ratios of aqueous $[Fe^{2+}]/[Fe^{3+}]$, which were calculated after total measured $[Fe^{2+}]$ and calculated $[Fe^{3+}]$ (= $[Fe_{tot}] - [Fe^{2+}]$) were speciated. For upstream sites (4, 5, 6, and 9), where pH ≤ 3.14, we assumed total $[Fe^{2+}]$ was 90% of Fe_{tot} based on earlier measurements of upstream MC samples (Runkel and Kimball, 2002). All inorganic analyte concentrations (Appendix 4A) in filtered samples were used to determine speciation and mineral saturation indices for selected sample sites.

4.4. Results

4.4.1. Field Observations

The stream pH was lowest at site 2 (Fig. 4.1) and increased downstream (Table 4.1). Copper and Fe concentrations decreased from site 2 to the downstream reach (sites 10-14) by a factor of 83 and 430, respectively (Table 4.1). Despite decreasing Cu concentration, the total mass flux of Cu increases from upstream to downstream, coincident with increasing discharge (Table 4.2).

Rock samples from the Silverledge mine tailings (Fig. 4.1) contain matrix-hosted, ~2 mm-sized cubic pyrite crystals. With acid digestion and ICP-AES, we determined that these cubic pyrite grains contain 180 mg Cu/kg. Due to the high concentration of Fe compared to Cu we were unsuccessful in conducting IEC for separating Cu from the sample matrix for these digestates; therefore, we were unable to measure the isotopic composition of trace Cu in this pyrite. The Carbon Lakes mine tailings (about 600 m southeast of the Koehler Tunnel, see figure 13 in Bove et al., 2007) contain samples of

enargite + pyrite + quartz (based on micro-XRD), and the Idarado mine tailings (about 2.2 km northeast of the Koehler Tunnel, see figure 13 in Bove et al., 2007) contain quartz-rich rock with segregated masses of chalcopyrite (verified by SEM and EDS).

The average $\delta^{65}Cu$ value of the enargite collected on site is -0.01 ± 0.10‰ (2σ), and that for chalcopyrite is 0.16 ± 0.10‰ (Table 4.1; Fig. 4.2). These $\delta^{65}Cu$ values fall within the 0 ± 0.5‰ range reported for unaltered, primary Cu sulfides collected worldwide (Markl et al., 2006; Asael et al., 2007).

Compared to minerals, stream water $\delta^{65}Cu$ values are higher (Table 4.1; Fig. 4.2), ranging from 1.38 to 1.69 ± 0.10‰. The $\delta^{65}Cu$ values do not differ between filtered and unfiltered samples from each site (within error), so only data for filtered samples are reported (Table 4.1). The isotopic composition of the spring (site 12) is indistinguishable from nearby stream water (sites 11, 13, 14), but slightly isotopically depleted relative to the upstream sites (Table 4.1; Fig. 4.2).

4.4.2. Chalcopyrite Leach Experiment

Dissolved [Cu] increased similarly over time in all chalcopyrite experiments (Table 4.3). Dissolved [Fe] remained relatively constant during all experiments, and was greatest in the nonautoclaved biotic experiment (Table 4.3). The additional Fe in this experiment was dissolved Fe^{2+} and dissolved or precipitated Fe^{3+} introduced with the *A. ferrooxidans* inoculum. The $[Fe^{2+}]$ decreased quickly during day 1 in all experiments, then stabilized (Table 4.3).

Leached Cu_{aq} in the abiotic chalcopyrite experiment was enriched in ^{65}Cu relative to the undissolved chalcopyrite (Cu_{min}^{o}) throughout the experiment. Fractionation is noted here as:

$$\Delta_{aq\text{-}min}^{o} = \delta^{65}Cu_{aq} - \delta^{65}Cu_{min}^{o} \quad (4.6)$$

Note this equation differs from equation (4.4) in that the $\delta^{65}Cu_{aq}$ is compared to that of the undissolved mineral, Cu_{min}^{o}, rather than the value for leached residual mineral, Cu_{min}. In the abiotic experiments, $\Delta_{aq\text{-}min}^{o}$ averaged 1.37 ± 0.14‰ (Table 4.3; Fig. 4.3). Leached Cu_{aq} in the biotic experiments was isotopically indistinguishable between nonautoclaved and autoclaved experiments. Average $\Delta_{aq\text{-}min}^{o}$ was smaller and of opposite sign compared to the abiotic experiment (-0.57 ± 0.14‰; Table 4.3; Fig. 4.3).

The average abiotic value for $\Delta_{aq\text{-}min}{}^{o}$ in this study is similar to $\Delta_{aq\text{-}min}$ observed by Mathur et al. (2005) during similar abiotic chalcopyrite leach experiments (1.36 ± 0.23‰). In contrast, the biotic value for $\Delta_{aq\text{-}min}{}^{o}$ in this study is significantly less than $\Delta_{aq\text{-}min}$ for the Mathur et al. biotic chalcopyrite leach experiment with *A. ferrooxidans* (0.38 ± 0.23‰).

4.4.3. Enargite-bearing Leach Experiment

Dissolved [Cu] increased in all enargite experiments, but was greatest in the nonautoclaved biotic experiment (Table 4.3). Dissolved [Fe] remained relatively constant during all experiments, and like the chalcopyrite experiments, was greatest in the nonautoclaved biotic experiment (Table 4.3). The [Fe^{2+}] maintained constant until day 7, then decreased slightly in all experiments (Table 4.3).

Leached Cu_{aq} in the abiotic enargite experiment was enriched in ^{65}Cu relative to the undissolved mineral (average $\Delta_{aq\text{-}min}{}^{o}$ = 0.98 ± 0.14‰; Table 4.3; Fig. 4.3). In contrast, values for Cu_{aq} in the biotic experiments were isotopically indistinguishable and only slightly greater than the undissolved mineral (average value for nonautoclaved experiment, $\Delta_{aq\text{-}min}{}^{o}$ = 0.03 ± 0.14‰, and for autoclaved experiment $\Delta_{aq\text{-}min}{}^{o}$ = 0.26 ± 0.14‰; Table 4.3; Fig. 4.3).

4.4.4. Solids in Biotic Leach Experiments

Each of the chalcopyrite and enargite biotic experiments contained both live and dead *A. ferrooxidans* cells, as well as ferric precipitates that form as a result of oxidation of Fe^{2+} in the medium, as observed under optical microscopy. Using micro-XRD, we were able to identify that the precipitates in the autoclaved biotic experiments were potassium jarosite. In constrast, for the nonautoclaved biotic experiments, micro-X-ray diffractograms did not reveal identifiable peaks.

4.4.5. TEM and EDS Characterization of Cells

A. ferrooxidans cells grown in medium containing aqueous Cu (0.1, 1 and 10 mM) exhibited electron-dense (i.e., metal-rich) areas within the cell and on the cell membranes (Fig. 4.4). Electron-dense granules appeared within the cells whether they

were grown in the presence of significant Cu or not. In addition, extracellular polymeric substances (EPS) were observed to surround the cells grown in the presence of 1 and 10 mM of Cu (but not in the 0 and 0.1 mM systems) (Fig. 4.4).

EDS for a cell grown in 10 mM Cu medium (Fig. 4.5) was used to measure elemental concentrations in areas within and near the cell. The atomic percentages of elements were normalized by that of carbon, which is ubiquitous throughout the sample; analyses showed that cellular cytoplasm, granules within the cell, the cell membranes, and extracellular precipitates all contained Cu (Fig. 4.5). The O:P for the granule in this cell is 3.3 ± 0.8, consistent with formation of a polyphosphate granule.

4.5. Model Results

4.5.1. Mineral Creek Chemistry

According to thermodynamic calculations, the most and second-most abundant aqueous Cu species were $(Cu(H_2O)_6)^{2+}$ and $CuSO_4^0$, respectively, accounting for almost 100% of Cu in stream samples. At sites 4-6 and 9 (pH ≈ 3.1) the supersaturated and least kinetically-hindered minerals calculated to form were K- and H-jarosite ($KFe_3(OH)_6(SO_4)_2$; $((H_3O)Fe_3(OH)_6(SO_4)_2)$. Note that goethite, hematite, and lepidocrocite were also calculated to be supersaturated, but goethite and hematite tend to be the last of multiple Fe oxide transformations (Cornell and Schwertmann, 2003), and lepidocrocite is less likely to form in SO_4-rich waters, so these minerals are less likely to precipitate directly from solution. Jarosite generally precipitates at pH < 2.5, and schwertmannite ($Fe_8O_8(OH)_6SO_4$-$Fe_8O_8(OH)_{4.5}(SO_4)_{1.75}$) precipitates between pH 2.8 and 4.5 (Bigham et al., 1996). However, schwertmannite was calculated to be undersaturated for all MC samples (saturation index, SI < -4.4) regardless of the value of the solubility constant chosen (Bigham et al., 1996; Yu et al., 1999; Kawano and Tomita, 2001; Majzlan et al., 2004). In contrast, the SI for K-jarosite was positive and relatively constant (SI = 4.5 to 5.7) at upstream sites (4-6, 9). Based on these observations, the constancy of $[Fe^{3+}]$ at these sites could be related to jarosite precipitation. Further downstream, at sites 10-12 and 14 (3.5 ≤ pH ≤ 4.2) K-jarosite was also calculated to be supersaturated, but less so than upstream (SI = 0.9 to 1.5). At the higher pH downstream sites (10, 11, 14), ferrihydrite ($Fe_5HO_8 \cdot 4H_2O$) was supersaturated (SI = 0.1 to 1.1),

suggesting that jarosite and/or ferrihydrite precipitation was possible at these sites. In the lower MC reach, (sites 10-11, 13-14), filtered [Fe] << unfiltered [Fe] (Appendix 4A, Table 4.2), consistent with precipitation of an Fe phase.

4.5.2. Speciation and Composition of Leach Media

Like the MC waters, in the leach experiments, dissolved Cu was calculated to be either $(Cu(H_2O)_6)^{2+}$ or $CuSO_4^0$, and both K- and H-jarosite were undersaturated initially. However, both phases were calculated to be highly supersaturated during both abiotic and biotic chalcopyrite and enargite leach experiments. Consistent with this calculation, micro-XRD results revealed K-jarosite precipitates in the autoclaved biotic experiments, presumably due to the increased temperatures during autoclaving (Margulis et al., 1976).

4.6. Discussion

The batch experiments can be described with a closed-system mass balance by defining the fraction of Cu in each reservoir (f_i):

$$\delta^{65}Cu_{min}{}^{o} = \delta^{65}Cu_{min}f_{min} + \delta^{65}Cu_{aq}f_{aq} + \delta^{65}Cu_{b}f_{b} \quad (4.7)$$

Here, super- and subscripts represent Cu in original chalcopyrite ($Cu_{min}{}^{o}$), in the dissolving mineral at any time in the experiment (Cu_{min}), in the aqueous phase (Cu_{aq}), and associated with bacteria and related ferric precipitates (Cu_b). In equation (4.7), f_i equals the moles of Cu in reservoir *i* divided by the moles of total Cu in the flask.

In the abiotic experiments, f_b was 0 so we calculated $\delta^{65}Cu_{min}$ using observations of f_{aq}, noting that $f_{min} = 1 - f_{aq}$. The value of f_{min} did not significantly differ from 1 in the abiotic experiments. Therefore, $Cu_{min} = Cu_{min}{}^{o}$ and $\Delta_{aq\text{-}min} = \Delta_{aq\text{-}min}{}^{o} = 1.37 \pm 0.14‰$ or $0.98 \pm 0.14‰$, within error, for chalcopyrite and enargite, respectively.

Values of $\Delta_{aq\text{-}min}$ for MC are similar to the values in these abiotic experiments, ranging from 1.22 to $1.53 \pm 0.14‰$ (chalcopyrite) or 1.39 to $1.70 \pm 0.14‰$ (enargite) (Table 4.1). These field observations are more similar to observations for Cu leached abiotically from chalcopyrite than from enargite (Fig. 4.3).

4.6.1. Fractionation of Copper in Mineral Creek

Enargite and chalcopyrite samples from near MC appeared unaltered, and have been reported as unoxidized primary ore (Schwarz, 1883). We therefore consider these $\delta^{65}Cu_{min}$ values to be similar to the $\delta^{65}Cu_{min}{}^{o}$ values for the original minerals. Consistent with this, these $\delta^{65}Cu_{min}$ values fall within the 0 ± 0.5‰ range reported for primary, unaltered Cu sulfides (Markl et al., 2006; Asael et al., 2007).

The Cu isotope fractionation in MC resembles abiotic rather than biotic sulfide leach experiments. However, oxidative sulfide dissolution by acidophilic microorganisms is well known in systems similar to MC (Nordstrom, 2000). Furthermore, we were able to culuture Fe- and S-oxidizing microorganisms from MC stream sites using Fe^{2+}- or S^0-based media (ATCC medium 125, Barron and Lueking, 1990). We conclude that in the field, $f_b << f_{aq}$, whereas in our flasks, f_b must have been larger.

This conclusion is consistent with the observation that nutrient-rich conditions in laboratory cultures support greater cell numbers than in natural environments, where microorganisms are often limited by essential nutrients such as C, N, P, etc. (Madigan et al., 2003). Even cell densities in systems with high photosynthetic and chemolithotrophic primary productivity in acidic, high-metal systems (e.g., López-Archilla et al., 2001; Niyogi et al., 2002) rarely reach laboratory values (e.g., Sharma et al., 2003).

4.6.2. Downstream Changes in Isotopic Composition

Copper isotope fractionation in MC decreases slightly downstream (Table 4.1; Fig. 4.2). Consistent with the inference of Fe precipitation in downstream MC, experiments have shown that Cu sorbed to ferrihydrite or goethite is 0.7 – 0.8‰ more enriched in ^{65}Cu than aqueous Cu (Balistrieri et al., 2008; Pokrovsky et al., 2008). While sorption of Cu_{aq} may have occurred, measured average discharge increased from site 4 to 14 by approximately 12-fold (Table 4.2). With increased discharge, the total net mass flux of Cu increased from upstream to downstream (Table 4.2). Thus, most of the changes in the isotopic composition of Cu_{aq} in the stream are attributed to Cu addition to the stream rather than to sorption.

4.6.3. Abiotic Copper Isotope Signatures

All values for $\Delta_{aq\text{-}min}$ reported for abiotic oxidative dissolution of Cu sulfides are positive, decreasing in the order chalcocite (3.00 ± 0.23‰, Mathur et al., 2005; 2.46 ± 0.12‰, Wall et al., 2007) > chalcopyrite (1.37 ± 0.14‰, this study, 1.36 ± 0.23‰, Mathur et al., 2005) > enargite (0.98 ± 0.14‰, this study). Positive $\delta^{65}Cu$ values indicate that ^{63}Cu is preferentially retained in the mineral, and ^{65}Cu is released to the aqueous phase during oxidation. Preferential solubilization of ^{65}Cu over ^{63}Cu is somewhat unexpected given that heavier isotopes generally concentrate in the environment with the stiffest bonds (Bigeleisen and Mayer, 1947; Urey, 1947; Criss, 1999; Schauble, 2004): ^{65}Cu-^{32}S bonds within sulfide minerals are expected to be harder to break than ^{63}Cu-^{32}S bonds. However, Schauble (2004) uses equilibrium theory to argue that bond stiffness is greater for higher oxidation states of any given element. Consistent with this, experimental evidence shows that redox reactions concentrate ^{65}Cu into the oxidized as opposed to the reduced phase (Zhu et al., 2002; Ehrlich et al., 2004; Mathur et al., 2005). In addition, in deposits where Cu^{+} and Cu^{2+} minerals coexist, secondary Cu^{2+} minerals are isotopically enriched in ^{65}Cu relative to primary Cu^{+} minerals (Larson et al., 2003; Mason et al., 2005; Markl et al., 2006; Asael et al., 2007).

Preferential release of $^{65}Cu^{2+}$ to solution is therefore here attributed to fractionation during formation of an oxidized layer on the surface of an isotopically homogeneous mineral. The isotopically heavy Cu^{2+} in the partially oxidized layer is also assumed to leach into solution faster than Cu^{+}. For example, published results from X-ray photoelectron spectroscopy and SEM show that when oxidatively dissolved in acidic ferric solutions, chalcopyrite develops a leach layer that is deficient in Cu and enriched in sulfate (as a jarosite-like phase) (Parker et al., 2003; Klauber, 2008), disulfide (S^{2-}) (Klauber et al., 2001; Parker et al., 2003), and/or S^{0} (Rimstidt et al., 1994; Klauber et al., 2001; Parker et al., 2003; Klauber, 2008). Freshly cleaved enargite surfaces exposed to acidic ferric solution also develop a Cu-deficient layer (Fantauzzi et al., 2007).

This model is somewhat similar to the previously described leach layer formation on hornblende, where it was observed that the isotopic composition of solubilized Fe differed from that in the starting mineral (Brantley et al., 2004). Following the treatment by Brantley et al. (2004) for release of a metal to solution from a leach layer, the rate of

change of Cu concentration in the leach layer on sulfide minerals (C) can be expressed as:

$$dC/dt = F_{ox}/x - kC \tag{4.8}$$

where F_{ox} is the rate per unit area of Cu oxidized, x is the thickness of the leach layer, and k is a rate constant describing Cu mobilization from the leach layer to solution. Following the assumptions of Brantley et al. (2004), the solution to (4.8) is:

$$^{6X}C(t) = \frac{^{6X}F_{ox}}{^{6X}kx}(1 - e^{-6Xkt}) + {}^{6X}C_0 e^{-6Xkt} \tag{4.9}$$

where superscript 6X represents 65 or 63, indicating that this equation can be used to describe both ^{65}Cu and ^{63}Cu concentrations, respectively, over time. The rate at which ^{65}Cu or ^{63}Cu is released to solution (R_{in}) is:

$$^{6X}R_{in} = {}^{6X}k\,{}^{6X}C(t) \tag{4.10}$$

Combining equations (4.9) and (4.10) gives:

$$\frac{^{65}R_{in}}{^{63}R_{in}} = \frac{\frac{^{65}F_{ox}}{x}(1 - e^{-65kt}) + {}^{65}k\,{}^{65}C_0 e^{-65kt}}{\frac{^{63}F_{ox}}{x}(1 - e^{-63kt}) + {}^{63}k\,{}^{63}C_0 e^{-63kt}} \tag{4.11}$$

Initially, at t = 0:

$$\frac{^{65}R_{in}}{^{63}R_{in}} = \frac{^{65}k\,{}^{65}C_0}{^{63}k\,{}^{63}C_0} \tag{4.12}$$

where $^{65}C_0/^{63}C_0$ represents the isotopic ratio of the undissolved mineral. Dividing equations (4.11) and (4.12) by $^{65}C_0/^{63}C_0$ gives the isotope fractionation factor ($\alpha_{aq\text{-}min}{}^{o} = (^{65}R_{in}/^{63}R_{in})/(^{65}C_0/^{63}C_0)$) between undissolved mineral and Cu instantaneously released to solution.

While it is most likely that $^{65}k < {}^{63}k$ due to a kinetic isotope effect, the rate of oxidation of $^{65}Cu^{+}$ is faster than that of $^{63}Cu^{+}$ as described above ($^{65}F_{ox}/^{63}F_{ox} > {}^{65}C_0/^{63}C_0$). Therefore, values of $\alpha_{aq\text{-}min}{}^{o}$ become greater than 1 (Fig. 4.6a). Fig. 4.6a is plotted with arbitrary time units (because we do not know the values of k or F_{ox} nor mineral surface area) under the assumptions of $^{63}k > {}^{65}k$ and $^{65}F_{ox}/^{63}F_{ox} > {}^{65}C_0/^{63}C_0$. For this model with constant values of $^{6X}F_{ox}$, the system reaches a steady state value of 1.0013. Of course, mass balance requires that $^{65}F_{ox}/^{63}F_{ox}$ cannot remain larger than $^{65}C_0/^{63}C_0$ forever but rather must decrease with time as ^{65}Cu is depleted in the unoxidized remnant of the

mineral. The steady state in Figure 4.6a is thus quasi-stationary rather than representing true steady state, and is simply due to the fact that our model does not incorporate the change in ${}^{6X}F_{ox}$ that must occur with time. The fractionation observed between MC stream water and chalcopyrite samples is assumed to be at some point in time within this quasi-stationary state (Fig. 4.6a). Eventually $\alpha_{aq\text{-}min}{}^{o}$ will return to 1, which occurs when the isotopic composition of released Cu is the same as that in the bulk mineral (i.e., ${}^{65}R_{in}/{}^{63}R_{in} = {}^{65}C_0/{}^{63}C_0$).

We also used the model to calculate the values of $\alpha_{aq\text{-}min}{}^{o}$ expected for the cumulative Cu concentration during abiotic chalcopyrite dissolution (Fig. 4.6b) in closed system experiments using the same ${}^{65}k/{}^{63}k$ as for Figure 4.6a. For these experiments, the instantaneous steady state model value of $({}^{65}F_{ox}/{}^{63}F_{ox})/({}^{65}C_0/{}^{63}C_0)$ is 1.0378, which is much greater than that for the field (1.0013). Note that the cumulative steady state $({}^{65}F_{ox}/{}^{63}F_{ox})/({}^{65}C_0/{}^{63}C_0)$ value that is most consistent with the chalcopyrite leach experiments is 1.0013. Because F_{ox} must be proportional to the mineral surface area (A) to water volume (V) ratio during far-from-equilibrium dissolution, a greater $({}^{65}F_{ox}/{}^{63}F_{ox})/({}^{65}C_0/{}^{63}C_0)$ value for the leach experiments is to be expected since A/V is smaller in the field than the laboratory. If this model is applicable to MC, the quasi-steady state leaching of Cu sulfide near MC has lasted at least since the onset of mining in 1871 (Jones, 2007).

4.6.4. Biotic Copper Isotope Signatures

While varying degrees of formation of an oxidized layer on Cu sulfide surfaces may explain abiotic Cu isotope fractionation during leaching, other effects are needed to explain the observed biotic fractionation. Acidophilic microorganisms have developed coping mechanisms for high metal concentrations (Valls and de Lorenzo, 2002), including microbially-mediated precipitation, metal biosorption (the uptake or binding of metals to cellular components) (e.g., Beveridge and Murray, 1976; Mullen et al., 1989), and enzymatic transformation (Bruins et al., 2000; Valls and de Lorenzo, 2002). Recently, biosorption has been observed even at low pH. For example, Fowle and Fein (2001) observed that 1.11 mg Cu/g biomass sorbed to *Bacillus subtilis* cells at pH 2.6,

and 0.2 mg Cu/g biomass sorbed to a river water consortia at pH 2.3 (Johnson et al., 2007).

The observed biotic Cu isotope fractionation is therefore attributed to the same processes as in abiotic oxidative dissolution, but with the addition of preferential association of $^{65}Cu_{aq}$ with cells and related precipitates. Differences between our nonautoclaved biotic results and those of Mathur et al. (2005) were expected given that the volume percent inoculum we used was 200 times that of Mathur et al. The larger inoculum is consistent with greater association of ^{65}Cu with cells/precipitates and lower $\delta^{65}Cu_{aq}$ relative to the Mathur et al. experiments. We conclude that differences in the $\delta^{65}Cu_{aq}$ in laboratory and field systems represents the balance in any given system between Cu released to solution (f_{aq}) and Cu interaction with cells and related precipitates (f_b).

Consistent with this model, the TEM and EDS characterization of *A. ferrooxidans* cells demonstrates that the addition of Cu_{aq} to the growth medium results in metal-rich areas on the cell membranes, in cellular cytoplasm, and in granules within the cell (Fig. 4.4 and 4.5). Similarly, when incubated with aqueous U^{6+}, *A. ferrooxidans* accumulated electron-dense material in extracellular polysaccharides and polyphosphate granules within cells (Merroun et al., 2003). These observations, along with previous experimental studies of Cu adsorption onto bacterial surfaces (Fowle and Fein, 2001; Johnson et al., 2007), suggest that in our biotic system Cu_{aq} associates with cells through both sorption/precipitation onto cell membranes and uptake of Cu_{aq} into cells, resulting in depletion of $^{65}Cu_{aq}$. Interestingly, the $\Delta_{aq\text{-}min}{}^{o}$ values for the autoclaved and nonautoclaved biotic experiments were the same, within error, consistent with fractionation due to association with live or dead cells. The most likely cause of the fractionation is thus sorption onto membranes or coprecipitation with related precipitates rather than uptake.

In contrast to these inferences, Pokrovsky et al. (2008) observed that Cu sorbed to *Pseudomonas aureofaciens* cells from about pH 2 to 3 was 0.99 ± 0.10‰ to 1.80 ± 0.15‰ depleted in ^{65}Cu relative to Cu_{aq}. The fractionation observed by Pokrovsky et al. (2008) is in the opposite direction relative to fractionation measured in previous microorganism-Cu_{aq} incubation experiments ($\Delta_{bacteria/ppts\text{-}solution}$ = 2.20 + 0.23‰, Mathur et al., 2005; $\Delta_{bacteria\text{-}solution}$ = 0.6‰, Borrok et al., 2008b). The different biotic fractionations

among multiple microbial experiments may result from differences in cell surface properties given that prokaryotes are best adapted to certain environments. *Pseudomonas spp.* live at neutral pH in soil and aquatic environments, while *Acidithiobacillus spp.* are typically found at pH 2 to 4 (Madigan et al., 2003).

4.6.5. Potential for Sorption to Precipitates

The biotic fractionation observed in our experiments is not attributed to sorption of Cu_{aq} enriched in ^{65}Cu onto ferric precipitates for the following reasons. Our experiments were conducted at pH 2.0, well below the adsorption edge for Cu_{aq} sorption onto hydrous ferric oxides (Smith, 1999), and below the lowest pH tested for isotope fractionation following Cu_{aq} sorption to ferrihydrite (pH = 3.0, Balistrieri et al., 2008) and goethite (pH = 4, Pokrovsky et al., 2008). Copper has also been observed to sorb to jarosite and schwertmannite (e.g., Swedlund and Webster, 2001; Gräfe et al., 2008), but only for pH > 3. Below pH 3, sorption was negligible.

In the *initial* leach medium, the Fe content decreased in the order nonautoclaved biotic > autoclaved biotic > abiotic (Table 4.3). The additional Fe in the biotic experiments was Fe^{2+} and Fe^{3+} introduced with the inoculum. If sorption of Cu_{aq} onto introduced jarosite was important in the autoclaved biotic experiments, we would expect to have seen a difference in $\Delta_{aq\text{-}min}{}^{o}$ between the autoclaved and nonautoclaved biotic experiments. In contrast, the $\Delta_{aq\text{-}min}{}^{o}$ values for these sets of experiments were within error (Table 4.3).

Ferrous ion content in the abiotic and autoclaved biotic experiments was expected to remain relatively constant, since abiotic oxidation of Fe^{2+} is slow under acidic conditions (Nordstrom and Southam, 1997), while a decrease in $[Fe^{2+}]$ was expected in the nonautoclaved biotic experiments. This decrease did not occur in the nonautoclaved biotic enargite experiments, even though we observed live cells with optical microscopy throughout this experiment. In contrast, the $[Fe^{2+}]$ decreased quickly over 1 day in all chalcopyrite leach experiments (Table 4.3), presumably as a result of oxidation of Fe^{2+} in the medium by Fe^{3+} released from chalcopyrite. There is no Fe in enargite, so this phenomenon was not observed in the enargite leach experiments.

4.6.6. Implications

The Cu isotope composition of MC is an isotopic signature of abiotic oxidative sulfide dissolution. The $\delta^{65}Cu$ values for MC are similar to those for Fisher Creek ($1 \leq \delta^{65}Cu \leq 2‰$), a small mountain stream draining the New World mining district in southern Montana, USA (Borrok et al., 2008). Chalcopyrite is the only documented major Cu sulfide mineral in the deposits near Fisher Creek (Elliot et al., 1992); thus, the isotopic composition of Fisher Creek suggests that the abiotic chalcopyrite dissolution signature is also evident in Fisher Creek. This signature might be useful for AMD remediation and ore prospecting.

4.7. Conclusions

This is the first survey of the Cu isotope composition of both minerals and stream water in a natural acidic environment. The large Cu isotope fractionation between leached Cu in AMD and Cu in primary sulfides determined for this mining-impacted stream in Colorado resembles that observed in abiotic sulfide leach experiments, where leached Cu is isotopically enriched in ^{65}Cu relative to sulfides. Abiotic fractionation is attributed to preferential oxidation of $^{65}Cu^{+}$ at the mineral surface, and formation of an oxidized layer. The isotopically heavy Cu^{2+} in the partially oxidized layer is then assumed to leach faster than Cu^{+}. When acidophilic, Fe- and S-oxidizing *A. ferrooxidans* are present at high concentrations in leach experiments, the fractionation between aqueous Cu and Cu in sulfides is negligible (enargite dissolution) or smaller and opposite (chalcopyrite dissolution) to abiotic dissolution. Regardless of which mineral is leached, when *A. ferrooxidans* participate in oxidative leaching, association of Cu_{aq} with cells and related precipitates may preferentially sequester $^{65}Cu_{aq}$, and therefore overprint any abiotic Cu isotope effects that may have occurred.

Laboratory experiments show clear differences in Cu isotope fractionation during abiotic and biotic leaching that we originally though might also be identifiable in the field where oxidative sulfide dissolution by acidophilic microorganisms is well known (Nordstrom, 2000). However, in MC, the Cu isotope signature of leaching resembles abiotic leaching, which we attribute to lower cell densities in the field system as compared to our nutrient-rich laboratory experiments.

Our laboratory and field investigations also suggest that abiotic dissolution of Cu sulfide minerals is recognizable by positive $\Delta_{aq\text{-}min}$ values. More research is needed to elucidate why $\Delta_{aq\text{-}min}$ differs among different Cu sulfides, and how these isotopic signatures might be used for both AMD remediation and ore prospecting.

4.8. References

Archer, C. and Vance, D. (2004) Mass discrimination correction in multiple-collector plasma source mass spectrometry: an example using Cu and Zn isotopes. *Journal of Analytical Atomic Spectrometry* **19**, 656-665.

Archer, C., Vance, D., Bermin, J., Perkins, J., Statham, P. J., Lohan, M. C., Ellwood, M. J., and Mills, R. A. (2008) The copper isotope geochemistry of rivers and the oceans. *Geophysical Research Abstracts* **10**, EGU2008-A-05179.

Asael, D., Matthews, A., Bar-Matthews, M., and Halicz, L. (2007) Copper isotope fractionation in sedimentary copper mineralization (Timna Valley, Israel). *Chemical Geology* **243**, 238-254.

Baker, B. J. and Banfield, J. F. (2003) Microbial communities in acid mine drainage. *FEMS Microbiology Ecology* **44**, 139-152.

Balistrieri, L. S., Borrok, D. M., Wanty, R. B., and Ridley, W. I. (2008) Fractionation of Cu and Zn isotopes during adsorption onto amorphous Fe(III) oxyhydroxide: Experimental mixing of acid rock drainage and ambient river water. *Geochimica Cosmochimica Acta* **72**, 311-328.

Barron, J. L. and Lueking, D. R. (1990) Growth and maintenance of *Thiobacillus ferrooxidans* cells. *Applied and Environmental Microbiology* **56**, 2801-2806.

Beard, B. L., Johnson, C. M., Cox, L., Sun, H., Nealson, K. H., and Aguilar, C. (1999) Iron Isotope Biosignatures. *Science* **285**, 1889-1892.

Beard, B. L., Johnson, C. M., Skulan, J. L., Nealson, K. H., Cox, L., and Sun, H. (2003) Application of Fe isotopes to tracing the geochemical and biological cycling of Fe. *Chemical Geology* **195**, 87-117.

Bertocci, U. and Wagman, D. D. (1985) Copper, Silver, and Gold. In: Bard, A. J., Parsons, R., and Jordan, J. Eds.), *Standard potentials in aqueous solution*. Marcel Dekker, Inc., New York.

Beveridge, T. J. and Murray, R. G. E. (1976) Uptake and retention of metals by cell walls of Bacillus subtilis. *Journal of Bacteriology* **127**, 1502-1518.

Bevilaqua, D., Leite, A. L. L. C., Garcia, J., O., and Tuovinen, O. H. (2002) Oxidation of chalcopyrite by *Acidithiobacillus ferrooxidans* and *Acidithiobacillus thiooxidans* in shake flasks. *Process Biochemistry* **38**, 587-592.

Bigeleisen, J. and Mayer, M. G. (1947) Calculation of equilbrium constants for isotopic exchange reactions. *Journal of Chemical Physics* **15**, 261-267.

Bigham, J. M., Schwertmann, U., Traina, S. J., Winland, R. L., and Wolf, M. (1996) Schwertmannite and the chemical modeling of iron in acid sulfate waters. *Geochimica Cosmochimica Acta* **60**, 2111-2121.

Boekema, C., Krupski, A. M., Varasteh, M., Parvin, K., van Til, F., van der Woude, F., and Sawatzky, G. A. (2004) Cu and Fe valence states in $CuFeS_2$. *Journal of Magnetism and Magnetic Materials* **272-276**, 559-561.

Borrok, D. M., Nimick, D. A., Wanty, R. B., and Ridley, W. I. (2008) Isotopic variations of dissolved copper and zinc in stream waters affected by historical mining. *Geochimica Cosmochimica Acta* **72**, 329-344.

Borrok, D. M., Wanty, R. B., Ridley, W. I., Wolf, R., Lamothe, P. J., and Adams, M. (2007) Separation of copper, iron, and zinc from complex aqueous solutions for isotopic measurement. *Chemical Geology* **242**, 400-414.

Bove, D. J., Hon, K., Budding, K. E., Slack, J. F., Snee, L. W., and Yeoman, R. A. (2001) Geochronology and Geology of Late Oligocene Through Miocene Volcanism and Mineralization in the Western San Juan Mountains, Colorado*U. S. Geological Survey Professional Paper 1642*.

Bove, D. J., Mast, M. A., Dalton, J. B., Wright, W. G., and Yager, D. B. (2007) Major styles of mineralization and hydrothermal alteration and related solid- and aqueous-phase geochemical signatures. In: Church, S. E., von Guerard, P., and Finger, S. E. Eds.), *U. S. Geological Survey Professional Paper 1651*.

Bove, D. J., Mast, M. A., Wright, W. G., Verplank, P. L., Meeker, G. P., and Yager, D. B. (2000) Geologic control on acidic and metal-rich waters in the Southeast Red Mountains area, near Silverton, Colorado*5th International Conference on Acid Rock Drainage*. Society for Mining, Metallurgy, and Exploration, Inc., Denver, CO.

Brantley, S. L., Liermann, L. J., Guynn, R. L., Anbar, A., Icopini, G. A., and Barling, J. (2004) Fe isotopic fractionation during mineral dissolution with and without bacteria. *Geochimica et Cosmochimica Acta* **68**, 3189-3204.

Brown, E., Skougstad, M. W., and Fishman, M. J. (1970) Methods for collection and analysis of water samples from dissolved minerals and gases, *U. S. Geological Survey Techniques of Water-Resource Investigations*.

Bruins, M. R., Kapil, S., and Oehme, F. W. (2000) Microbial resistance to metals in the environment. *Ecotoxicology and Environmental Safety* **45**, 198-207.

Bullen, T. D., White, A. F., Childs, C. W., Vivit, D. V., and Schulz, M. S. (2001) Demostration of significant abiotic iron isotope fractionation. *Geology* **29**, 699-702.

Cornell, R. and Schwertmann, U. (2003) *The Iron Oxides: Structure, Properties, Reactions, Occurences and Uses*. Wiley-VCH.

Criss, R. E. (1999) *Principles of stable isotope distribution*. Oxford University Press, New York.

Ehrlich, H. L. (1964) Bacterial oxidation of arsenopyrite and enargite. *Economic Geology* **59**, 1306-1312.

Ehrlich, S., Butler, I., Halicz, L., Rickard, D., Oldroyd, A., and Matthews, A. (2004) Experimental study of the copper isotope fractionation between aqueous Cu(II) and covellite, CuS. *Chemical Geology* **209**, 259-269.

Elliot, J. E., Kirk, A. R., and Johnson, T. W. (1992) Field Guide: Gold-copper-silver deposits of the New World district. *Northwest Geology* **20-21**, 1-20.

Escobar, B., Huenupi, E., and Wiertz, J. V. (1997) Chemical and biological leaching of enargite. *Biotechnology Letters* **19**, 719-722.

Falco, L., Pogliani, C., Curutchet, G., and Donati, E. (2003) A comparison of bioleaching of covellite using pure cultures of *Acidithiobacillus ferrooxidans* and *Acidithiobacillus thiooxidans* or a mixed culture of *Leptospirillum ferrooxidans* and *Acidithiobacillus thiooxidans*. *Hydrometallurgy* **71**, 31-36.

Fantauzzi, M., Elsener, B., Atzel, D., Lattanzi, P., and Rossi, A. (2007) The surface of enargite after exposure to acidic ferric solutions: an XPS/XAES study. *Surface and Interface Analysis* **39**, 908-915.

Fowle, D. A. and Fein, J. B. (2001) Quantifying the effects of *Bacillus subtilis* cell walls on the precipitation of copper hydroxide from aqueous solution. *Geomicrobiology journal* **18**, 77-91.

Garcia, O. J., Bigham, J. M., and Tuovinen, O. H. (2007) Oxidation of isochemical FeS_2 (marcasite-pyrite) by *Acidithiobacillus thiooxidans* and *Acidithiobacillus ferrooxidans*. *Minerals Engineering* **20**, 98-101.

Goh, S. W., Buckley, A. N., Lamb, R. N., Rosenberg, R. A., and Moran, D. (2006) The oxidation states of copper and iron in mineral sulfides, and the oxides formed on initial exposure of chalcopyrite and bornite to air. *Geochimica Cosmochimica Acta* **70**, 2210-2228.

Gräfe, M., Beattie, D. A., Smith, E., Skinner, W. M., and Singh, B. (2008) Copper and arsenate co-sorption at the mineral-water interfaces of goethite and jarosite. *Journal of Colloid and Interface Science* **322**, 399-413.

Graham, S., Pearson, N., Jackson, S., Griffin, W., and O'Reilly, S. Y. (2004) Tracing Cu and Fe from source to porphyry: in situ determination of Cu and Fe isotope ratios in sulfides from the Grasberg Cu-Au deposit. *Chemical Geology* **207**, 147-169.

Hoare, J. P. (1985) Oxygen. In: Bard, A. J., Parsons, R., and Jordan, J. Eds.), *Standard potentials in aqueous solution*. Marcel Dekker, Inc., New York.

Icopini, G. A., Anbar, A. D., Ruebush, S. S., Tien, M., and Brantley, S. L. (2004) Iron isotope fractionation during microbial reduction of iron: The importance of adsorption. *Geology* **32**, 205-208.

Johnson, D. B. and Hallberg, K. B. (2003) The microbiology of acidic mine waters. *Research in Microbiology* **154**, 466-473.

Johnson, K. J., Szymanowski, J. E. S., Borrok, D. M., Huynh, T. Q., and Fein, J. B. (2007) Proton and metal adsorption onto bacterial consortia: Stability constants for metal-bacterial surface complexes. *Chemical Geology* **239**, 13-26.

Jones, W. R. (2007) History of mining and milling practices and production in San Juan County, Colorado, 1871-1991. In: Church, S. E., von Guerard, P., and Finger, S. E. Eds.), *U. S. Geological Survey Professional Paper 1651*.

Kawano, M. and Tomita, K. (2001) Geochemical modeling of bacterially induced mineralization of schwertmannite and jarosite in sulfuric acid spring water. *American Mineralogist* **86**, 1156-1165.

Kilpatrick, F. A. and Cobb, E. D. (1985) Measurement of discharge using tracers, *U. S. Geological Survey Techniques of Water Resource Investigations*.

Klauber, C. (2008) A critical review of the surface chemistry of acidic ferric suphate dissolution of chalcopyrite with regards to hindered dissolution. *International Journal of Mineral Processing* **86**, 1-17.

Klauber, C., Parker, A., van Bronswijk, W., and Watling, H. (2001) Sulphur speciation of leached chalcopyrite surfaces as determined by X-ray photoelectron spectroscopy. *International Journal of Mineral Processing* **62**, 65-94.

Larson, P. B., Maher, K., Ramos, F. C., Chang, Z., Gaspar, M., and Meinert, L. D. (2003) Copper isotope ratios in magmatic and hydrothermal ore-forming environments. *Chemical Geology* **201**, 337-350.

López-Archilla, A. I., Marin, I., and Amils, R. (2001) Microbial community composition and ecology of an acidic aquatic environment: Rio Tinto River, Spain. *Microbial Ecology* **41**, 20-35.

Lovely, D. R. and Phillips, E. J. P. (1986) Organic matter mineralization with reduction of ferric iron in anaerobic sediments. *Applied and Environmental Microbiology* **51**, 683-689.

Madigan, M. T., Martinko, J. M., and Parker, J. (2003) *Brock Biology of Microorganisms*. Prentice Hall, Upper Saddle River, NJ.

Majzlan, J., Navrotsky, A., and Schwertmann, U. (2004) Thermodynamics of iron oxides: Part III. Enthalpies of formation and stability of ferrihydrite (~Fe(OH)3), schwertmannite (~FeO(OH)3/4(SO4)1/8), and ε-Fe2O3. *Geochimica Cosmochimica Acta* **68**, 1049-1059.

Maréchal, C. N. and Albarède, F. (2002) Ion-exchange fractionation of copper and zinc isotopes. *Geochimica Cosmochimica Acta* **66**, 1499-1509.

Maréchal, C. N., Télouk, P., and Albarède, F. (1999) Precise analysis of copper and zinc isotopic compositions by plasma-source mass spectrometry. *Chemical Geology* **156**, 251-273.

Margulis, E. V., Getskin, N. A., Zapuskalova, N. A., and Beisekeeva, L. I. (1976) Hydrolytic precipitation of iron in the Fe2(SO4)3-KOH-H2O system. *Russian Journal of Inorganic Chemistry* **20**, 996-999.

Markl, G., Lahaye, Y., and Schwinn, G. (2006) Copper isotopes as monitors of redox processes in hydrothermal mineralization. *Geochimica Cosmochimica Acta* **70**, 4215-4228.

Mason, T. F. D., Weiss, D. J., Chapman, J. B., Wilkinson, J. J., Tessalina, S. G., Spiro, B., Horstwood, M. S. A., Spratt, J., and Coles, B. J. (2005) Zn and Cu isotope variability in the Alexandrinka volcanic-hosted massive sulfide (VHMS) ore deposit, Urals, Russia. *Chemical Geology* **221**, 170-187.

Mathur, R., Ruiz, J., Titley, S., Liermann, L., Buss, H., and Brantley, S. L. (2005) Cu isotopic fractionation in the supergene environment with and without bacteria. *Geochimica et Cosmochimica Acta* **69**, 5233-5246.

Merroun, M., Hennig, C., Rossberg, A., Reich, T., and Selenska-Pobell, S. (2003) Characterization of U(VI)-*Acidithiobacillus ferrooxidans* complexes using EXAFS, transmission electron microscopy, and energy-dispersive X-ray analysis. *Radiochimica Acta* **91**, 583-591.

Mullen, M. D., Wolf, D. C., Ferris, F. G., Beveridge, T. J., Flemming, C. A., and Bailey, G. W. (1989) Bacterial Sorption of Heavy Metals. *Applied and Environmental Microbiology* **55**, 3143-3149.

Nielsen, A. M. and Beck, J. V. (1972) Chalcocite oxidation and coupled carbon dioxide fixation by *Thiobacillus ferrooxidans*. *Science* **175**, 1124-1126.

Niyogi, D. K., Lewis, W. M. J., and McKnight, D. M. (2002) Effects of stress from mine drainage on diversity, biomass, and function of primary producers in mountain streams. *Ecosystems* **5**, 554-567.

Nordstrom, D. K. (2000) Advances in the Hydrogeochemistry and Microbiology of Acid Mine Waters. *international Geology Review* **42**, 499-515.

Nordstrom, D. K. and Southam, G. (1997) Geomicrobiology of sulfide mineral oxidation. *Reviews in Mineralogy and Geochemistry* **35**, 361-390.

Parker, A., Klauber, C., Kougianos, A., Watling, H., and van Bronswijk, W. (2003) An X-ray photoelectron spectroscopy study of the mechanism of oxidative dissolution of chalcopyrite. *Hydrometallurgy* **71**, 265-276.

Parkhurst, D. L. and Appelo, C. A. J. (1999) User's guide to PHREEQC (Version 2)--a computer program for speciation, batch-reaction, one-dimensional transport, and inverse geochemical calculations. In: Report, U. S. G. S. W. R. I. (Ed.),*U.S. Geological Survey*.

Pearce, C. I., Pattrick, R. A. D., Vaughan, D. J., Henderson, C. M. B., and van der Laan, G. (2006) Copper oxidation state in chalcopyrite: Mixed Cu d9 and d10 characteristics. *Geochimica Cosmochimica Acta* **70**, 4635-4642.

Pokrovsky, O. S., Viers, J., Emnova, E. E., Kompantseva, E. I., and Freydier, R. (2008) Copper isotope fractionation during its interaction with soil and aquatic microorganisms and metal oxy(hydr)oxides: Possible structural control. *Geochimica Cosmochimica Acta* **72**, 1742-1757.

Pokrovsky, O. S., Viers, J., and Freydier, R. (2005) Zn stable isotope fractionation during its adsorption on oxides and hydroxides. *Journal of Colloid Interface Science* **291**, 192-200.

Rimstidt, J. D., Chermak, J. A., and Gagen, P. M. (1994) Rates of reaction of galena, sphalerite, chalcopyrite, and arsenopyrite with Fe(III) in acidic solutions. In: Alters, C. N. and Blowes, D. W. Eds.), *Environmental geochemistry of sulfide oxidation*. American Chemical Society, Washington, DC.

Rodríguez, Y., Ballester, A., Blazquez, M. L., González, F., and Muñoz, J. A. (2003a) Study of bacterial attachment during the bioleaching of pyrite, chalcopyrite, and sphalerite. *Geomicrobiology Journal* **20**, 131-141.

Rodríguez, Y., Ballester, A., Blázquez, M. L., González, F., and Muñoz, J. A. (2003b) New information on the chalcopyrite bioleaching mechanism at low and high temperature. *Hydrometallurgy* **71**, 47-56.

Ross, P. N. (1985) Hydrogen. In: Bard, A. J., Parsons, R., and Jordan, J. Eds.), *Standard potentials in aqueous solution*. Marcel Dekker, Inc., New York.

Rouxel, O., Fouquet, Y., and Ludden, J. N. (2004) Copper isotope systematics of the Lucky Strike, Rainbow, and Logatchev sea-floor hydrothermal fields on the Mid-Atlantic Ridge. *Economic Geology* **99**, 585-600.

Runkel, R. L. and Kimball, B. A. (2002) Evaluating Remedial Alternatives for an Acid Mine Drainage Stream: Application of a Reactive Transport Model. *Environmental Science and Technology* **36**, 1093-1101.

Schauble, E. A. (2004) Applying stable isotope fractionation theory to new systems. *Reviews in Mineralogy and Geochemistry* **55**, 65-111.

Schemel, L. E., Kimball, B. A., and Bencala, K. E. (2000) Colloid formation and metal transport through two mixing zones affected by acid mine drainage near Silverton, Colorado. *Applied Geochemistry* **15**, 1003-1018.

Schwarz, T. E. (1883) Remarks on occurrences of ore in mines near Silverton*Colorado Scientific Society Proceedings*.

Sharma, P. K., Das, A., Rao, K. H., and Forssberg, K. S. E. (2003) Surface characterization of Acidithiobacillus ferrooxidans cells grown under different conditions. *Hydrometallurgy* **71**, 285-292.

Shields, W. R., Goldich, S. S., Garner, E. L., and Murphy, T. J. (1965) Natural variation in the abundance ratio and atomic weight of copper. *Journal of Geophysical Research* **70**, 479-491.

Smith, K. S. (1999) Metal sorption on mineral surfaces: an overview with examples relating to mineral deposits. In: Plumblee, G. S. and Logsdon, M. J. Eds.), *The Environmental Geochemistry of Mineral Deposits*. Society of Economic Geologists, Inc. .

Smith, K. S. and Huyck, J. L. O. (1999) An overview of the abundance, relative mobility, bioavailability, and human toxicity of metals. In: Plumblee, G. S. and Logsdon, M. J. Eds.), *The Environmental Geochemistry of Mineral Deposits*. Society of Economic Geologists, Inc. .

Swedlund, P. J. and Webster, J. G. (2001) Cu and Zn ternary surface complex formation with SO4 on ferrihydrite and schwertmannite. *Applied Geochemistry* **16**, 503-511.

Tributsch, H. (2001) Direct versus indirect bioleaching. *Hydrometallurgy* **59**, 177-185.

Urey, H. C. (1947) The thermodynamic properties of isotopic substances. *Journal of the Chemical Scoiety (London)*, 562-581.

Valls, M. and de Lorenzo, V. (2002) Exploiting the genetic and biochemical capacities of bacteria for the remediation of heavy metal pollution. *FEMS Microbiology Reviews* **26**, 327-338.

Wiederhold, J. G., Kraemer, S. M., Teutsch, N., Borer, P. M., Halliday, A. N., and Kretzschmar, R. (2006) Iron isotope fractionation during proton-promoted, ligand-controlled, and reductive dissolution of goethite. *Evironmental Science and Technology* **40**, 3787-3793.

Wincott, P. L. and Vaughan, D. J. (2006) Spectroscopic Studies of Sulfides. *Reviews in Mineralogy and Geochemistry* **61**, 181-229.

Wirt, L., Leib, K. J., Bove, D. J., Mast, M. A., Evans, J. B., and Meeker, G. P. (1999) Determination of chemical-constituent loads during base-flow and storm runoff conditions near historical mines in Prospect Gulch, upper Animas River watershed, southwestern, Colorado. U.S. Geological Survey.

Yu, J.-Y., Heo, B., Choi, I.-K., Cho, J.-P., and Chang, H.-W. (1999) Apparent solubilities of schwertmannite and ferrihydrite in natural stream waters polluted by mine drainage. *Geochimica Cosmochimica Acta* **63**, 3407-3416.

Yu, J.-Y., McGenity, T. J., and Coleman, M. L. (2001) Solution chemistry during the lag phase and exponential phase of pyrite oxidation by *Thiobacillus ferrooxidans*. *Chemical Geology* **175**, 307-317.

Zhdanov, S. I. (1985) Sulfur, Selenium, Tellurium, and Polonium. In: Bard, A. J., Parsons, R., and Jordan, J. Eds.), *Standard potentials in aqueous solution*. Marcel Dekker, Inc., New York.

Zhu, X. K., Guo, Y., Williams, R. J. P., O' Nions, R. K., Matthews, A., Belshaw, N. S., Canters, G. W., de Waal, E. C., Weser, U., Burgess, B. K., and Salvato, B. (2002) Mass fractionation processes of transition metal isotopes. *Earth and Planetary Science Letters* **200**, 47-62.

Zhu, X. K., O' Nions, R. K., Guo, Y., Belshaw, N. S., and Rickard, D. (2000) Determination of natural Cu-isotope variation by plasma-source mass spectrometry: implications for use as geochemical tracers. *Chemical Geology* **163**, 139-149.

Table 4.1. Chemistry and Cu isotopic composition of MC stream samples.

Sample[a] #	pH	[Cu] mg/kg	[Fe] mg/kg	$\delta^{65}Cu$[b] ‰	n[c]	$\Delta_{aq\text{-}En}$[d]	$\Delta_{aq\text{-}Cpy}$[e]
En	-	-	-	-0.01	9	-	-
Cpy	-	-	-	0.16	1	-	-
2-1	2.70	25	560	1.67	4	1.68	1.51
2-2	2.63	24	560	1.68	3	1.69	1.52
3	2.86	17	270	1.69	3	1.70	1.53
4	3.01	7	93	1.64	2	1.65	1.48
5	3.03	7.2	93	1.61	1	1.62	1.45
6	2.99	7.1	87	1.65	2	1.66	1.49
7	3.01	6.7	82	1.67	3	1.68	1.51
8	3.02	5.9	71	1.60*	3	1.61	1.44
9	3.20	5.3	70	1.64	2	1.65	1.48
10	5.06	0.4	1.5	1.62	1	1.63	1.46
11	5.24	0.3	1.4	1.48	2	1.49	1.32
12	3.70	0.2	1.5	1.38*	4	1.39	1.22
13	4.79	0.3	1.3	1.46	3	1.47	1.30
14	4.67	0.4	1.6	1.52	3	1.53	1.36

[a]Only filtered results are shown since no differences exist between filtered and unfiltered samples

[b]$\delta^{65}Cu$ values calculated according to Eqn. 5, with 2σ = 0.10‰.

[c]n = number of replicate isotope analyses

[d]$\Delta_{aq\text{-}min} = \delta^{65}Cu_{aq} - \delta^{65}Cu_{min}$, where aq = stream $\delta^{65}Cu$ values and min = En $\delta^{65}Cu$ value

[e]Ditto, min = Cpy $\delta^{65}Cu$ value

*The 2σ for replicate measurements is $\leq$ 0.14‰

Table 4.2. Chemistry and discharge measurements for selected MC stream samples.

Site #	Date	pH	Discharge L/s	Fe^{2+} mg/L	Fe_{tot} mg/L	% Fe^{2+}	[b]Cu mg/L	Cu mass flux mg/s
4	8/22/05	3.10	3.87	[a]80.11	[b]89.01	[a]90	6.824	26
5	8/22/05	3.10	3.91	[a]75.61	[b]84.01	[a]90	6.312	25
6	8/22/05	3.14	4.01	[a]49.63	[b]55.15	[a]90	4.765	19
9	8/22/05	3.11	4.08	[a]48.18	[b]53.53	[a]90	4.402	18
10	8/22/05	4.22	44.00	2.84	[c]3.36	85	0.815	36
11	8/22/05	4.22	44.14	2.93	[c]3.47	84	0.801	35
12	8/22/05	3.50	-	0.68	[c]1.53	44	0.319	-
14	8/22/05	4.19	46.86	2.8	[c]3.42	82	0.790	37

[a]Fe^{2+} values are assumed to be 90% of Fe_{tot}, based on previous measurements (see text)
[b]Measured in additional MC samples by ICP-MS
[c]Measured in additional MC samples by colorimetry
- not measured/applicable

Table 4.3. Chemistry and Cu isotopic compositions of laboratory samples.

Sample	Collection day	pH	[Cu] (mg/kg)	% Cu leached[a]	[Fe] (mg/kg)	[Fe^{2+}] (mg/kg)	$\delta^{65}Cu$[b] (‰)	n[c]	$\Delta_{aq\text{-}min}o$[d] (‰)	$\alpha_{aq\text{-}min}o$[e]
Chalcopyrite abiotic leach experiments										
Mineral	0	-	-	-	-	-	-0.01	2	-	-
Leach	0	2.0	BD	-	4469	4485	-	-	-	-
Leach	1	2.2	146	2.1	4645	1943	1.64	3	1.65	1.0017
Leach	7	-	351	5.1	4848	1722	1.08	3	1.09	1.0011
Leach	14	2.8	455	6.6	4805	1829	-	-	-	-
Chalcopyrite nonautoclaved biotic leach experiments										
Mineral	0	-	-	-	-	-	-0.01	2	-	-
Leach	0	2.0	BD	-	5017	3830	-	-	-	-
Leach	1	2.2	149	2.2	5146	2583	-0.43*	3	-0.42	0.9996
Leach	7	-	274	4.0	5090	2007	-0.94	3	-0.93	0.9991
Leach	14	2.2	528	7.6	5121	1890	-0.49	3	-0.48	0.9995
Chalcopyrite autoclaved biotic leach experiments										
Mineral	0	-	-	-	-	-	-0.01	2	-	-
Leach	0	1.9	BD	-	4559	4166	-	-	-	-
Leach	1	2.0	144	2.1	4385	1719	-0.23	3	-0.22	0.9998
Leach	7	-	275	4.0	4728	2113	-0.70*	3	-0.69	0.9993
Leach	14	2.1	475	6.9	4703	871	-0.68	3	-0.67	0.9993
Enargite-bearing abiotic leach experiments										
Mineral	0	-	-	-	-	-	0.29	4	-	-
Leach	0	2.0	BD	-	4469	4485	-	-	-	-
Leach	1	2.1	0.58	0.01	4409	4375	-	-	-	-
Leach	7	-	1.79	0.02	4719	4404	1.21	3	0.92	1.0009
Leach	14	2.2	2.50	0.03	4698	3499	1.34	2	1.05	1.0011
Enargite-bearing nonautoclaved biotic leach experiments										
Mineral	0	-	-	-	-	-	0.29	4	-	-
Leach	0	2.0	BD	-	5017	3830	-	-	-	-
Leach	1	2.2	1.80	0.02	5008	4127	0.13	3	-0.16	0.9998
Leach	7	-	2.96	0.03	5181	4336	0.46	3	0.17	1.0002
Leach	14	2.2	4.28	0.04	5094	3669	0.36	2	0.07	1.0001
Enargite-bearing autoclaved biotic leach experiments										
Mineral	0	-	-	-	-	-	0.29	4	-	-
Leach	0	1.9	BD	-	4559	4166	-	-	-	-
Leach	1	2.0	1.53	0.02	4680	3874	0.42*	4	0.13	1.0001
Leach	7	-	2.28	0.02	4728	4015	0.48	3	0.19	1.0002
Leach	14	2.1	3.08	0.03	4669	3477	0.77	2	0.48	1.0005

[a] %Cu leached = (mol Cu_{aq}/mol Cu_{total}) x 100

[b] $\delta^{65}Cu$ values calculated according to Eqn. 5, with $2\sigma = 0.10‰$

[c] n = number of replicate isotope analyses

[d] $\Delta_{aq\text{-}min}{}^{o} = \delta^{65}Cu_{aq} - \delta^{65}Cu_{min}{}^{o}$, where aq = leach $\delta^{65}Cu$ values and min^{o} = $\delta^{65}Cu$ value for undissolved mineral at day 0

[e] $\alpha_{aq\text{-}min}{}^{o} = (\delta^{65}Cu_{aq} + 1000)/(\delta^{65}Cu_{min}{}^{o} + 1000)$

BD = below detection; - = not measured

*The 2σ for replicate measurements is $\leq 0.14‰$

Appendix 4A.

The physical and chemical parameters for Mineral Creek stream sites. Temperature, specific conductance (K_{sc}), and pH were measured in-stream during sample collection. Cations were measured with ICP-AES, and anions were measured using IC.

Site #	Date	Treat-ment	Temp. °C	K_{sc} µS/cm	pH	Al mg/kg	Ba mg/kg	Ca mg/kg	Cu mg/kg	Fe mg/kg	K mg/kg	Mg mg/kg	Mn mg/kg	Na mg/kg	Ni mg/kg	Si mg/kg	Sr mg/kg	Zn mg/kg	F mg/kg	Cl mg/kg	NO_3 mg/kg	SO_4 mg/kg
2	8/19/05	filtered	-	-	-	66	0.03	330	25	560	4.0	46	51	43	0.38	19	11	145	10	1.1	-	2400000
2	8/19/05	unfiltered	5.4	4860	2.70	65	0.03	330	24	570	4.1	45	49	43	0.36	19	11	140	-	-	-	-
2	8/23/05	filtered	5.4	5010	2.63	67	0.03	320	26	560	4.2	46	50	44	0.37	19	11	150	9.6	1.1	-	2500000
3	8/23/05	filtered	12	3660	2.86	47	0.01	250	17	270	2.0	39	38	30	0.30	20	8.3	110	12	0.9	-	1700000
4	8/19/05	filtered	-	-	-	20	0.03	127	7.0	*	1.2	21	17	17	0.13	11	4.1	44	5.6	5.4	-	840
4	8/19/05	unfiltered	14.1	1600	3.01	20	0.03	126	6.9	95	1.1	21	17	17	0.12	11	4.1	45	-	-	-	-
5	8/19/05	filtered	-	-	-	20	0.03	126	7.2	*	1.1	20	17	17	0.13	11	4.1	45	5.3	5.4	-	1020
5	8/19/05	unfiltered	14.5	1670	3.03	20	0.03	126	7.5	94	1.0	20	17	17	0.13	11	4.1	45	-	-	-	-
6	8/19/05	filtered	-	-	-	20	0.03	125	7.1	*	1.1	20	17	17	0.13	11	4.1	47	5.0	5.5	-	940
6	8/19/05	unfiltered	14.4	1670	2.99	20	0.03	127	7.0	90	1.1	21	17	17	0.13	11	4.1	46	-	-	-	-
7	8/19/05	filtered	-	-	-	19	0.03	122	6.7	82	1.2	20	16	17	0.11	11	3.9	43	5.2	5.6	-	930
7	8/19/05	unfiltered	13.7	1640	3.01	19	0.03	122	6.7	84	1.0	20	16	17	0.13	11	3.9	42	-	-	-	-
8	8/19/05	filtered	-	-	-	17	0.03	118	5.9	71	0.8	19	15	16	0.10	11	3.7	39	4.8	5.5	-	810
8	8/19/05	unfiltered	13.6	1500	3.02	17	0.03	119	5.9	73	1.0	19	15	15	0.10	11	3.6	38	-	-	-	-
9	8/19/05	filtered	-	-	-	15	0.03	103	5.3	*	0.9	17	13	14	0.10	10	3.3	35	4.2	5.3	1.3	760
9	8/19/05	unfiltered	8.1	1430	3.20	15	0.03	102	5.2	71	1.0	17	13	14	0.12	10	3.3	34	-	-	-	-
10	8/17/05	filtered	-	-	-	0.8	0.03	21	0.4	*	0.3	2.3	1.0	2.5	0.02	2.3	0.5	3	0.6	1.1	1.0	95
10	8/17/05	unfiltered	14.5	211	5.05	1.2	0.03	21	0.4	4.6	0.3	2.3	1.0	2.5	0.02	2.3	0.5	3	-	-	-	-
11	8/17/05	filtered	-	-	-	0.4	0.03	20	0.3	*	0.3	2.2	0.8	2.3	0.01	2.2	0.46	3	0.3	1.1	1.3	92
11	8/17/05	unfiltered	14.2	190	5.24	0.9	0.03	21	0.3	3.9	0.3	2.2	0.8	2.3	0.01	2.3	0.46	3	-	-	-	-
12	8/17/05	filtered	-	-	-	0.8	0.02	20	0.2	*	0.9	2.1	1.6	4.5	0.01	3.2	0.68	10	0.3	3.4	1.0	140
12	8/17/05	unfiltered	5.9	413	3.70	0.7	0.02	21	0.2	1.6	0.8	2.2	1.6	4.2	0.03	3.2	0.67	11	-	-	-	-
13	8/17/05	filtered	-	-	-	0.6	0.03	22	0.3	1.3	0.3	2.3	0.9	2.4	0.01	2.3	0.48	3	0.3	1.2	6.4	94
13	8/17/05	unfiltered	13.7	205	4.79	0.9	0.03	21	0.3	3.8	0.4	2.3	0.9	2.4	0.00	2.4	0.48	3	-	-	-	-
14	8/17/05	filtered	-	-	-	0.9	0.03	21	0.4	*	0.3	2.4	1.0	2.6	0.02	2.4	0.52	3	0.4	1.2	0.2	100
14	8/17/05	unfiltered	13.2	209	4.67	1.2	0.03	21	0.4	4.9	0.4	2.4	1.0	2.6	0.02	2.4	0.51	3	-	-	-	-

* see Table 4.2 for Fe^{2+} and Fe^{3+} values used in thermodynamic calculations

- = not applicable

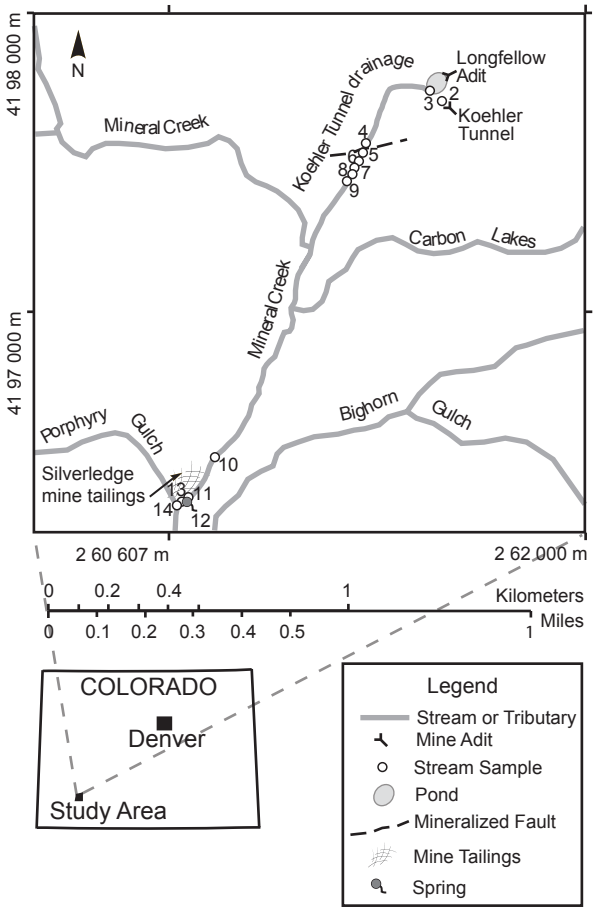

Figure 4.1. Location map for the MC drainage area showing stream sample locations. Notable mining features include the Longfellow Adit and Koehler Tunnel, which drain the interior of mineralized Red Mountain No. 3, and the Silverledge mine tailings. A mineralized fault transects the upper reach of the stream. Stream sample numbers correspond to those in Table 4.1.

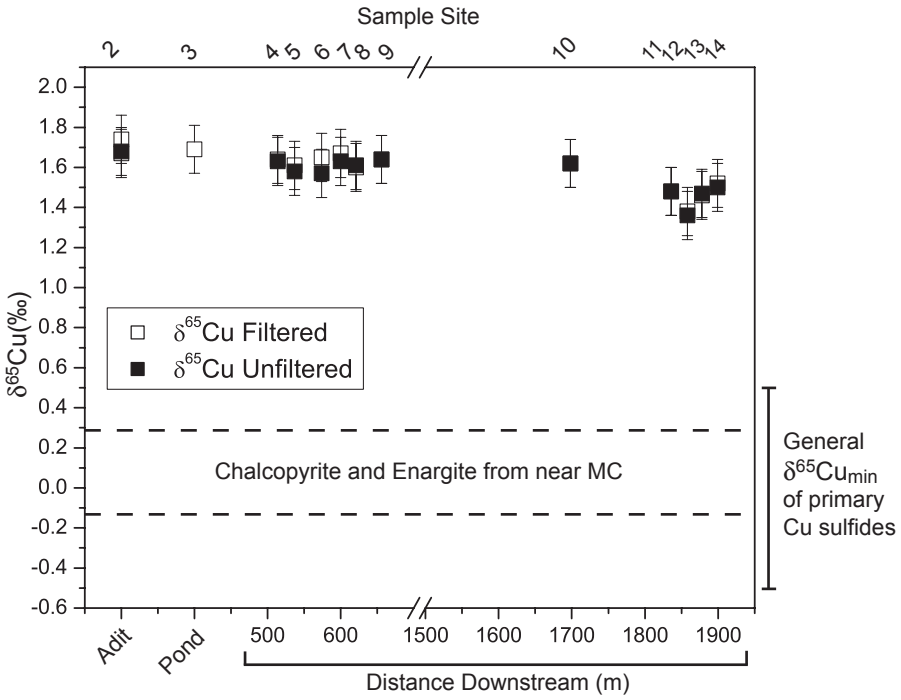

Figure 4.2. The $\delta^{65}Cu$ values for filtered and unfiltered MC samples and the range of $\delta^{65}Cu$ values for enargite and chalcopyrite samples. The sample site names correspond to those in Fig. 4.1. The general range of $\delta^{65}Cu_{min}$ values for primary terrestrial Cu sulfides (see text for references) is also shown.

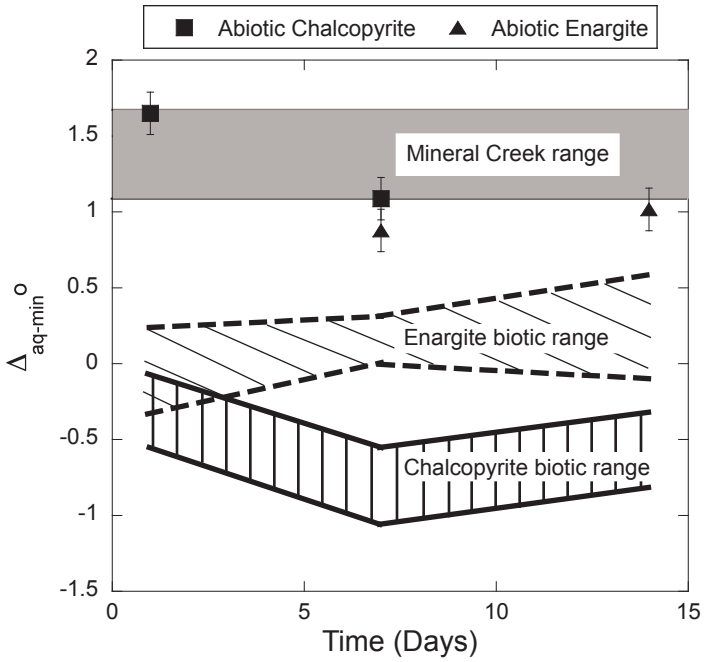

Figure 4.3. The $\Delta_{aq\text{-}min^o}$ values ($\Delta_{aq\text{-}min^o} = \delta^{65}Cu_{aq} - \delta^{65}Cu_{min^o}$, where Cu_{aq} is leached Cu and Cu_{min^o} is Cu in the original mineral) for abiotic leach experiments. Because $\Delta_{aq\text{-}min^o}$ was similar for the nonautoclaved and autoclaved biotic experiments (Table 4.3), ranges for the biotic chalcopyrite and enargite experiments are shown. The range of $\Delta_{aq\text{-}min}$ values for MC are also shown.

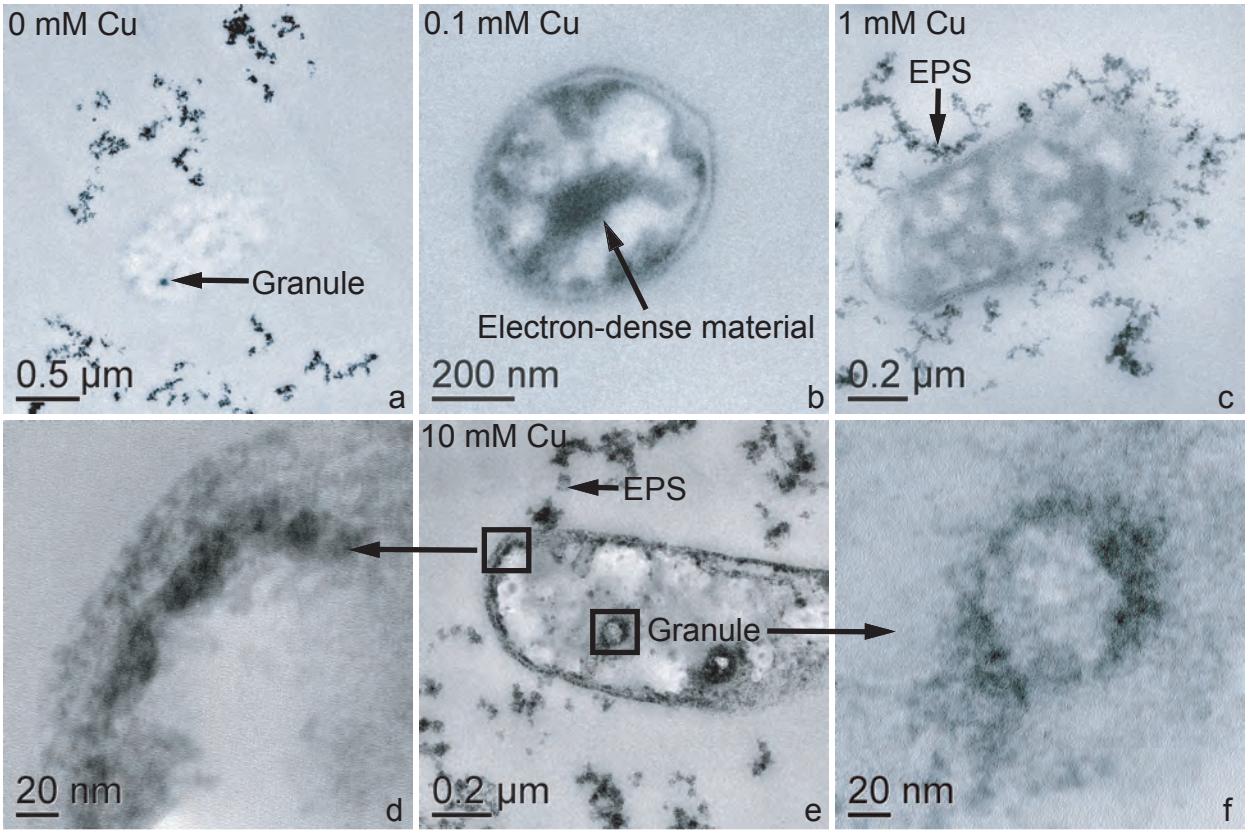

Figure 4.4. Transmission electron micrographs of *A. ferrooxidans* cells grown in medium containing 0, 0.1, 1, and 10 mM Cu. Note the electron-dense (darker) portions, representing metal-rich areas, in the cytoplasm (panels b, c, and e), in polyphosphate granules within the cell (panels a, e), on the cell membranes (panels b, c, d, and e), and in extracellular polymeric substances (EPS) surrounding the cell (panels c, e, and f). Note that panels d and f are higher resolution micrographs of the cell imaged in panel e. Although not pictured here, polyphosphate granules were found inside cells grown in all treatments.

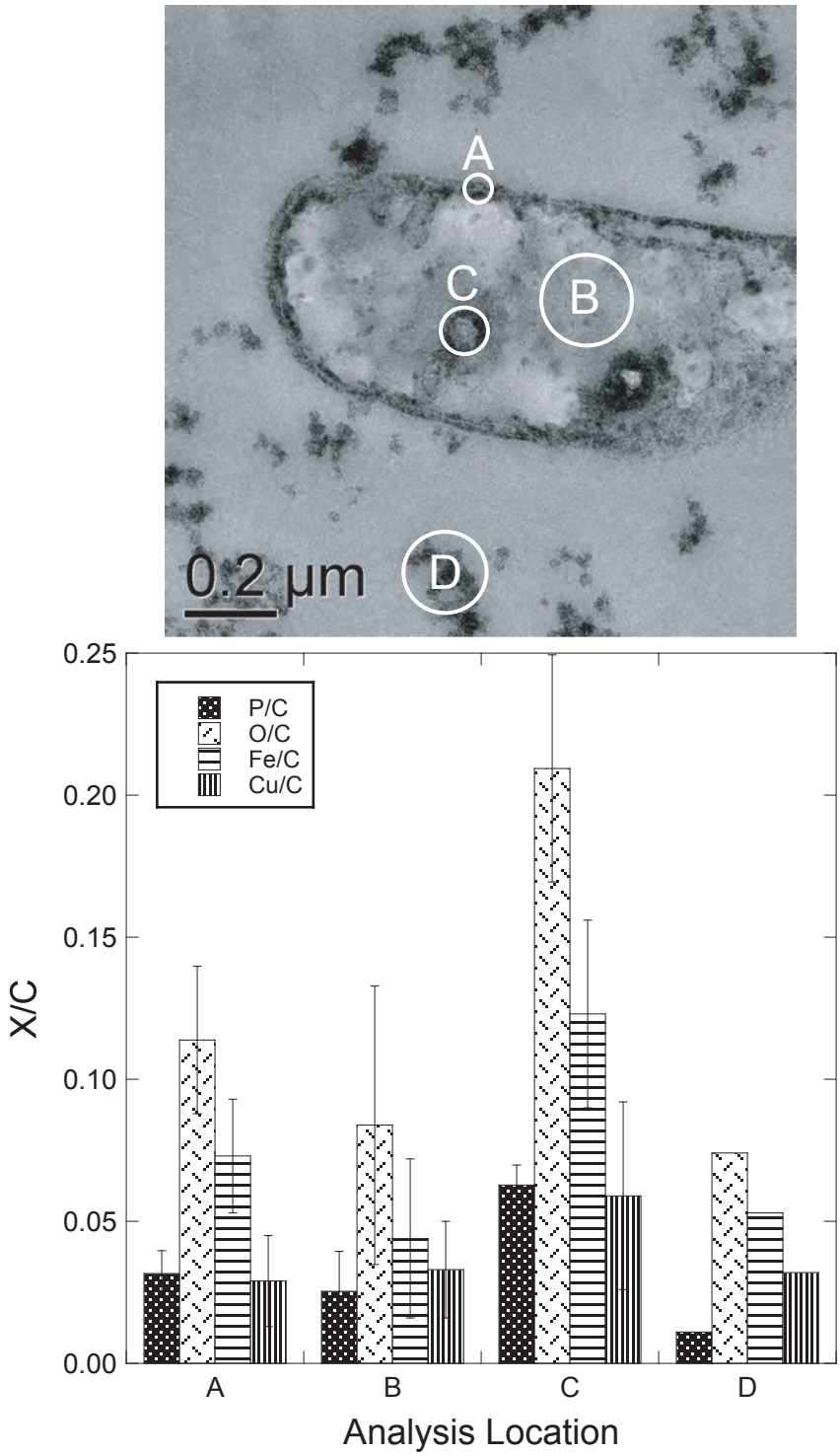

Figure 4.5. Upper image is a transmission electron micrograph of an *A. ferrooxidans* cell grown in 10 mM Cu with areas analyzed with EDS annotated. Lower graph indicates amotic % ratios for spot locations in upper image as measured by EDS. Analysis locations include cell membranes (A), the cytoplasm (B), a polyphosphate granule (C), and extracellular material (D). After background values for each element were removed, the ratios show that all analysis locations contain Cu. Error bars, if present, represent the standard deviation of multiple measurements. The x-ray beam spot-size is roughly equal to the diameter of the circles.

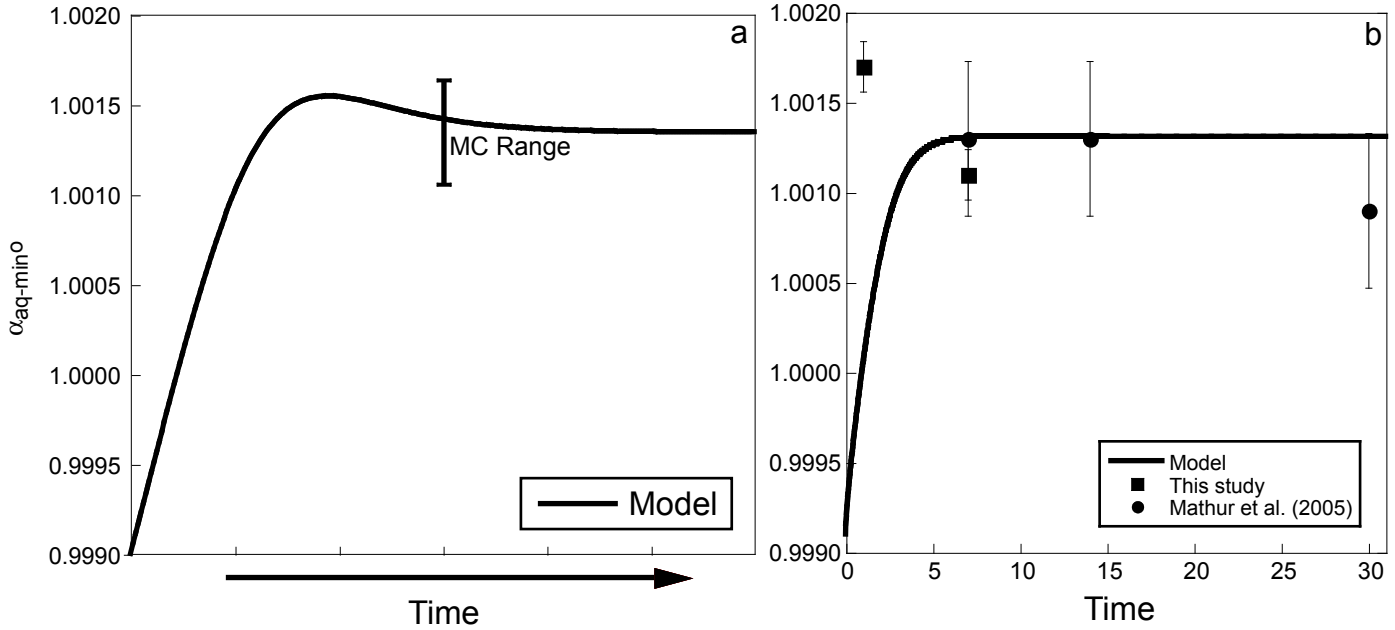

Figure 4.6. Measured (MC Range or symbols) and calculated (line) values of $\alpha_{aq\text{-}min^o}$ during abiotic chalcopyrite dissolution. Model values of $\alpha_{aq\text{-}min^o}$ are noted for an open system (instantaneous values, plot a), and for a closed system (cumulative values, plot b). Model values were set as follows: $^{65}k/^{63}k = 0.999$, x = 10 (for both (a) and (b)) and $^{65}F_{ox}/^{63}F_{ox}/^{65}C_0/^{63}C_0 = 1.0013$ (a), $^{65}F_{ox}/^{63}F_{ox}/^{65}C_0/^{63}C_0 = 1.0378$ (b). Note that the cumulative steady state $(^{65}F_{ox}/^{63}F_{ox})/(^{65}C_0/^{63}C_0)$ in (b) is 1.0013. Also, in plot (b) time is arbitrary for calculated values and represents days for measured values. For illustration, ratios of ^{6X}k and $^{6X}F_{ox}$ and x were chosen to model fit the data (see text).

Chapter 5

Bacterially-Mediated Precipitation of Jarosite: Implications for Copper Mobility and Isotopes in Acidic Environments

5.0. Abstract

The interaction of metals with microbial cells is an important factor in metal cycling, yet few studies have documented this interaction under acidic conditions. Previous experiments showed that the isotopic composition of Cu leachates from Cu sulfides were depleted in ^{65}Cu relative to ^{63}Cu when *Acidithiobacillus ferrooxidans* cells and related precipitates were present as compared to abiotic leachates. In an effort to understand this isotopic difference, we grew *A. ferrooxidans* in a Cu-bearing medium to determine how it interacts with Cu at pH = 2 and 22 ± 2ºC. Based on TEM and EDS, the highest Cu concentrations within cells occur near polyphosphate granules. Microscopic X-ray fluorescence (μ-XRF) observations show that cells of *A. ferrooxidans* grown in 1mM Cu may contain 0.11 ± 0.01 to 6.19 ± 0.28 fg Cu/cell. In the presence of cells, jarosite precipitates formed within 4 days. In contrast, abiotic experiments contained only amorphous precipitates as determined by x-ray and electron diffraction. Jarosite grains in biotic experiments grew in diameter from 0.5 to 1.5 μm over 5 days. Initial grains formed aggregates that were likely to have encircled cells. The lack of jarosite in experiments without cells and the cell-shaped growth patterns are consistent with nucleation of jarosite aggregates on *A. ferrooxidans* cell surfaces followed by mineral grain growth. Fe-oxidizing microorganisms growing in low pH, metal-rich systems may benefit from cell-controlled jarosite precipitation because this impurity-rich mineral commonly entrains toxic trace metals, such as Cu, into an insoluble form. Although we do not present new Cu isotopic results, these new observations are consistent with previous Cu isotope experiments if jarosite hosts isotopically heavy Cu relative to the growth medium. Further work is warranted to determine whether isotopic, chemical, and structural characteristics of jarosite function as a biosignature of microbial Fe-oxidation.

5.1. Introduction

The ubiquity of microorganisms and their roles in important geochemical processes is well known. Microbial cells are found in deep-sea hydrothermal fluids (e.g. Mandernack and Tebo, 1993; Edwards et al., 2005), groundwaters (e.g., Mahmood and Rama, 1993; Corapcioglu and Kim, 1995), brines (e.g. Harvey et al., 1982), neutral freshwaters (e.g. Geesey et al., 1977), and acidic freshwaters (e.g.Ferris et al., 1989; Hunt et al., 2001). The presence of microbiota can affect the chemical behavior of important elements, including toxic metals. For example, Beveridge and Murray (1976) were among the first to show that metals are selectively bound to the cell wall of a gram-positive bacterium. We now know that anionic functional groups within extracellular polymers that extend from cell walls are responsible for binding positively charged metals (e.g., Beveridge and Murray, 1980; Fein et al., 1997; Kelly et al., 2002; Boyanov et al., 2003; Jiang et al., 2004; Naja et al., 2005; Guiné et al., 2006). These metal-bacteria interactions have significant implications for metal sequestration in aqueous systems (Fein et al., 1997) as metal binding to cell walls can be a precursor to mineral precipitation (Fowle and Fein, 2001; Wightman and Fein, 2005).

Few studies have focused on acidophilic microorganism-metal interaction at low pH (Naja et al., 2005; Ginn and Fein, 2008; Kenney and Fein, 2009). In acidic, metal-rich environments near the Earth's surface, Fe-oxidizing microorganisms take advantage of the slow chemical oxidation of dissolved Fe(II) to Fe(III) (Schwertmann and Fitzpatrick, 1992; Nordstrom and Southam, 1997) by catalyzing this reaction for their energy needs. Microbial production of Fe(III) at low pH results in precipitation of the Fe-bearing minerals ferrihydrite, goethite, jarosite, and schwertmannite (Bigham et al., 1996a). Such minerals are known to scavenge trace metals during precipitation (Martínez and McBride, 1998; Hammarstrom et al., 2005; Hochella et al., 2005; Sidenko and Sherriff, 2005; Gunsinger et al., 2006; Cánovas et al., 2007).

In previous experiments, leached Cu was isotopically enriched in ^{65}Cu (based on $^{65}Cu/^{63}Cu$) relative to sulfides when bacteria were absent, and isotopically indentical to or depleted in ^{65}Cu relative to sulfides when *Acidithiobacillus ferrooxidans*, an Fe- and S-oxidizing Preteobacterium, was present (Mathur et al., 2005; Kimball et al., 2009). The isotopic differences were attributed to association of dissolved Cu enriched in ^{65}Cu with

cells (Mathur et al., 2005) or a combination of cells and Fe(III)-bearing precipitates that formed during growth (Kimball et al., 2009). Because the biotic Cu isotope signature described above was similar regardless of whether the cells were alive or heat-killed (Kimball et al., 2009), the major process affecting dissolved Cu isotopes was likely co-precipitation of ^{65}Cu with Fe(III)-precipitates.

To characterize the association of dissolved Cu with *A. ferrooxidans* cells and related precipitates, we used Transmission Electron Microscopy (TEM), and Energy Dispersive X-ray Spectroscopy (EDS) to probe the chemistry of subcellular and extracellular features. We also used X-ray Fluorescence Microscopy (μ-XRF) to measure the spatial distribution and concentration of Cu within single cells, and Micro-x-ray Diffraction (μ-XRD) to document the formation of jarosite during *A. ferrooxidans* growth. In addition to measuring the quantity of Cu within single cells, we discuss the possibility that jarosite formation is biologically controlled for the purpose of preventing Fe(III) and trace metals such as Cu from entering the cell at toxic levels. We use our observations to interpret the previous isotopic experiments and to elucidate the implications for using jarosite as a biosignature of microbial Fe-oxidation.

5.2. Methods

5.2.1. Cell growth

Acidithiobacillus ferrooxidans cells (ATCC® 13598) were grown on a modified $FeSO_4$-based medium consisting of the following: (in g/L) 0.8 $(NH_4)_2SO_4$, 2.0 $MgSO_4 \cdot 7H_2O$, 0.4 K_2HPO_4, Wolfes Mineral Solution (5mL), and 20.0 $FeSO_4 \cdot 7H_2O$, with the pH adjusted to 2.0 with concentrated H_2SO_4 (ATCC medium 2039). To separate batches of medium we added 0, 0.025, 0.25, or 2.5 g/L $CuSO_4 \cdot 5H_2O$ to make 0, 0.1, 1, and 10 mM Cu treatments, respectively. Cells were maintained in each medium at 22 ± 2ºC on a shaker set to 200 rpm, and were subcultured every 1-15 weeks prior to the experiment.

Cells analyzed by microscopic and spectroscopic techniques were allowed to grow for 2, 6, or 7 days before preparation for TEM. The first time we did TEM, the cultures experienced variable ambient temperatures during shipment for 4 days, and then were harvested and prepared for TEM at the Pacific Northwest National Laboratory after 6 days. In those samples, cell growth was confirmed after 5 days by the appearance of

orange precipitates, typical of the Fe precipitates related to *A. ferrooxidans* growth (Lazaroff et al., 1982; Barron and Lueking, 1990; Wang et al., 2006; Liu et al., 2007; Wang et al., 2007; Gramp et al., 2008; Gramp et al., 2009; Liao et al., 2009; Sasaki et al., 2009). In the second growth experiment, cultures were maintained at 22 ± 2ºC on a shaker set to 200 rpm, and were harvested and prepared for TEM at the Pennsylvania State University after 2 and 7 days. Orange precipitates in these samples appeared after 1 day of growth. In subsequent text, these two sample sets are referred to as *slow-growth* and *fast-growth*, respectively.

5.2.2. TEM and EDS

Aliquots of each culture, containing a cell and precipitate suspension, were centrifuged (4,000 - 8,000 × g; 1 - 2 min.), the supernatant discarded, and the cell/precipitate pellet was fixed in 2.5% glutaraldehyde. Aliquots of controls without cells containing abiotic precipitates were harvested the same way. The pellet was washed several times in PBS buffer, dehydrated in solutions of water + ethanol of increasing concentration, embedded in LR White resin and cured at 60ºC overnight. Hardened resin blocks were sectioned to 70 nm with a Diatome 45-degree diamond knife using a Leica UCT ultramicrotome (Leica Microsystems) and mounted on 200 mesh copper grids with formvar support film coated with carbon or on 150 mesh nickel grids with carbon coating. Unstained sections were examined at 120 kV using a Tecnai T-12 TEM (FEI Company) at the Pacific Northwest National Laboratory. Images were digitally collected and analyzed using DigitalMicrograph software (Gatan Inc.). We also used a JEOL 2010 high-resolution TEM equipped with an Oxford ISIS X-ray EDS microanalysis system for quantitative spectroscopy of elemental abundance. We used the electron diffraction capability of this instrument to examine the crystallinity of precipitates in biotic and abiotic experiments. A few samples were also viewed with a JEOL JEM 1200 EXII at Pennsylvania State University.

5.2.3. μ-XRF

The resin blocks sectioned for TEM and EDS were also sectioned for μ-XRF. These sections were 120 nm thick and were mounted onto 200 mesh alphanumeric gold

grids with formvar and carbon coating. Cells to be analyzed were imaged beforehand using TEM. We performed μ-XRF on these samples at beam line 2-ID-D at the Advanced Photon Source, Argonne National Laboratory, IL, USA (Cai et al., 2000). Samples were analyzed at 295 K under a He atmosphere using a 10 keV monochromatic X-ray incident beam focused to 0.15(V) x 0.2H μm^2 using a dual-zone plate and an order sorting aperture device (Yun et al., 1999). The beam was rastered across the sample in approximately 15 × 15 μm dimensions, with 0.5 μm step size for 0.5 s/point to collect low-resolution images and verify cell locations. Once accurate cell locations were found, higher resolution scans of approximately 3 - 5 × 3 - 5 μm, 0.1 μm step size, and 2 - 4 s/point were collected. Each pixel on the map corresponds to the integration of a specific region of interest around the Kα fluorescence energy for each element observed. Raw intensities were normalized to concentrations with thin film glass standards SRM 1832 and 1833 (National Institute of Standards and Technology, Gaithersburg, MD). Elemental maps were generated and analyzed with the program MAPS v 1.6.1.2 (Vogt, 2003).

5.2.4. μ-XRD

Well-mixed subsamples of abiotic and biotic cultures in the 0 and 1 mM Cu media were extracted after 2 - 8 days of fast growth. The subsamples were centrifuged (3 min.; 16,000 × g) and the supernatant was discarded. This process was repeated three times, and the final supernatant was not discarded, but instead used to create a dense slurry of cells and precipitates that was then injected into 1.0 mm quartz glass capillaries (Charles Supper Company, Natick, MA). The slurry was then analyzed using μ-XRD (Ragaku, DMAX-Rapid), using MoKα radiation (50 kV, 40 mA). We used a 0.8 mm collimator, an exposure time of 120 s, and we rotated the omega axis of the sample from 0 – 10° at 10°/s and the phi axis of the sample from -20 – 30° at 1°/s. Peak identification was accomplished using JADE version 7.0 (Materials Data, Inc.). To better compare spectra for each day, measured intensities were normalized by the intensity that occurred at 2θ = 40 in each spectrum. This intensity is representative of background values.

5.3. Results

5.3.1. TEM and EDS

Extracellular precipitates formed in the slow-growth experiments were aggregates of grains 20 - 50 nm in diameter after 6 days (Fig. 5.1). These precipitates did not diffract electrons, although we cannot definitively rule out that the precipitates were crystalline given the small grainsize. Extracellular precipitates in the fast-growth experiments were grains about 0.5 μm in size after 2 days (Fig. 5.1, 5.2a), and 1.5 μm in size after 7 days (Fig. 5.2b). These precipitates diffracted electrons, and were determined to be jarosite based on μ-XRD (see below). Aggregates of jarosite precipitates were commonly observed to surround voids in the micrographs of samples after 2 days of growth. Voids were rod shaped and typically 0.60 ± 0.23 μm in length and 0.38 ± 0.16 μm in width, similar to cells (Fig. 5.1e, 5.2a). This commonly observed distribution was not observed in the micrographs of samples after 7 days of growth (Fig. 5.2b). Abiotic controls showed no signs of microbial growth in any experiment, and white precipitates formed within a day of medium preparation in the abiotic flasks. In contrast to biotic experiments, abiotic precipitates formed after 2 days were globular and 0.5 to 0.75 μm in diameter (Fig. 5.3). Furthermore, unlike precipitates that formed in the presence of *A. ferrooxidans*, the abiotic precipitates did not diffract electrons. EDS measurements showed that the P/Fe of biotic precipitates was 0.2 and 0 (atomic %) for slow- and fast-growth experiments, respectively, and 0.6 ± 0.04 in abiotic precipitates (Fig. 5.3).

Microbial cell morphology was similar among fast-growing cells grown in 0, 1, and 10 mM Cu medium (Fig. 5.1). The most prominent morphological difference among the slow-growth cells was that in 1 mM Cu, small mineral aggregates were organized into long, slender chains that emanated from cells (Fig. 5.1b). Based on their similarity to previous cellular structures (e.g., Hunter and Beveridge, 2005; Reese and Guggenheim, 2007), these chains are assumed to be extracellular polymeric substances (EPS) that were encrusted with minerals (Fig. 5.1b). Encrusted EPS were not found to emanate from slow-growth cells in 1, 0.1, and 10 mM Cu, but the extracellular precipitates in these experiments resembled those associated with EPS in the 1 mM Cu experiments (Fig. 5.1a, b, c). EPS were not visible in the fast-growth experiments, but this does not preclude their existence since the TEM samples were not stained, and EPS could be

present but not visible.

Electron-dense granules appeared within cells grown in all biotic experiments (Figs. 5.1, 5.3). The average P/O for these granules was 0.27 ± 0.04 and 0.39 ± 0.09 for slow- and fast-growing cells, respectively, based on EDS (Fig. 5.3). These P/O values are suggestive of polyphosphate granules (Alvarez and Jerez, 2004).

5.3.2. μ-XRF

Figure 5.4 shows μ-XRF elemental mapping results for slow-growth and fast-growth cells. With the MAPS software, one can select a region of interest (ROI) within the elemental maps to calculate the concentration of a given element in $\mu g/cm^2$ for each pixel within the ROI. Using TEM images of cells as a guide, we selected ROIs that encompassed single cells. Knowing the thickness of the thin section (120 nm), we calculated the average volumetric concentration of an element within the ROI (in $\mu g/\mu m^3$). *A. ferrooxidans* are rod-shaped, and 0.5 - 0.6 μm wide by 1.0 - 2.0 μm long (Nemati et al., 1998). Assuming the geometry of the rod-shaped cells can be approximated by a cylinder, the cell volume of *A. ferrooxidans* ranges from 0.196 - 0.565 μm^3. With these values, and assuming the average elemental concentration of a section is representative of that within the entire cell, we calculated the total mass of a given element in a single cell (Table 5.1) (Kemner et al., 2004). Higher Cu, Fe, and P concentrations occur in slow-growth cells as compared to fast-growing cells (Fig. 5.4; Table 5.1). In both slow-growth and fast-growth experiments, Cu and Fe concentrations are highest near polyphosphate granules (Fig. 5.4).

5.3.3. μ-XRD

The μ-XRD patterns for abiotic and biotic precipitates after 2 days of growth were typical of amorphous material (Fig. 5.5). After 8 days, the amorphous material was still observed in abiotic experiments (Fig. 5.5a,c), but in fast-growth biotic experiments, crystalline material was observed (Fig. 5.5b,d). Each defined peak for precipitates in the biotic experiments corresponded to jarosite. The medium contained 12 mM NH_4^+, 4.6 mM K^+ and 0.085 mM Na^+ (Na^+ from the Wolfes Mineral Solution), so mixed jarosite $(K^+, Na^+, NH_4^+, H_3O^+)Fe_3(SO_4)_2(OH)_6$ was likely formed.

5.4. Discussion

5.4.1. Extracellular Mineral Precipitation

A solid solution forms between jarosite and alunite with K^+, Na^+, H_3O^+, and rarely NH_4^+, occupying the A sites and Fe^{3+} and Al^{3+} occupying the B sites (Welch et al., 2008). Minerals with $Fe^{3+} > Al^{3+}$ in their composition belong to the jarosite family, and minerals with $Fe^{3+} < Al^{3+}$ belong to the alunite family (Dutrizac and Jambor, 2000). Jarosite commonly forms near oxidized sulfide deposits and in acid sulfate soils on Earth (Dutrizac and Jambor, 2000) and has been identified at Meridiani Planum on Mars(Klingelhöfer et al., 2004). In such environments it is presumed that weathering of sulfides, particularly pyrite, provides the Fe(III), sulfate, and acid, which leaches silicate minerals and releases K^+ and Na^+. Generally, jarosite precipitates from oxic, acid solutions (pH < 3) that contain threshold level concentrations of Fe^{3+} (10-3 M, Brown, 1971), Na^+ (0.05 molar, Dutrizac, 1999), and K^+ (0.02 molar, Brown, 1970). When synthesized abiotically in the laboratory, ammoniojarosite [$(NH_4)Fe_3(SO_4)_2(OH)_6$] forms at 36 ºC after 27 days, 65 ºC after 8 days, and 95 ºC within 24 hours (Wang et al., 2007). Potassium jarosite, the most commonly formed end-member composition (Dutrizac and Jambor, 2000), has been synthesized abiotically within 4 hours at 95ºC (Baron and Palmer, 1996; Driscoll and Leinz, 2005).

Jarosite that forms in the presence of *A. ferrooxidans* at room temperature takes days to weeks to form (Wang et al., 2007; Gramp et al., 2008; Gramp et al., 2009; Sasaki et al., 2009). In our experiments at 22 ± 2ºC, jarosite was identified by μ-XRD after 4 days in fast-growth biotic experiments, and was not identified in parallel abiotic experiments over the course of 8 days. These studies suggest that although abiotic synthesis of sodium, potassium, and ammonium jarosite is theoretically possible at 25 ºC, the abiotic rates are slow (i.e., months) compared to biogenic formation. Jarosite has been shown previously to form in cultures of *A. ferrooxidans* (Wang et al., 2007; Gramp et al., 2008; Gramp et al., 2009; Sasaki et al., 2009), as well as in mixed Fe-oxidizing cultures (Wang et al., 2007; Gramp et al., 2009), and in cultures of the Fe-oxidizing archeaon *Sulfolobus metallicus* (Wang et al., 2007; Gramp et al., 2009). Jarosite formation appears to be independent of microbial species, but is instead linked to microbial oxidation of

dissolved Fe(II) to Fe(III) generally.

The biogenic jarosite precipitates formed in the fast-growth experiments contained no P, while P was detected in the abiotic precipitates (Fig. 5.3). Biogenic jarosite devoid of P is consistent with lower dissovled P concentrations in the fast-growth experiments due to uptake of P and storage in polyphosphate granules. In the abiotic experiments, dissolved P was available to sorb to the amorphous precipitates. The maximum possible HPO_4^{2-} concentration in the medium was 2.3 mM. The P concentrations in acidic settings where jarosite tends to form are usually lower, given that P is rapidly scavenged by acid-tolerant organisms or sorbed to ferric (oxyhydr)oxides (Tate et al., 1995). It is possible that P acted as an inhibitor to jarosite precipitation in the abiotic experiments, although there is no direct evidence to suggest this effect in the literature.

Biogenic formation of jarosite is believed to be indirect (Wang et al., 2007; Gramp et al., 2009). In other words, the formation of jarosite is not related to enzymatically-driven processes, and is therefore considered to form due to "biologically induced mineralization" (Lowenstam and Weiner, 1989). This differs from "biologically controlled mineralization," whereby minerals are formed directly from enzymatic reactions that control the nucleation, growth, and morphology of a mineral (Lowenstam and Weiner, 1989; Roden, 2008).

While biogenic formation of jarosite is conventionally thought to be biologically-induced, we present evidence that it is biologically-controlled. In the slow-growth experiments in 1 mM Cu medium, precipitates appear to have encrusted EPS (Fig. 5.1b). Additionally, figures 5.1e and 5.2a show aggregates that surround cell-shaped voids. These aggregates with cell-shaped voids were common in the fast-growth experiments after 2 days. We did not find cells within these voids, but this may result from a sample preparation artifact, where fixative diffusion into the cell was hindered by the mineral layer (Schädler et al., 2008), causing cells to lyse during dehydration. Alternately, the cells may have shed the outer mineral layer to prevent entombment, a process proposed for neutrophilic Fe-oxidizing microorganisms (e.g., Chan et al., 2004; Chan et al., 2009). Precipitates with cell-shaped voids were not evident after 7 days of growth, perhaps due to Ostwald ripening of the preexisting aggregated grains. The larger size of the jarosite

precipitates at 7 days and absence of smaller grains (Fig. 5.2) supports this hypothesis.

Nucleation of Fe (oxyhydr)oxides onto extracellular material produced by microorganisms has been observed previously. For example, Chan et al. (2004) and (2009) found nanocrystalline Fe (oxyhydr)oxides templated onto organic polymers from freshwater biofilms. The polymers were characterized as acidic microbial polysaccharides with carboxyl functional groups (Chan et al., 2009). The authors infer that microbial production of extracellular polysaccharides encourages localized precipitation of Fe (oxyhydr)oxides, which prevents Fe from entering the cell and decreases the pH near the cell membrane through hydrolysis, thereby strengthening the proton motive force near the cell wall. Precipitation of Fe (oxyhydr)oxides in this scenario benefits the microorganism, making it appropriate to consider that precipitates templated onto EPS could be classified as biologically-controlled (Perry et al., 2007). If the formation of jarosite were to serve a similar purpose for Fe-oxidizing microorganisms, it too might be considered a biologically-controlled mineral. Hydrogen ions are not limiting in the environments where jarosite forms, however, so biologically-controlled Fe (oxyhydr)oxide mineralization to decrease the pH near the cell is not necessary for acidophilic Fe-oxidizing microorganisms.

Binding of Fe(III) to deprotonated acidic functional groups on cell surfaces is required for microbial templation of Fe mineralization. Protonation of acidic functional groups at low pH will generally prevent other positively charged species from binding. Despite this, sorption of dissolved Fe onto microbial cells at low pH has been documented previously. For example, Wightman and Fein (2005) found that non-metabolizing *Bacillus subtilis* cells removed about 75% and 85% of aqueous Fe from solution (initial [Fe] = 1 ppm) at a bacterial concentration of 2 g/L and pH of 1.5 and 2.0, respectively. Additionally, *A. ferrooxidans* cells were shown to have zero surface charge at pH 2 when grown on ferrous Fe, according to zeta-potential studies (Sharma et al., 2003). Above pH 2 the cells were negatively charged (Sharma et al., 2003), which would promote binding of positively charged metals.

Negatively charged functional groups are found within microbial EPS (Douglass and Beveridge, 1998). *A. ferrooxidans* express differential EPS production, depending upon the growth conditions. Cells grown on pyrite produced 13 times more EPS than

cells grown on ferrous sulfate (Gehrke et al., 1998). This is not surprising, since *A. ferrooxidans* utilize EPS to attach to sulfide mineral substrates (e.g. Harneit et al., 2006). The EPS of both ferrous sulfate- and pyrite-grown cells contain neutral sugars, glucuronic acid, and Fe(III) (Gehrke et al., 1998). In the presence of pyrite, Fe(III) bound to EPS mediates cellular attachment to and attack of pyrite surfaces (Gehrke et al., 1998; Sand and Gehrke, 2006). The role of EPS for ferrous sulfate-grown cells is more obscure, but may be to nucleate Fe (oxyhydr)oxide mineralization, as was shown for Fe-oxidizing microorganisms near neutral pH (Chan et al., 2004; Chan et al., 2009). In low pH, metal-rich environments, the benefit to the cell of controlling Fe mineralization might be to entrain both Fe(III) and trace metals, such as Cu, away from the cell and into an insoluble form. In this context, *A. ferrooxidans* control on jarosite precipitation might be considered a metal-resistance mechanism.

5.4.2. Intracellular Mineral Precipitation

The polyphosphate granules that form within *A. ferrooxidans* cells (Figs. 5.1, 5.3, 5.4) are biologically-controlled minerals (according to Perry et al., 2007). Polyphosphate granules are common in Acidithiobacilli (Shively et al., 1970) and are believed to function as storage for nutrient P (Teske and Nelson, 2005), and to increase tolerance for intracellular heavy metals (Keasling and Hupf, 1996; Seufferheld et al., 2008 and references therein). For example, Alvarez and Jerez (2004) document that growth in high Cu concentration causes phosphate efflux from *A. ferrooxidans* to increase. They infer that polyphosphate granules within the cell break down through hydrolysis, allowing the formation of metal-phosphate complexes, which are then transported out of the cell. The proximity of higher Cu and Fe concentrations within cells to polyphosphate granules in this work (Fig. 5.4) suggests that excess metals in the cytoplasm bind to polyphosphate, which could lead to formation of metal-phosphate complexes that can be expelled from the cell if necessary. Strains of *A. ferrooxidans* have been adapted to grow in as much as 0.6 M Cu, but Cu concentrations above 0.3 M can be considered toxic to non-adapted strains of this bacterium (Boyer et al., 1998). Higher phosphate efflux during growth in medium containing 100 mM Cu was also observed with the archaeon *Sulfolobus metallicus* (Remonsellez et al., 2006). Interestingly, *Sulfolobus solfataricus* did not

accumulate polyphosphate granules and could not tolerate more than 5 mM Cu concentration (Remonsellez et al., 2006). This highlights that polyphosphate granules are found within both bacteria and archaea, and their presence is consistent with overcoming the stresses imposed by metal-rich environments (Seufferheld et al., 2008).

5.4.3. Copper Incorporation into Cells and Jarosite

The amount of Cu within a single *A. ferrooxidans* cell (≈ 0.1 – 6.2 fg/cell; Table 5.1) is comparable to the amount of Cu sorbed to other microorganisms under acidic conditions. Fowle and Fein (2001) observed that 1.1 mg Cu/g biomass sorbed to *Bacillus subtilis* cells at pH 2.6, and 0.2 mg Cu/g biomass sorbed to a river water consortia at pH 2.3 (Johnson et al., 2007). Assuming that the typical mass of an *A. ferrooxidans* cell can be approximated by 9.5×10^{-13} g (Neidhardt et al., 1990), we calculate a range of $0.12 \pm 0.01 – 6.5 \pm 0.3$ mg Cu/g biomass taken up by *A. ferrooxidans*, based on the data presented in Table 5.1. Significantly, this amount of Cu was removed from solution at low pH (= 2.0).

The amount of Cu within a single *A. ferrooxidans* cell becomes important when considering the density of cells in some environments. The Tinto River in southwestern Spain has a pH of 2.2 and extremely high metal concentrations (Fe 2.3 g/L, Zn 0.22 g/L, Cu 0.11 g/L) (López-Archilla et al., 2001). The combined average density of Fe- and S-oxidizing microorganisms in riverbed slurries collected from various sampling sites along the Tinto River was 6.7×10^5 cells/mL (in spring), 6.3×10^6 cells/mL (in summer), and 3.2×10^6 cells/mL (in autumn) (López-Archilla et al., 2001). Assuming that 3.4×10^6 cell/mL is a reasonable approximation for the density of Fe- and S-oxidizing cells in biofilms found in acidic, metal-rich environments, and that all Fe- and S-oxidizing microorganisms can withstand high metal concentrations, we calculate 0.00034 – 0.021 mg Cu/L as an estimate of the possible amount of Cu within metal-resistant cells in a saturated biofilm. This amount of Cu could potentially affect aqueous saturation states and mineral solubility. Thus, future study of how microbial cells and biofilms immobilize and release metals is worthwhile.

Another possible sink for Cu in acidic environments is co-precipitation with jarosite. The jarosite-alunite system can accommodate many elements within the crystal

structure (Papike et al., 2006a), and this mineral is known to scavenge toxic metals (Dutrizac and Jambor, 2000). Approximately 2 wt % Cu can substitute for Fe in sodium jarosite (Dutrizac, 1984). The rate of synthetic K-jarosite dissolution at room temperature ranges from 2.0×10^{-10} mol jarosite m^{-2} s^{-1} at pH 8 (Smith et al., 2006; Elwood Madden et al., 2009) to 1-3 $\times 10^{-9}$ mol jarosite m^{-2} s^{-1} at pH 2 (Baron and Palmer, 1996; Smith et al., 2006; Elwood Madden et al., 2009) and 7.0×10^{-9} mol jarosite m^{-2} s^{-1} at pH 5 (Elwood Madden et al., 2009). Experiments with environmental samples of jarosite gave a lower dissolution rate of 4.4×10^{-12} mol jarosite m^{-2} s^{-1} at pH 3 (Welch et al., 2008). If pH remains low (2.5 <), and arid conditions predominate, then jarosite should remain stable (Elwood Madden et al., 2004), making jarosite a potentially more permanent sink for Cu than microbial cells at low pH.

Incorporation of Cu enriched in ^{65}Cu into jarosite is consistent with previous experiments that showed residual dissolved Cu depleted in ^{65}Cu when *A. ferrooxidans* were present relative to when *A. ferrooxidns* were absent (Mathur et al., 2005; Kimball et al., 2009). This work indicates that jarosite was likely present in previous experiments with *A. ferrooxidans* and absent in previous experiments without *A. ferrooxidans*. Preferential co-precipitation of ^{65}Cu into the solid phase is expected given that heavier isotopes generally concentrate in the environment with the stiffest bonds (Bigeleisen and Mayer, 1947; Urey, 1947; Criss, 1999; Schauble, 2004). Copper substitutes for Fe in jarosite (Dutrizac, 1984), and Fe is bonded octahedrally to O in the crystal structure (Dutrizac and Jambor, 2000; Welch et al., 2008). When Cu substitutes for Fe in Pb-Cu-jarosite, Cu is bonded tetrahedrally to 4 O, with Cu-O bond lengths of 1.94 – 1.95 Å based on extended X-ray absorption fine structure spectroscopy (EXAFS) (Hudson-Edwards et al., 2008). Approximately half of the dissolved Cu in the 1 mM Cu medium was calculated to be $(Cu(H_2O)_6)^{2+}$, and the other half was $CuSO_4^0$ according to the chemical equilibrium-solving program PHREEQC and associated minteq.v4 thermodynamic database (Parkhurst and Appelo, 1999). Published bond lengths for the Cu-O bonds formed in $(Cu(H_2O)_6)^{2+}$ (Table 5.3), based on EXAFS measurements, range from 1.97 Å to 2.38 Å (Korshin et al., 1998; Fulton et al., 2000). The Cu-O bond length measured by EXAFS for aqueous $Cu(SO_4) \cdot 5H_2O$ is 2.20 Å (Koul and Padilla, 1985). Because Cu-O bonds in jarosite are shorter, they are likely stiffer and stronger than the

longer Cu-O bonds formed in the aqueous species (Table 5.3). As a result, it is conceivable that ^{65}Cu-O bonds are preferred over ^{63}Cu-O bonds in jarosite. Further study of the Cu isotope composition of trace Cu in jarosite is needed to verify this hypothesis.

If isotopically heavy Cu is preferentially co-precipiated with jarosite, the remaining Cu in solution will be relatively depleted in ^{65}Cu. The δ^{65}Cu values of stream water affected by acid mine drainage (AMD) ranged from 1.24‰ – 1.79‰, which resemble the δ^{65}Cu values (0.98‰ – 1.74‰) for Cu leached from sulfides in experiments without cells and associated jarosite precipitates (Kimball et al., 2009). In comparison, the δ^{65}Cu values for Cu leached from sulfides in the presence of live and dead cells and precipitates ranged from -0.57‰ – 0.87‰ (Kimball et al., 2009). The observation of relatively heavy dissolved Cu in the AMD-impacted stream could be consistent with lack of precipitation of jarosite in that environment. While thermodynamic calculations revealed that the stream was highly supersaturated with respect to jarosite (Kimball et al., 2009), the pH of the stream ($2.6 \leq pH \leq 5.2$) was above the pH (2.5) that jarosite generally precipitates (Bigham et al., 1996b). Copper isotope measurements may prove to be a valuable tool in characterizing the incorporation of Cu into secondary Fe (oxyhydr)oxide minerals.

5.4.4. Jarosite as a Biosignature

Jarosite was observed at Meridiani Planum using the Mössbauer spectrometer on NASA's Opportunity rover (Klingelhöfer et al., 2004). Jarosite is most often a secondary mineral, so its presence on Mars indicates weathering of the basaltic host rock by acidic, oxidative fluids. Such conditions could have supported life, thus, jarosite is believed to be a possible biosignature of microbial life on Mars (Skelley et al., 2004; Squyres and Knoll, 2005; Aubrey et al., 2006; Kotler et al., 2008). A biosignature is a physical and/or chemical remnant of life preserved in rocks and sediments. To be considered a biosignature of microbial Fe-oxidation, biogenic jarosite must be distinguishable from abiogenic jarosite, which, to our knowledge, has not been accomplished for environmental samples. Wang et al. (2007) synthesized biogenic ammoniojarosite (from 22 – 65ºC) and abiogenic ammoniojarosite (from 35 – 95ºC) and could not find major differences in XRD patterns, chemical composition, color, or surface area between the two sample types. Others have identified amino acids and other organic compounds

associated with terrestrial jarosite samples (Skelley et al., 2004; Aubrey et al., 2006; Kotler et al., 2008), but the origin of these organic compounds is not necessarily contemporaneous with jarosite mineralization.

It is possible that chemical composition, crystal habit, and surface area are diagnostic features of abiogenic and biogenic jarosite (Table 5.2). In jarosites from hydrothermal environments, where mineralization was likely not affected by microorganisms, prominent growth zones with alternating near-end-member jarosite ($KFe_3(OH)_6(SO_4)_2$) and natrojarosite ($NaFe_3(OH)_6(SO_4)_2$) were observed (Papike et al., 2006a; Papike et al., 2007; Burger et al., 2009). These presumably abiogenic hydrothermal jarosites exhibit fibrous, euhedral grains that are 10s to 100s of μm in size (Lueth et al., 2005; Papike et al., 2006a; Papike et al., 2006b).

In contrast, jarosite depositing today on andesitic rock surfaces near an acidic ($2.89 \leq pH \leq 3.37$) spring at 24.5ºC forms aggregated spherical particles with diameters of 5 – 10 μm (Kawano and Tomita, 2001). This jarosite is believed to result from microbially-induced mineralization because the Fe(III) concentrations downstream from the spring effluent can only be explained by microbial Fe(II) oxidation (Kawano and Tomita, 2001). Biogenic jarosite mineralization is expected to be more rapid than abiogenic jarosite mineralization at low temperature and pH because Fe(III) is not limiting. Consequently, biogenic jarosite grains are likely smaller and more anhedral than abiogenic grains formed at a similar temperature. The crystal habit and size of the spring jarosite is closer to that observed for the biogenic jarosite formed in the present study. Synthesized biogenic ammoniojarosite exhibited a surface area of 0.30 – 0.91 m^2/g (Wang et al., 2007). The surface area of larger, euhedral abiogenic jarosite is likely smaller.

If biogenic jarosite mineralization is indeed faster than abiogenic mineralization, then the likelihood of formation of end-member jarosite compositions is expected to be lower in biogenic jarosite. Consistent with this, Gramp et al. (2009) observed that ideal end-member compositions of jarosite are rare in biological systems. Future investigation of the isotopic, chemical, and structural characteristics of abiogenic and biogenic jarosite are needed to assess whether jarosite can be considered a biosignature of microbial Fe-oxidation.

5.5. Conclusions

While jarosite has been shown in the literature to form abiogenically, the rate is slower (i.e., months) than that for biogenic formation at earth surface conditions. In ferrous sulfate medium with or without dissolved Cu at 22 ± 2°C and pH = 2, jarosite was observed to precipitate in the presence of *A. ferrooxidans*, but not in abiotic experiments within the experimental period of 8 days. Biogenic jarosite grew from 0.5 μm diameter grains that formed aggregates around cell-shaped centers at 2 days to grains of 1.5 μm diameter at 7 days. The cell-related distribution of jarosite at 2 days and the absence of jarosite in abiotic experiments are consistent with aggregate nucleation by EPS on *A. ferrooxidans* cell surfaces followed by mineral grain growth through Ostwald ripening. Nucleation of jarosite onto cells in low pH, metal-rich environments may be of benefit to microorganisms because jarosite can entrain both Fe(III) and trace metals away from the cell and into an insoluble form. Preferential co-precipitation of isotopically heavy Cu with jarosite is consistent with isotopic observations reported for dissolved Cu in our earlier publication (Kimball et al., 2009).

A single *A. ferrooxidans* cell may contain a range of 0.11 ± 0.01 to 6.19 ± 0.28 fg Cu/cell, which amounts to 0.12 ± 0.01 – 6.5 ± 0.3 mg Cu/g biomass. Within cells, the highest Cu concentration occurs near polyphosphate granules. This observation, combined with published results showing higher phosphate efflux from *A. ferrooxdans* when grown in high Cu concentration, suggests that polyphosphate granules serve as a metal-defense mechanism, whereby metal-phosphate complexes are formed and transported out of the cell when necessary.

Based upon published results and this work, jarosite forms rapidly with a mixed composition, small grain size (20 nm – 10 μm), and high surface area (0.30 – 0.91 m^2/g) in the presence of Fe-oxidizing microorganisms as compared to abiogenic genesis. Further work is warranted to determine whether isotopic, chemical, and structural characteristics of jarosite are reliable biosignatures of microbial Fe-oxidation.

5.6. References

Alvarez, S. and Jerez, C. (2004) Copper ions stimulate poluphosphate degradation and phosphate efflux in Acidithiobacillus ferrooxidans. *Applied and Environmental Microbiology* **70**, 5177-5182.

Aubrey, A., Cleaves, H., Chalmers, J., Skelley, A., Mathies, R., Grunthaner, F., Ehrenfreund, P., and Bada, J. (2006) Sulfate minerals and organic compounds on Mars. *Geology* **34**, 357-360.

Baron, D. and Palmer, C. D. (1996) Solubility of jarosite at 4-35°C. *Geochimica Cosmochimica Acta* **60**, 185-195.

Barron, J. L. and Lueking, D. R. (1990) Growth and maintenance of *Thiobacillus ferrooxidans* cells. *Applied and Environmental Microbiology* **56**, 2801-2806.

Beveridge, T. J. and Murray, R. G. E. (1976) Uptake and retention of metals by cell walls of Bacillus subtilis. *Journal of Bacteriology* **127**, 1502-1518.

Beveridge, T. J. and Murray, R. G. E. (1980) Sites of metal deposition in the cell wall of Bacillus subtilis. *Journal of Bacteriology* **141**, 876-887.

Bigeleisen, J. and Mayer, M. G. (1947) Calculation of equilbrium constants for isotopic exchange reactions. *Journal of Chemical Physics* **15**, 261-267.

Bigham, J., Schwertmann, U., and Pfab, G. (1996a) Influence of pH on mineral speciation in a bioreactor simulating acid mine drainage. *Applied Geochemistry* **11**, 845-849.

Bigham, J. M., Schwertmann, U., Traina, S. J., Winland, R. L., and Wolf, M. (1996b) Schwertmannite and the chemical modeling of iron in acid sulfate waters. *Geochimica Cosmochimica Acta* **60**, 2111-2121.

Boyanov, M. I., Kelly, S. D., Kemner, K. M., Bunker, B. A., Fein, J. B., and Fowle, D. A. (2003) Adsorption of cadmium to *Bacillus subtilis* bacterial cell walls: a pH-dependent x-ray absorption fine structure spectroscopy study. *Geochimica et Cosmochimica Acta* **67**, 3299-3311.

Boyer, A., Magnin, J.-P., and Ozil, P. (1998) Copper ion removal by Thiobacillus ferrooxidans biomass. *Biotechnology Letters* **20**, 187-190.

Brown, J. (1970) A chemical study of some synthetic potassium-hydronium jarosites. *Canadian Mineralogy* **10**, 696-703.

Brown, J. (1971) Jarosite-goethite stabilities at 25°C, 1 atm. *Mineralium Deposita* **6**, 245-252.

Burger, P., Papike, J., Shearer, C., and Karner, J. (2009) Jarosite growth zoning as a recorder of fluid evolution. *Geochimica et Cosmochimica Acta* **73**, 3248-3259.

Cai, Z., Lai, B., Yun, W., Ilinski, P., Legnini, D., Maser, J., and Rodrigues, W. (2000) A hard x-ray scanning microprobe for fluorescence imaging and microdiffraction at the Advanced Photon Source. In: Meyer-Ilse, W., Warwick, T., and Attwood, D. Eds.)*X-Ray Microscopy: Proceedings of the Sixth International Conference*. American Institute of Physics, New York.

Cánovas, C. R., Olías, M., Nieto, J. M., Sarmiento, A. M., and Cerón, J. C. (2007) Hydrogeochemical characteristics of the Tinto and Odiel Rivers (SW Spain). Factors controlling metal contents. *Science of the Total Environment* **373**, 363-382.

Chan, C., De Stasio, G., Welch, S., Girasole, M., Frazer, B., Nesterova, M., Fakra, S., and Banfield, J. (2004) Microbial polysaccharides template assembly of nanocrystal fibers. *Science* **303**, 1656-1658.

Chan, C. S., Fakra, S. C., Edwards, D. C., Emerson, D., and Banfield, J. F. (2009) Iron oxyhydroxide mineralization on microbial extracellular polysaccharides. *Geochimica et Cosmochimica Acta* **73**, 3807-3818.

Corapcioglu, M. Y. and Kim, S. (1995) Modeling facilitated contaminant transport by mobile bacteria. *Water Resources Research* **31**, 2693-2697.

Criss, R. E. (1999) *Principles of stable isotope distribution*. Oxford University Press, New York.

Douglass, S. and Beveridge, T. J. (1998) Mineral formation by bacteria in natural microbial communities. *FEMS Microbiology Ecology* **26**, 79-88.

Driscoll, R. and Leinz, R. (2005) Methods for synthesis of some jarosites*Techniques and Methods 5-D1*. U.S. Geological Survey.

Dutrizac, J. (1984) The behaviour of impurities during jarosite precipitation. In: Bautista, R. (Ed.), *Hydrometallurgical Process Fundamentals*. Plenum Press, New York.

Dutrizac, J. (1999) Effectiveness of different jarosite species as seed for the precipitation of sodium jarosite. *Journal of Metals* **51**, 30-42.

Dutrizac, J. and Jambor, J. (2000) Jarosites and their application in hydrometallurgy. *Reviews in Mineralogy and Geochemistry* **40**, 405-452.

Edwards, K. J., Bach, W., and McCollom, T. M. (2005) Geomicrobiology in oceanography: microbe-mineral interactions at and below the seafloor. *Trends in Microbiology* **13**, 449-456.

Elwood Madden, M., Bodnar, R., and Rimstidt, J. (2004) Jarosite as an indicator of water-limited chemical weathering on Mars. *Nature* **431**, 821-823.

Elwood Madden, M., Madden, A. S., and Rimstidt, J. (2009) How long was Meridiani Planum wet? Applying a jarosite stopwatch to determine the duration of aqueous diagenesis. *Geology* **37**, 635-638.

Fein, J. B., Daughney, C. J., Yee, N., and Davis, T. A. (1997) A chemical equilibrium model for metal adsorption onto bacterial surfaces. *Geochimica et Cosmochimica Acta* **61**, 3319-3328.

Ferris, F. G., Schultze, S., Witten, T. C., Fyfe, W. S., and Beveridge, T. J. (1989) Metal interactions with microbial biofilms in acidic and neutral pH environments. *Applied and Environmental Microbiology* **55**, 1249-1256.

Fowle, D. A. and Fein, J. B. (2001) Quantifying the effects of *Bacillus subtilis* cell walls on the precipitation of copper hydroxide from aqueous solution. *Geomicrobiology Journal* **18**, 77-91.

Fulton, J. L., Hoffmann, M. M., Darab, J. G., Palmer, B. J., and Stern, E. A. (2000) Copper(I) and copper(II) coordination structure under hydrothermal conditions at 325ºC: An X-ray absorption fine structure and molecular dynamics study. *Journal of Physical Chemistry A* **104**, 11651-11663.

Geesey, G. G., Richardson, W. T., Yeomans, H. G., Irvin, R. T., and Costerton, J. W. (1977) Microscopic examination of natural sessile bacterial populations from an alpine stream. *Canadian Journal of Microbiology* **23**, 1733-1736.

Gehrke, T., Telegdi, J., Thierry, D., and Sand, W. (1998) Importance of extracellular polymeric substances from *Thiobacillus ferrooxidans* for bioleaching. *Applied and Environmental Microbiology* **64**, 2743-2747.

Ginn, B. R. and Fein, J. B. (2008) The effect of species diversity on metal adsorption onto bacteria. *Geochimica et Cosmochimica Acta* **72**, 3939-3948.

Gramp, J., Jones, F., Bigham, J., and Tuovinen, O. (2008) Monovalent cation concentrations determine the types of Fe(III) hydroxysulfate precipitates formed in bioleach solutions. *Hydrometallurgy* **94**, 29-33.

Gramp, J., Wang, H., Bigham, J., Jones, F., and Tuovinen, O. (2009) Biogenic synthesis and reduction of Fe(III)-hydroxysulfates. *Geomicrobiology Journal* **26**, 275-280.

Guiné, V., Spadini, G., Sarret, G., Muris, M., Delolme, C., Gaudet, J. P., and Martins, J. M. F. (2006) Zinc sorption to three Gram-negative bacteria: combined titration, modeling, and EXAFS study. *Environmental Science and Technology* **40**, 1806-1813.

Gunsinger, M. R., Ptacek, C. J., Blowes, D. W., Jambor, J., and Moncur, M. C. (2006) Mechanisms controlling acid neutralization and metal mobility within a Ni-rich tailings impoundment. *Applied Geochemistry* **21**, 1301-1321.

Hammarstrom, J. M., Seal, R. R. II, Meier, A. L., and Kornfeld, J. M. (2005) Secondary sulfate minerals associated with acid drainage in the eastern US: recycling of metals and acidity in surficial environments. *Chemical Geology* **215**, 407-431.

Harneit, K., Goksel, A., Kock, D., Klock, J.-H., Gehrke, T., and Sand, W. (2006) Adhesion to metal sulfide surfaces by cells of *Acidithiobacillus ferrooxidans*, *Acidithiobacillus thiooxidans*, and *Leptospirillum ferrooxidans*. *Hydrometallurgy* **83**, 245-254.

Harvey, R. W., Lion, L. W., Young, L. Y., and Leckie, J. O. (1982) Enrichment and association of lead and bacteria at particulate surfaces in a salt-marsh surface layer. *Journal of Marine Resources* **40**, 1201-1211.

Hochella, M. F. J., Moore, J. N., Putnis, C. V., Putnis, A., Kasama, T., and Eberl, D. D. (2005) Direct observation of heavy metal-mineral association from the Clark Fork River Superfund Complex: Implications for metal transport and bioavailability. *Geochimica Cosmochimica Acta* **69**, 1651-1663.

Hudson-Edwards, K. A., Smith, A. M. L., Dubbin, W. E., Bennett, A. J., Murphy, P. J., and Wright, K. (2008) Comparison of the structures of natural and synthetic Pb-Cu-jarosite-type compounds. *European Journal of Mineralogy* **20**, 241-252.

Hunt, A. P., Hamilton-Taylor, J., and Parry, J. D. (2001) Trace metal interactions with epilithic biofilms in small acidic mountain streams. *Archiv fur Hyrobiologie* **153**, 155-176.

Hunter, R. C. and Beveridge, T. J. (2005) High-resolution visualization of *Pseudomonas aeruginosa* PAO1 biofilms by freeze-substitution transmission electron microscopy. *Journal of Bacteriology* **187**, 7619-7630.

Jiang, W., Saxena, A., Song, B., Ward, B. B., Beveridge, T. J., and Myneni, S. C. B. (2004) Elucidation of functional groups on gram-positive and gram-negative bacterial surfaces using infrared spectroscopy. *Langmuir* **20**, 11433-11442.

Johnson, K. J., Szymanowski, J. E. S., Borrok, D. M., Huynh, T. Q., and Fein, J. B. (2007) Proton and metal adsorption onto bacterial consortia: Stability constants for metal-bacterial surface complexes. *Chemical Geology* **239**, 13-26.

Kawano, M. and Tomita, K. (2001) Geochemical modeling of bacterially induced mineralization of schwertmannite and jarosite in sulfuric acid spring water. *American Mineralogist* **86**, 1156-1165.

Keasling, J. and Hupf, G. (1996) Genetic manipulation of polyphosphate metabolism affects cadmium tolerance in *Escherichia coli*. *Applied and Environmental Microbiology* **62**, 743-746.

Kelly, S. D., Kemner, K. M., Fein, J. B., Fowle, D. A., Boyanov, M. I., Bunker, B. A., and Yee, N. (2002) X-ray absorption fine structure determinations of pH-dependent U-bacterial cell wall interactions. *Geochimica et Cosmochimica Acta* **66**, 3855-3871.

Kemner, K., Kelly, S., Lai, B., Maser, J., O'Loughlin, E., Sholto-Douglas, D., Cai, Z., Schneegurt, M., Kulpa, C., and Nealson, K. (2004) Elemental and redox analysis of single bacterial cells by X-ray microbeam analysis. *Science* **306**, 686-687.

Kenney, J. P. L. and Fein, J. B. (2009) Surface reactivity of acidophilic and alkaliphilic bacteria as determined by potentiometric titrations. *Geochimica et Cosmochimica Acta* **73**, A640.

Kimball, B. E., Mathur, R., Dohnalkova, A. C., Wall, A. J., Runkel, R. L., and Brantley, S. L. (2009) Copper isotope fractionation in acid mine drainage. *Geochimica et Cosmochimica Acta* **73**, 1247-1263.

Klingelhöfer, G., Morris, V., Bernhardt, B., Schröder, C., Rodionov, D., de Souza Jr., P., Yen, A., Gellert, R., Evlanov, E., Zubkov, B., Foh, J., Bonnes, U., Kankeleit, E., Gütlich, P., Ming, D., Renz, F., Wdowiak, T., Squyres, W., and Arvidson, R. (2004) Jarosite and hematite at Meridiani Planum from Opportunity's Mössbauer Spectrometer. *Science* **306**, 1740-1745.

Korshin, G. V., Fenkel, A. I., and Stern, E. A. (1998) EXAFS study of the inner shell structure in copper(II) complexes with humic substances. *Environmental Science and Technology* **32**, 2699-2705.

Kotler, J., Hinman, N., Yan, B., Stoner, D., and Scott, J. (2008) Glycine indentification in natural jarosites using laser desorption Fourier Transform Mass Spectrometry: Implications for the search for life on Mars. *Astrobiology* **8**, 253-266.

Koul, P. N. and Padilla, B. D. (1985) EXAFS studies of some copper and cobalt compounds and complexes in aqueous solution and polycrystalline form. *X-Ray Sptectrometry* **14**, 152-156.

Lazaroff, N., Sigal, W., and Wasserman, A. (1982) Iron oxidation and precipitation of ferric hydroxysulfates by resting *Thiobacillus ferrooxidans* cells. *Applied and Environmental Microbiology* **43**, 924-938.

Liao, Y., Zhou, L., Liang, J., and Xiong, H. (2009) Biosynthesis of schwertmannite by *Acidithiobacillus ferrooxidans* cell suspensions under different pH condition. *Materials Science and Engineering C* **29**, 211-215.

Liu, J., Li, B., Zhong, D., Xia, L., and Qui, G. (2007) Preparation of jarosite by *Acidithiobacillus ferrooxidans* oxidation. *Journal of the Central South University of Technology* **5**, 623-628.

López-Archilla, A. I., Marin, I., and Amils, R. (2001) Microbial community composition and ecology of an acidic aquatic environment: Rio Tinto River, Spain. *Microbial Ecology* **41**, 20-35.

Lowenstam, H. and Weiner, S. (1989) *On Biomineralization*. Oxford University Press, Oxford.

Lueth, V., Rye, R., and Peters, L. (2005) "Sour gas" hydrothermal jarosite: ancient to modern acid-sulfate mineralization in the southern Rio Grande Rift. *Chemical Geology* **215**, 339-360.

Mahmood, S. K. and Rama, R. P. (1993) Microbial abundance and degradation of polycyclic aromatic hydrocarbons in soil. *Bulletin of Environmental Contamination and Toxicology* **50**, 486-491.

Mandernack, K. W. and Tebo, B. M. (1993) Manganese scavenging and oxidation at hydrothermal vents and in vent plumes. *Geochimica et Cosmochimica Acta* **57**, 3907-3923.

Martínez, C. E. and McBride, M. B. (1998) Coprecipitates of Cd, Cu, Pb, and Zn in iron oxides: Solid transformation and metal solubility after aging and thermal treatment. *Clays and Clay Minerals* **46**, 537-545.

Mathur, R., Ruiz, J., Titley, S., Liermann, L., Buss, H., and Brantley, S. L. (2005) Cu isotopic fractionation in the supergene environment with and without bacteria. *Geochimica et Cosmochimica Acta* **69**, 5233-5246.

Naja, G., Mustin, C., Volesky, B., and Berthelin, J. (2005) A high-resolution titrator: a new approach to studying binding sites of microbial biosorbents. *Water Research* **39**, 579-588.

Neidhardt, F. C., Ingraham, J. L., and Schaechter, M. (1990) *Physiology of the Bacterial Cell: A Molecular Approach*. Sinauer Associates, Inc., Sunderland, Massachesetts.

Nemati, M., Harrison, S., Hansford, G., and Webb, C. (1998) Biological oxidation of ferrous sulphate by *Thiobacillus ferrooxidans*: a review on the kinetic aspects. *Biochemical Engineering Journal* **1**, 171-190.

Nordstrom, D. K. and Southam, G. (1997) Geomicrobiology of sulfide mineral oxidation. *Reviews in Mineralogy and Geochemistry* **35**, 361-390.

Papike, J., Burger, P., Karner, J., Shearer, C., and Lueth, V. (2007) Terrestrial analogs of martian jarosites: Major, minor element systematics and Na-K zoning in selected samples. *American Mineralogist* **92**, 444-447.

Papike, J., Karner, J., and Shearer, C. (2006a) Comparative planetary mineralogy: Implications of martian and terrestrial jarosite. A crystal chemical perspective. *Geochimica et Cosmochimica Acta* **70**, 1309-1321.

Papike, J., Karner, J., Spilde, M., and Shearer, C. (2006b) Terrestrial analogs of martian sulfates: Major and minor element systematics of alunite-jarosite from Goldfield, Nevada. *American Mineralogist* **91**, 1197-1200.

Parkhurst, D. L. and Appelo, C. A. J. (1999) User's guide to PHREEQC (Version 2)--a computer program for speciation, batch-reaction, one-dimensional transport, and inverse geochemical calculations. In: Report, U. S. G. S. W. R. I. (Ed.),*U.S. Geological Survey*.

Perry, R., Mcloughlin, N., Lynne, B., Sephton, M., Oliver, J., Perry, C., Campbell, K., Engel, M., Farmer, J., Brasier, M., and Staley, J. (2007) Definingh biominerals and organominerals: Direct and indirect indicators of life. *Sedimentary Geology* **201**, 157-179.

Reese, S. and Guggenheim, B. (2007) A novel TEM contrasting technique for extracellular polysaccharides in In Vitro biofilms. *Microscopy Research and Technique* **70**, 816-822.

Remonsellez, F., Orell, A., and Jerez, C. (2006) Copper tolerance of the thermoacidophilic archaeon *Sulfolobus metallicus*: possible role of polyphosphate metabolism. *Microbiology* **152**, 59-66.

Roden, E. (2008) Microbiological controls on geochemical kinetics 1: fundamentals and case study on microbial Fe(III) oxide reduction. In: Brantley, S. L., Kubicki, J. D., and White, A. F. Eds.), *Kinetics of Water-Rock Interaction*. Springer, New York.

Sand, W. and Gehrke, T. (2006) Extracellular polymeric substances mediate bioleaching/biocorrosion via interfactial processes involving iron(III) ions and acidophilic bacteria. *Research in Microbiology* **157**, 49-56.

Sasaki, K., Nakamuta, Y., Hirajima, T., and Tuovinen, O. (2009) Raman characterization of secondary minerals formed during chalcopyrite leaching with *Acidithiobacillus ferrooxidans*. *Hydrometallurgy* **95**, 153-158.

Schädler, S., Burkhardt, C., and Kappler, A. (2008) Evaluation of electron microscopic sample preparation methods and imaging techniques for characterization of cell-mineral aggregates. *Geomicrobiology Journal* **25**, 228-239.

Schauble, E. A. (2004) Applying stable isotope fractionation theory to new systems. *Reviews in Mineralogy and Geochemistry* **55**, 65-111.

Schwertmann, U. and Fitzpatrick, R. (1992) Iron Minerals in Surface Environments. In: Skinner, H. and Fitzpatrick, R. Eds.), *Biomineralization: Processes of Iron and Manganese: Modern and Ancient Environments*. Catena Verlag, Cremlingen, Germany.

Seufferheld, M., Alvarez, H., and Farias, M. (2008) Role of pholyphosphates in microbial adaptation to extreme environments. *Applied and Environmental Microbiology* **74**, 5867-5874.

Sharma, P. K., Das, A., Rao, K. H., and Forssberg, K. S. E. (2003) Surface characterization of *Acidithiobacillus ferrooxidans* cells grown under different conditions. *Hydrometallurgy* **71**, 285-292.

Shively, J., Decker, G., and Greenwalt, J. (1970) Comparative ultrastructure of the *Thiobacilli*. *Journal of Bacteriology* **101**, 618-627.

Sidenko, N. V. and Sherriff, B. L. (2005) The attenuation of Ni, Zn, and Cu, by secondary Fe phases of different crystallinity from surface and ground water of two sulfide mine tailings in Manitoba, Canada. *Applied Geochemistry* **20**, 1180-1194.

Skelley, A., Scherer, J., Aubrey, A., Grover, W., Ivester, R., Ehrenfreund, P., Grunthaner, F., Bada, J., and Mathies, R. (2004) Development and evaluation of a microdevice for amino acid biomarker detection and analysis on Mars. *Proceedings of the National Academy of Sciences* **102**, 1041-1046.

Smith, A. M. L., Hudson-Edwards, K. A., Dubbin, W. E., and Wright, K. (2006) Dissolution of jarosite [$KFe_3(SO_4)_2(OH)_6$] at pH 2 and 8: Insights from batch experiments and computational modelling. *Geochimica Cosmochimica Acta* **70**, 608-621.

Squyres, S. and Knoll, A. (2005) Sedimentary rocks at Meridiani Planum: Origin, diagenesis, and implications for life on Mars. *Earth and Planetary Science Letters* **240**, 1-10.

Tate, C. M., Broshears, R. E., and McKnight, D. M. (1995) Phosphate dynamics in an acidic mountain stream: Interactions involving algal uptake, sorption by iron oxide, and photoreduction. *Limnology and Oceanography* **40**, 938-946.

Teske, A. and Nelson, D. (2005) The Genera Beggiatoa and Thioploca. In: Dworkin, M., Falkow, S., Rosenberg, E., Schleifer, K.-H., and Stackerbrandt, E. Eds.), *The Prokaryotes: A Handbook on the Biology of Bacteria*. Springer-Verlag, New York.

Urey, H. C. (1947) The thermodynamic properties of isotopic substances. *Journal of the Chemical Scoiety (London)*, 562-581.

Vogt, S. (2003) MAPS: A set of software tools for analysis and visualization of 3D X-ray fluorescence data sets. *Journal De Physique IV* **104**, 635-638.

Wang, H., Bigham, J., Jones, F., and Tuovinen, O. (2007) Synthesis and properties of ammoniojarosites prepared with iron-oxidizing acidophilic microorganisms at 22-65°C. *Geochimica et Cosmochimica Acta* **71**, 155-164.

Wang, H., Bigham, J., and Tuovinen, O. (2006) Formation of schwertmannite and its transformation to jarosite in the presence of acidophilic iron-oxidizing microorganisms. *Materials Science and Engineering C* **26**, 588-592.

Welch, S., Kirste, D., Christy, A., Beavis, F., and Beavis, S. (2008) Jarosite dissolution II - Reaction kinetics, stoichiometry and acid flux. *Chemical Geology* **254**, 73-86.

Wightman, P. G. and Fein, J. B. (2005) Iron adsorption by *Bacillus subtilis* bacteral cell walls. *Chemical Geology* **216**, 177-189.

Yun, W., Lai, B., Cai, Z., Maser, J., Legnini, D., Gluskin, E., Chen, Z., Krasnoperova, A., Vladimirsky, Y., Cerrina, F., Di Fabrizio, E., and Gentili, M. (1999) Nanometer focusing of hard x rays by phase zone plates. *Review of Scientific Instruments* **70**, 2238-2241.

Table 5.1. Elemental masses calculated using μ-XRF data and MAPS software

	fg Cu/cell min	sd	fg Cu/cell max	sd	fg Fe/cell min	sd	fg Fe/cell max	sd	fg P/cell min	sd	fg P/cell max	sd
slow-growth	2.15	0.10	6.19	0.28	4.94	0.46	14.24	1.33	3.28	0.57	9.44	1.65
fast-growth	0.11	0.01	0.32	0.02	0.91	0.24	2.62	0.69	1.33	0.23	3.83	0.66

min = the mean value assuming a minimum cell volume of 0.196 μm^3
max = the mean value assuming a maximum cell volume of 0.565 μm^3
sd = 1 standard deviation

Table 5.2. Proposed characteristics of abiogenic and biogenic jarosite

	Chemical Composition	Crystal Habit	Surface Area	References
Abiogenic	Contains nearly pure end-member compositions of jarosite and natrojarosite in alternating growth zones	fibrous, euhedral grains; 10s to 100s of μm	< 0.30 m^2/g	Lueth, 2005 #41; Burger, 2009 #38; Papike, 2007 #37; Papike, 2006 #34
Biogenic	Devoid of end-member compositions; mixed jarosite is common	aggregated spherical particles; 20 nm - 10 μm	0.30 - 0.91 m^2/g	Kawano, 2001 #42; Wang, 2007 #9; Gramp, 2009 #12; This Study

Table 5.3. Bond lengths for Cu-O bonds in various phases

Phase	Bond description	Bond length (Å)	Bond description	Bond length (Å)	Reference
Pb-Cu-jarosite	Cu-O tetrahedra	1.94 - 1.95			Hudson-Edwards et al. (2008)
$[Cu(H_2O)_6]^{2+}$	4 equatorial Cu-O	1.97 ± 0.01	2 axial Cu-O	2.24 ± 0.03	Korshin et al. (1998)
$[Cu(H_2O)_6]^{2+}$	4 equatorial Cu-O	1.97	2 axial Cu-O	2.38	Fulton et al. (2000)
$Cu(SO_4).5H_2O$	aqueous Cu-O	2.20			Koul & Padilla (1985)

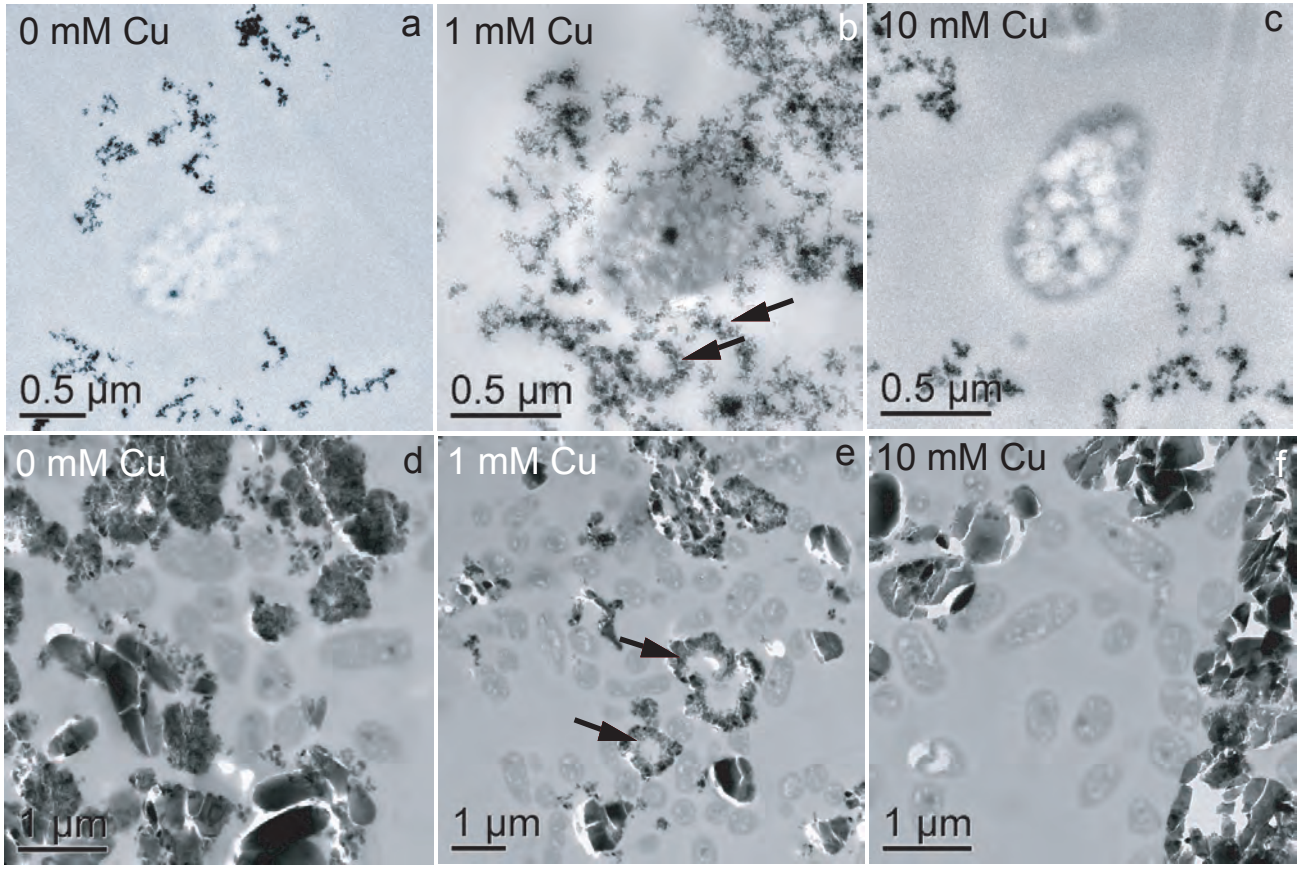

Figure 5.1. TEM images of slow-growth cells (a,b,c) and fast-growth cells (d,e,f) from samples grown in solutions of different Cu concentration. Cells are less electron-dense than the precipitates. Some precipitates in the fast-growth experiments have a cracked appearance, which is an artifact of thin sectioning. Arrows in (b) point to mineral encrusted extracellular polymeric substances (EPS), which were only visible in the slow-growth 1 mM Cu experiments. Extracellular precipitates in the other slow-growth experiments resemble those that encrust EPS in the 1 mM Cu experiments. Arrows in (e) point to aggregates of precipitates that form cell-shaped voids, which were common in the fast-growth experiments after 2 days of growth. We did not find cells within these voids, but this may result from a sample preparation artifact or shedding of the mineral layer to prevent entombment.

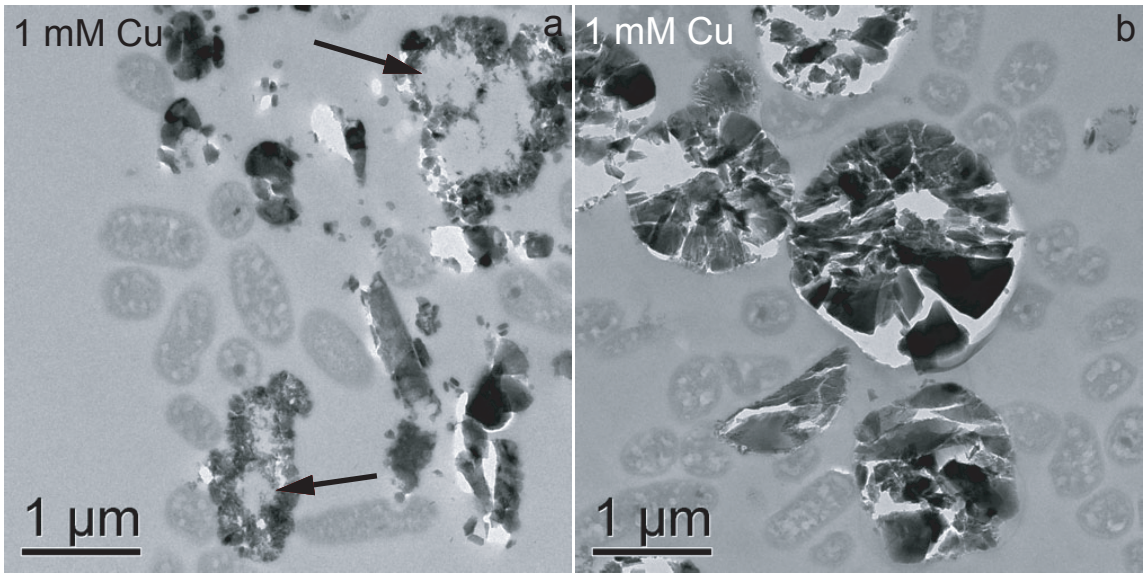

Figure 5.2. TEM images of fast-growing cells grown in solutions containing 1 mM Cu after 2 days of growth (a) and 7 days of growth (b). Note how the jarosite precipitates grew in size by 7 days, perhaps due to Ostwald ripening of the smaller aggregates observed at 2 days. Arrows in (a) point to precipitates with cell-shaped voids, which were common in the fast-growth experiments after 2 days of growth.

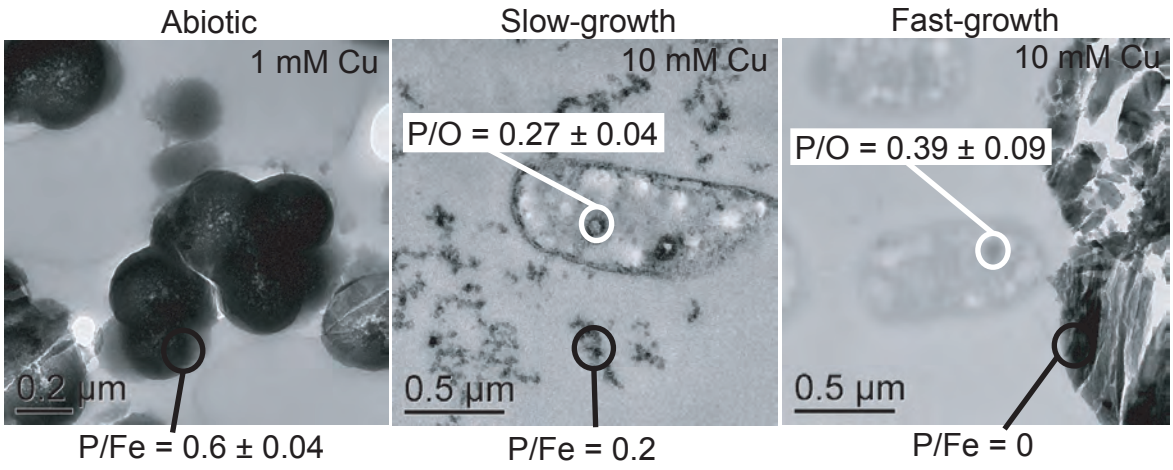

Figure 5.3. TEM images of abiotic, slow-growth, and fast-growth experiments. The average elemental ratios for precipitates in all experiments and polyphosphate granules within the biotic experiments are also displayed.

Figure 5.4. TEM and false-color μ-XRF images of slow-growth cells (left) and fast-growth cells (right). Higher Cu, Fe, and P concentrations occur in slow-growth cells and related precipitates relative to fast-growth cells. In both experiments, higher Cu concentrations tend to occur near polyphosphate granules.

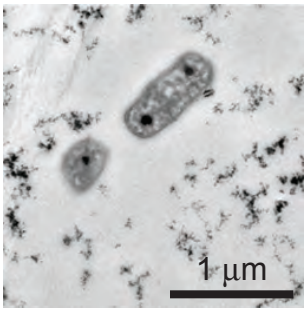

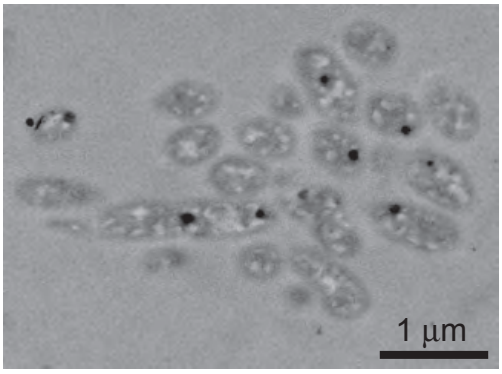

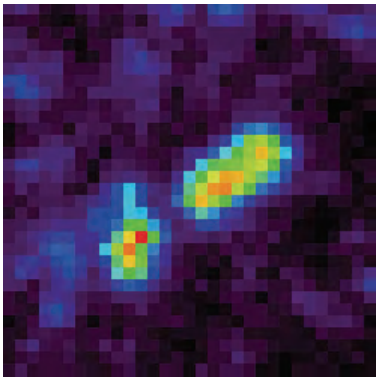

0.057 0.240

µg Cu/cm²

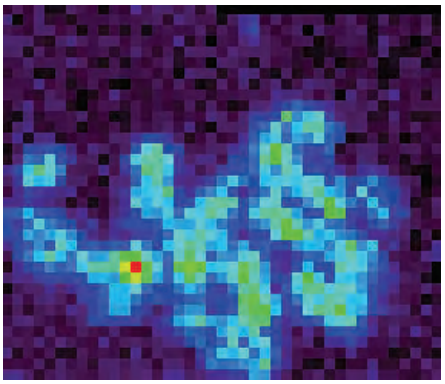

0.003 0.014

µg Cu/cm²

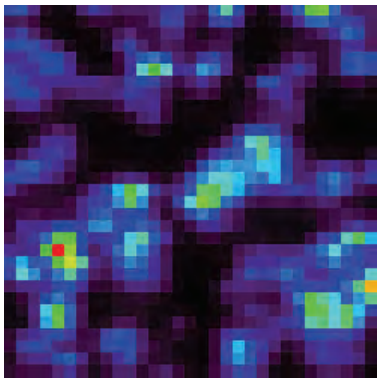

0.020 1.270

µg Fe/cm²

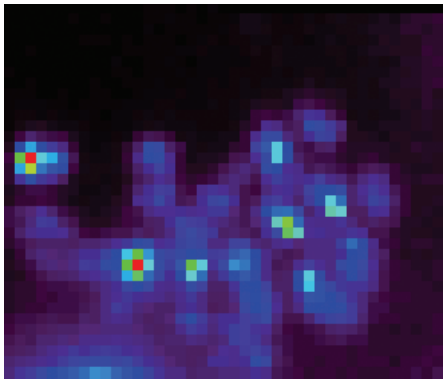

0.006 0.292

µg Fe/cm²

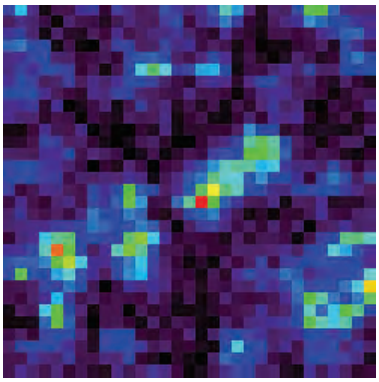

0 0.647

µg P/cm²

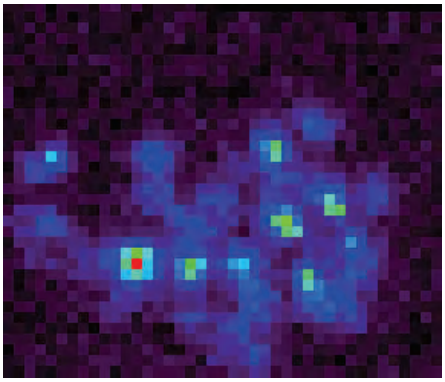

0.013 0.386

µg P/cm²

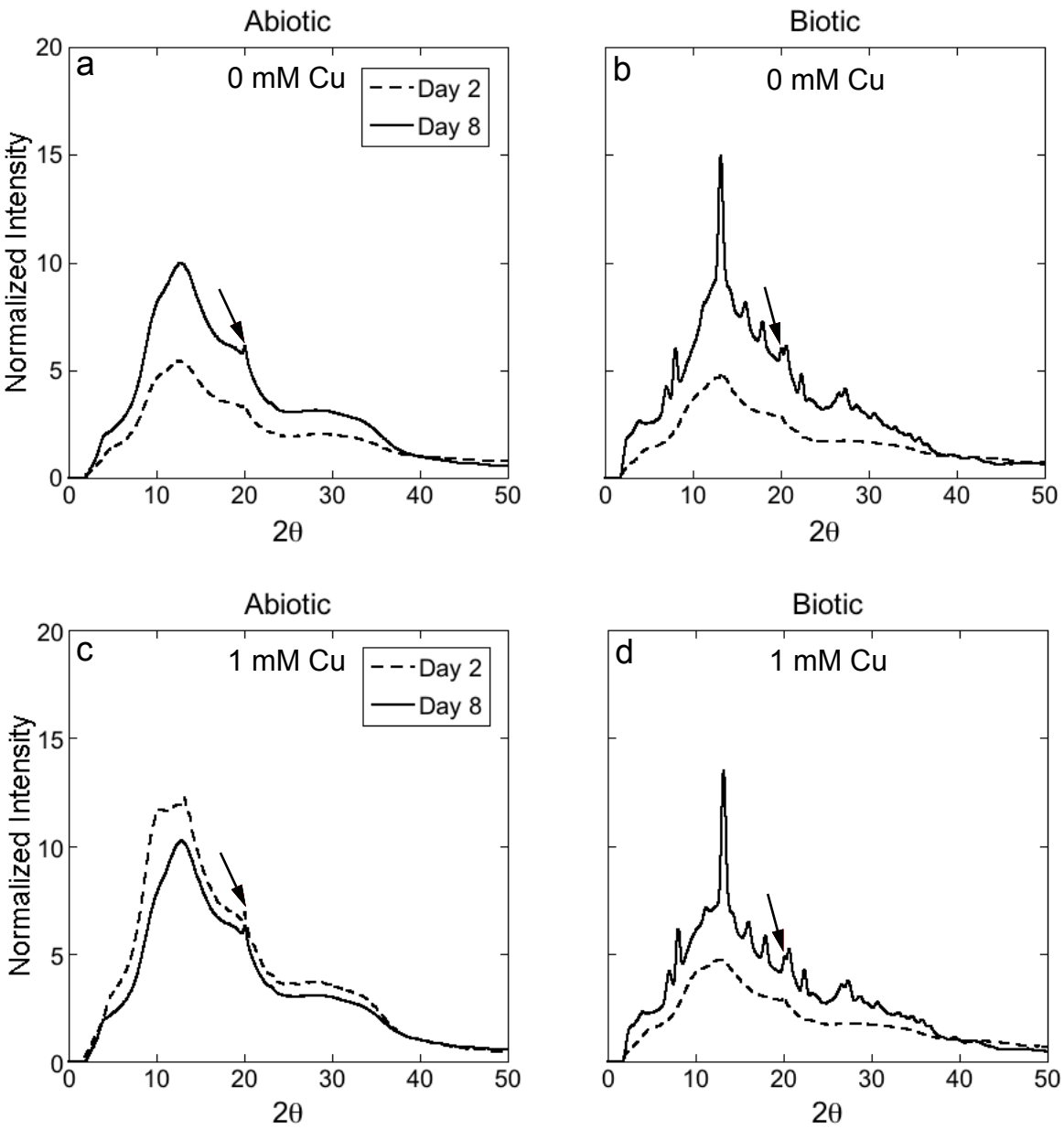

Figure 5.5. Normalized μ-XRD patterns for abiotic precipitates (a) and biotic precipitates (b) in 0 mM Cu medium, and abiotic precipitates (c) and biotic precipitates (d) in 1 mM Cu medium. The peak that appears at 2θ = 20 (indicated by an arrow) in both the abiotic and biotic patterns is due to the presence of Ni in the collimator. All other peaks occurred on day 8 in biotic experiments only and correspond to jarosite. The diffraction pattern backgrounds and intensities were variable from one time point to the next; however, the general trend was toward increasing crystallinity for (b) and (d), and no change in crystallinity for (a) and (c). For clarity, only diffraction patterns for days 2 and 8 are shown.

Vita – Bryn E. Kimball

Education

PhD Geosciences/Biogeochemistry, Pennsylvania State University Dec. 2009
Dissertation title: Biogeochemical Cycling of Copper in Acid Mine Drainage

BS Geosciences with Honors, *Summa Cum Laude*, U. of Oregon 2004
Thesis title: Investigation of Hot Spring Water Composition, Mt. St. Helens, Washington, 1986-2002

Selected Awards and Honors

Center for Environmental Kinetics Analysis Graduate Assistantship, *Penn State* 2008
Student Research Grant, *International Association of Geochemistry* 2008
Centennial Research Award, *Penn State College of Earth and Mineral Science* 2006
Science to Achieve Results Fellowship, *The U.S. Environmental Protection Agency* 2005
Biogeochemical Research Initiative for Education Fellowship, *Penn State* 2004
Inducted into Phi Beta Kappa 2004
Women in Physical Sciences Fellowship, *U. of Oregon* 2002

Selected Research Experience

Graduate Research Assistant, Penn State Geosciences Department August 2004 – present
Copper Isotope Fractionation in Acid Mine Drainage, Chalcopyrite and Enargite Dissolution, Acidophilic Bacteria-Aqueous Copper Interaction

Field Assistant, U. of Oregon Geosciences Department August 2004
Mapped areas of the Tien Shan Mountains, Kyrgyzstan

Undergraduate Research Assistant, U. of Oregon Geosciences Dept. Sept. 2003 – May 2004
Used FTIR to measure the H_2O content in Mt. St. Helens plagioclase melt inclusions (with Dr. Paul Wallace and Dr. Katharine Cashman)

Teaching Experience

Teaching Assistant, Penn State Geosciences Department August 2008 – Dec. 2008
Environmental Geology

Teaching Assistant, Penn State Geosciences Department August 2006 – Dec. 2006
Techniques in Environmental Geochemistry

Publications

Kimball B. E., Mathur R., Dohnalkova A. C., Wall A. J., Runkel R. L., and Brantley S. L. (2009) Copper isotope fractionation in acid mine drainage. *Geochimica et Cosmochimica Acta* **73**:1247-1263.

Kimball B. E., Dohnalkova A. C., Kemner K., Lai B., Macalady J., and Brantley S. L. (2009) Using TEM and μ-XRF to characterize bacterially-mediated precipitation of dissolved copper. *Geochimica et Cosmochimica Acta* **73**(13), A656.

Kimball B. E., Mathur R., Dohnalkova A., and Brantley S. L. (2008) Copper isotopic fractionation in acid mine drainage. *Geochimica et Cosmochimica Acta* **72**, A473.

Kimball B. E., Brantley S. L., and Mathur R. (2007) Using copper isotopes to distinguish biotic and abiotic effects on acid mine drainage. *Geochimica et Cosmochimica Acta* **71**(15), A485.